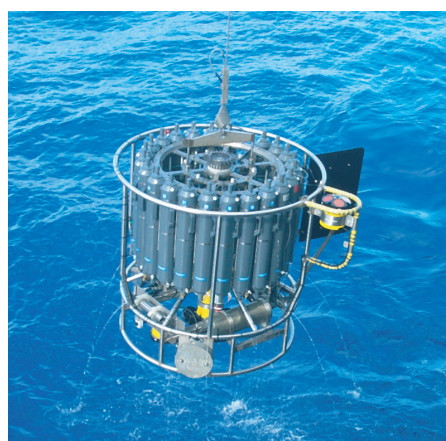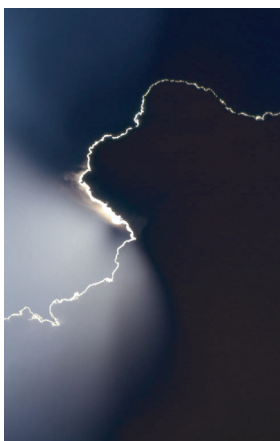# Validation of climate system models with mid-Holocene palaeobotanic data for the Northern Extratropics

Jens Wohlfahrt

Hinweis

Die Berichte zur Erdsystemforschung werden vom Max-Planck-Institut für Meteorologie in Hamburg in unregelmäßiger Abfolge herausgegeben.

Sie enthalten wissenschaftliche und technische Beiträge, inklusive Dissertationen.

Die Beiträge geben nicht notwendigerweise die Auffassung des Instituts wieder.

Die "Berichte zur Erdsystemforschung" führen die vorherigen Reihen "Reports" und "Examensarbeiten" weiter.

Notice

The Reports on Earth System Science are published by the Max Planck Institute for Meteorology in Hamburg. They appear in irregular intervals.

They contain scientific and technical contributions, including Ph. D. theses.

The Reports do not necessarily reflect the opinion of the Institute.

The "Reports on Earth System Science" continue the former "Reports" and "Examensarbeiten" of the Max Planck Institute.

Anschrift / Address

Max-Planck-Institut für Meteorologie
Bundesstrasse 53
20146 Hamburg
Deutschland

Tel.: +49-(0)40-4 11 73-0
Fax: +49-(0)40-4 11 73-298
Web: www.mpimet.mpg.de

Layout:

Bettina Diallo, PR & Grafik

Titelfotos:
vorne:
Christian Klepp - Jochem Marotzke - Christian Klepp
hinten:
Clotilde Dubois - Christian Klepp - Katsumasa Tanaka

Validation of climate system models with mid-Holocene palaeobotanic data for the Northern Extratropics

Jens Wohlfahrt

aus Altenkirchen

Hamburg 2010

Jens Wohlfahrt
Max-Planck-Institut für Meteorologie
Bundesstrasse 53
20146 Hamburg
Germany

Validation of climate system models
with mid-Holocene palaeobotanic data
for the Northern Extratropics

B4 modern

AO-6ka

AOV-6ka
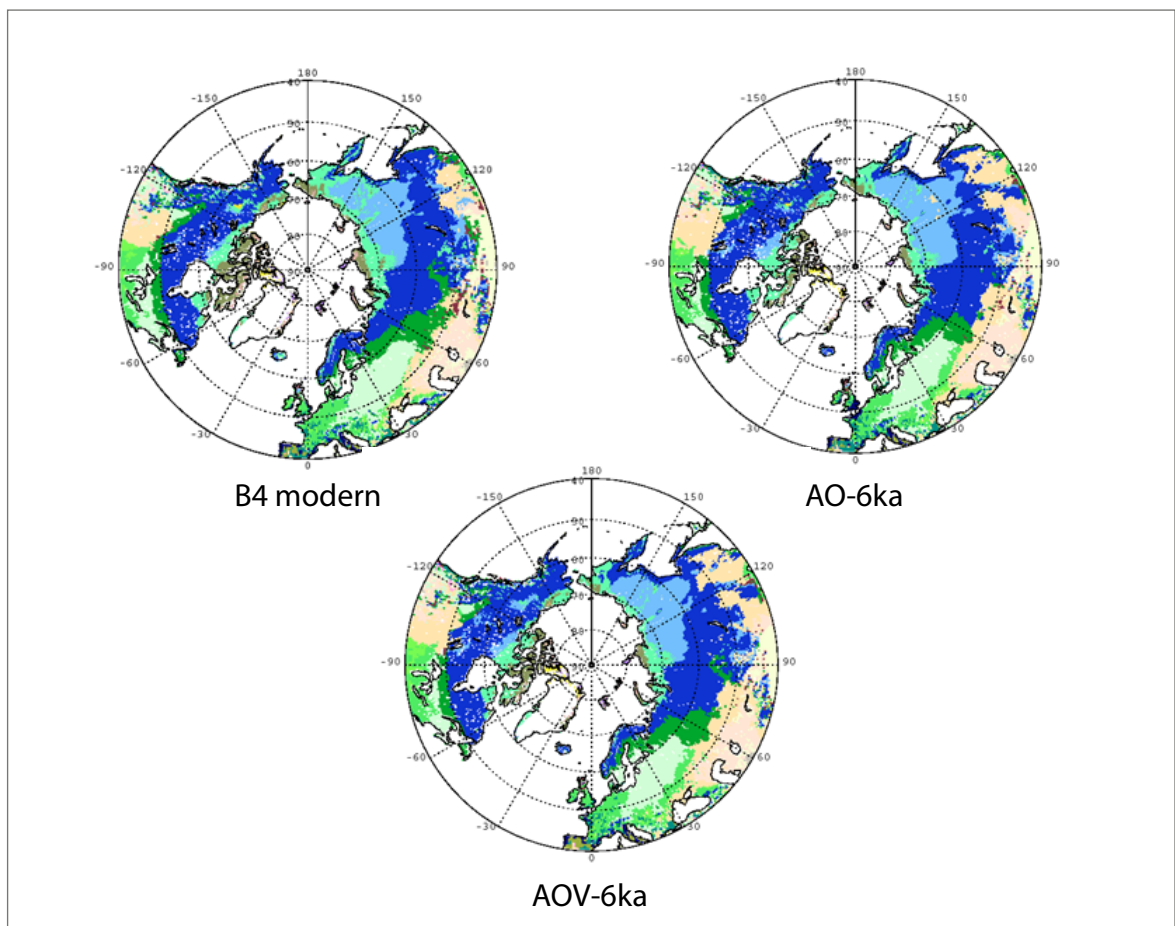
Jens Wohlfahrt

Hamburg 2010

Table of contents

Zusammenfassung

In der vorliegenden Arbeit werden Klimasimulationen von globalen Modellen der Zirkulation der Atmosphäre und des Ozeans mit Hilfe eines diagnostischen Vegetationsmodells und Pollendaten analysiert. Die Untersuchungen konzentrieren sich auf die mittleren und hohen Breiten der nördlichen Hemisphäre (Extratropen) und den Veränderungen auf Grund unterschiedlicher Randbedingungen im mittleren Holozän vor 6000 Jahren (6ka).

Anhand einer Serie von Simulationen mit Atmosphäre- (A), Ozean- (O) und Vegetations- (V) Modellen werden die saisonalen Veränderungen zwischen heutigem und Holozänem Klima und daraus folgende Vegetationsveränderungen in den Extratropen untersucht. Der Einfluss von Ozean- und Vegetationsrückkopplungen durch Meereis-Albedo und Schnee-Vegetations-Albedo, sowie daraus resultierende Synergie Effekte werden untersucht. Während des mittleren Holozän waren die nördlichen Extratropen - bei intensiverer Sonneneinstrahlung im Sommer und zugleich geringerer im Winter - ganzjährig wärmer als heute. Die atmosphärische Erwärmung im Sommer führt über die Wärmespeicherung der Ozeane zu einer Erwärmung im Herbst. Durch diese Verlängerung der Wachstumsperiode im Herbst dringen boreale Wälder weiter nach Norden vor. Diese neu besiedelten dunkleren Waldbereiche können sich im Frühling, anders als die schneebedeckte Tundra, schneller erwärmen. Nur auf Grund gemeinsamer Effekte (Synergien) zwischen Meereis-Albedo und Schnee-Vegetations-Albedo Rückkopplungen ergeben sich in der Atmosphäre-Ozean-Vegetation-Simulation (AOV) mildere Winter für das mittlere Holozän. Die Ergebnisse werden mit weiteren Atmosphäre-Ozean-Simulationen (AO) auf spezifische und konforme Veränderungen verglichen und mit Paläovegetationsdaten evaluiert. Abschließend wird mit dieser Analysemethode ein weiterentwickeltes Atmosphäre-Ozean-Vegetation-Modell untersucht. Alle Simulationen zeigen eine durch Pollendaten gestützte nördliche Verschiebung der borealen Baumgrenze sowie der temperierten Wälder in Nordamerika. Regionale Abkühlungssignale sind in Osteuropa und Zentral-Kanada zu erkennen. Bei allen Simulationen ist in Eurasien eine deutliche Ausbreitung arider Vegetation zu finden, die nicht durch Paläodaten gestützt werden kann. Diese Tendenz der Versteppung im Zentraleurasischen Kontinent wird in den AOV-Simulationen verstärkt. In Westeuropa zeigen die Simulationen deutliche Unterschiede und wechseln von warm temperierten gegenüber kalt temperierten Wäldern bis hin zu savannenartiger Vegetation. Übereinstimmungen mit Paläovegetationsdaten sind in diesem Bereich von Modell zu Modell unterschiedlich und variieren in einem kleinen regionalen Maßstab.

Abstract

Climate simulations with global circulation models (GCM) of atmosphere and ocean are analysed using a diagnostic vegetation model (BIOME4) and palaeovegetation data of pollen. The reconstructions with the BIOME4 model characterize combinations of climate parameters that induce vegetation distribution which is comparable to the used pollen data set. This validation is focused on the mid and high northern latitudes (Extratropics) and changes forced by different boundary conditions at the mid-Holocene about 6000 years before present (6ka). At that time higher orbital forcing in summer and lower orbital forcing in winter on the Northern Hemisphere produced an annual warming that is reflected in the palaeovegetation.

With an ensemble of atmosphere (A), atmosphere-ocean (AO) and atmosphere-ocean-vegetation (AOV) simulations of the same model the seasonal differences and the resulting changes of vegetation between present (control run) and 6ka are examined. Ocean and vegetation feedbacks are separated and the synergistic effect between sea-ice albedo and snow-vegetation albedo is analysed. The orbital induced warming of the atmosphere in summer generates a warming of the oceans in autumn which leads to a prolongation of the growing season and a northward migration of boreal forest. In spring the forest-covered regions appear to be darker than the snow-covered tundra and leads to further warming. As a consequence only the AOV simulation produces a year-round warming in the northern Extratropics. These results are compared to a series of other AOGCM simulation with different models. Specific and robust changes are evaluated and assessed with pollen data. These analysing methods are used to examine an AO and an AOV simulation with the recent ECHAM5-MPIOM-LPJ model. All simulations show a decline in tundra area, an asymmetric northward shift of boreal forests and a small northward shift of temperate forests in North-America in agreement with the palaeovegetation data. Regional cooling signals are recognized in East-Europe and Central-Canada. Another main response to mid-Holocene climate change refers to the increased distribution of temperate grassland caused by drier interior environments in central Eurasia. This robust signal is not supported by palaeovegetation data. Even the models with dynamic vegetation cannot reverse this trend. Most differences in the reconstruction of the vegetation from the model simulations are located in Europe. Warm temperate forests vary with cold temperate forests and savannah types in small scale distances and the agreement with pollen data alters from North to South.

1. Introduction

1.1 Overview

The high latitudes of the Northern Hemisphere have experienced significant warming since the last part of the 20th century, accompanied by a significant increase in ocean surface temperature, a decrease in sea-ice extent as well as thickness, a decrease in snow cover over the land as well as upon the ice sheets, and also a change in vegetation cover and seasonal duration (Chapman and Walsh 1993; Martin et al. 1997; Myneni et al. 1997; Overpeck et al. 1997; Parkinson et al. 1999; Serreze et al. 2000; Zhou et al. 2001; Lucht et al. 2002; Parmesan and Yohe 2003 ; ACIA 2004). The observed changes in climate are consistent with climate-model predictions on the consequences of increased atmospheric CO_2 concentrations, suggesting that greenhouse warming has already started in the high latitudes (IPCC AR4). Climate-model predictions of the response to anthropogenic changes in atmospheric composition suggest that the Arctic is particularly sensitive to the change in radiative forcing (Cubash et al. 2001) because of two powerful positive feedbacks: changes in the extent and duration of sea-ice cover in the Arctic Ocean (Curry et al. 1996; Hewitt et al. 2001; Vavrus and Harrison 2003; Mikolajewicz et al. 2007.), and changes in the albedo of the land surface as a consequence of changes in snow cover and the extent of forest, which masks the effect of snow cover to a large extent (Harvey 1988; Douville and Royer 1996; Bonan et al. 1992; Levis et al. 2000; Brovkin et al. 2003).

Mid-Holocene observations

A variety of environmental indicators (e.g. vegetation cover, lake level) show that Northern Hemisphere climates were considerably different from present during the mid-Holocene (ca. 6000 years ago, 6 ka). The most pronounced changes occur in the subtropics and the subpolar regions. Whereas in the Afro-Asian region the expansion of moisture-demanding vegetation and the presence of large lakes attest to an

enhancement of the Northern Hemisphere monsoons (Street-Perrott and Perrott 1993; Jolly et al. 1998; Yu et al. 1998; Prentice et al. 2000), in the mid- to high-northern latitudes, the expansion of boreal forest at the expense of tundra indicates warmer conditions during the growing season (TEMPO 1996; Tarasov et al. 1998; Edwards et al. 2000; MacDonald et al. 2000; Prentice et al. 2000; Williams et al. 2000; CAPE Project Members 2001; Bigelow et al. 2003). Both of these regional changes are associated with changes in incoming solar radiation (insolation) resulting from changes in the Earth's orbit: at 6 ka, northern-hemisphere insolation was ca 5 % stronger than today during summer and ca 5 % less than today in winter (see Chapter 4.4.1, Figure 4-13).

Mid-Holocene simulations

Simulations with general circulation models (GCMs) of the atmosphere (AGCMs) show that the observed changes in regional climates at 6 ka are partly caused by the atmospheric response to orbital forcing (Kutzbach 1981; Kutzbach and Otto-Bliesner 1982; Kutzbach and Street-Perrott 1985; Kutzbach and Guetter 1986; COHMAP members 1988; TEMPO 1996; Masson and Joussaume 1997; Joussaume et al. 1999; Brovkin et al. 2002; Weber et al. 2004). However, analyses conducted in the Palaeoclimate Modelling Intercomparison Project (PMIP: Joussaume and Taylor 2000) show that the AGCMs do not reproduce the pronounced asymmetry in the changes in the tundra-taiga boundary shown by the observations (TEMPO 1996; Kohfeld and Harrison 2000). These mismatches between simulated and observed regional climates indicate the importance of feedbacks in amplifying or modifying the atmospheric response to orbital forcing. Changes in ocean conditions have been invoked as important feedbacks on high-latitude climates (Kutzbach and Liu 1997; Hewitt and Mitchell 1998; Liu et al. 1999; Otto-Bliesner 1999; Braconnot et al. 2000a; Texier et al. 2000; Liu et al. 2004) as well as feedbacks indicated by changes of the terrestrial conditions (Ni et al. 2004; Renssen et al. 2004).

1.2 Research focus of this study

1.2.1   Assessment of the diagnostic model BIOME4

In this validation of climate system models with different complexity, ranging from atmosphere-only general circulation models (AGCM) to models with coupled atmosphere, ocean and vegetation components (AOVGCM), the analyses are focussing on the changes in the mid- to high-northern latitudes for mid-Holocene climate (6 ka). The spatial focus is motivated by the existence of a synthesis of pollen data from the high latitudes created as part of the Pan-Arctic INitiative project (PAIN: Bigelow et al. 2003). These data provide a target against which to assess the realism of the 6 ka simulations. To facilitate comparisons with these data, the output of climate system models is used to drive an equilibrium vegetation model (BIOME4: Kaplan et al. 2003) in order to derive the changes in vegetation patterns implied by the simulated climate changes. The simulated vegetation integrates changes in the seasonal cycles of temperature and moisture, and thus provides a simple diagnostic of regional climate changes.

Furthermore, this study presents a critical assessment of the BIOME4 model by comparing the potential modern standard vegetation reconstruction of the simulation with the data set of Biome6000/PAIN for present (0ka). Nevertheless this estimation is restricted and pertains on the region north of 40 °N, it displays the necessity of a critical use of BIOME4 vegetation simulation as both approaches do not generally match and indicate sensitive areas.

1.2.2   Analyses of atmosphere, ocean and vegetation response in a GCM

In Chapter 3, the strength of the individual feedback processes reflecting the interchanges between different model components are evaluated using existing mid-Holocene simulations made with the Institute Pierre Simone Laplace (IPSL)

atmosphere ocean general circulation model (AOGCM) asynchronously coupled to an equilibrium vegetation model (BIOME1; Prentice et al. 1992). The effects to vegetation change are diagnosed with reconstructed vegetation maps simulated with the global equilibrium vegetation model BIOME4 (Kaplan et al 2003). In a set of simulations with different combined climate system components the impact of orbital forcing is separated and systematic feedbacks of the ocean and the land can be addressed. The deviation of amplified and weakened signals of the separated feedbacks compared to the coupled AOVGCM simulation allows an assessment of the synergies as a result of changes that cannot be assigned to compound model feedbacks. Conspicuous regional changes of vegetation cover are located and ascertained in the context of climate conditions determine the vegetation distribution. The investigated features are verified against the observed palaeovegetation data. Therefore the simulated vegetation is compared with a combination of the PAIN data set with the Biome6000 data set to refill and cover the examined extratropical region north of the 40th latitude north.

1.2.3   Validation of GCMs

In a second step (Chapter 4) these results are tested with different simulations of several GCMs. It will be analysed if the responses to insolation changes as a consequence of orbital forcing (Berger 1978) shown by the IPSL model are model specific or characteristic for the Northern Hemisphere in 6 ka simulations and can be confirmed in general. This part of the validation is divided into two phases, where firstly the basic similarities of coupled ocean-atmosphere general circulation models (AOGCMs) is verified and in a subsequent phase the ECHAM3-LSG simulation out of the first phase is compared to simulations by its improved and new established successor ECHAM5-MPIOM with an additional version of fully coupled dynamic vegetation as a representative of one of the most comprehensive state of the art model.

Six modelling groups have run coupled AOGCM simulations for 6 ka (Chapter 4.3: Hewitt and Mitchell 1998; Otto-Bliesner 1999; Braconnot et al. 2000b; Voss and Mikolajewicz 2001; Weber 2001; Kitoh and Murakami 2002; Mikolajewicz et al. 2003). These simulations document the importance of ocean feedbacks for Northern Hemisphere climates, and should allow qualifying the strength of this feedback. However, the existing 6 ka AOGCM simulations use slightly different specifications of the 6 ka climate forcing, so the diagnosis of differences caused by model parameterisation is not entirely straightforward. Dissimilarities in the model constructions, as analyses of AGCM simulations show, can be important for the simulation of regional climates (PMIP: Harrison et al. 1998; Joussaume et al. 1999). However, comparison of these simulations is suitable to identify in how far specific regional climate changes are robust, and how large the differences are between models in their response to the same prescribed radiative forcing.

New developments in climate system models have to be tested for their capability to confirm applications in the sense of steady or even enhanced quality (Chapter 4.4). Thus, the innovated ECHAM5-MPIOM-LPJ model (Schurgers et al. 2007) for transient and long time scale simulations is examined and compared to the previous ECHAM3-LSG simulation (Voss and Mikolajewicz 2001) which is evaluated within the range of the six models of the first phase. This model is run in two different modes; one with the standard set up of the atmosphere-ocean components and one with added fully coupled interactive vegetation from the Lund-Potsdam-Jena dynamic global vegetation model (LPJ: Sitch et al. 2003). In addition to the assessment of changes in vegetation distribution and their reliability of realism in comparison to observed palaeobotanic data, a variability study of the control runs is realised and the direction of migration by vegetation types is quantitatively analysed.

2. Methods

2.1 BIOME data and model

2.1.1   The Biome6000/PAIN data set

Main results of this validation of climate simulations arise from comparisons with observed data. The aim of the analyses of pollen data sets is to estimate the quality of the model results and a potential interpretation of global and regional climate patterns and to detect and locate intra-model improvements. Therefore a combination of two related data sets for modern and mid-Holocene vegetation reconstruction is used.

All sites between 40 and 55 °N are derived from updated versions of the Biome6000 data (Prentice and Webb 1998; Prentice et al. 2000; Harrison et al. 2001; Bigelow et al. 2003; Pickett et al. 2004; available for download at http://www.bridge bris.ac.uk/resources/Databases/BIOMES_data). The collaboration collected large-scale continental fieldwork observations in the Global Palaeovegetation Mapping Project and was linked to the International Geosphere-Biosphere Programs IGBP-GAIM, IGBP-DIS, IGBP-GCTE and IGBP-PAGES (http://www.igbp.net). The Palaeovegetation Mapping Project provides global maps describing the vegetation patterns documented by pollen and plant macrofossils from individual sites for the mid-Holocene at 6000 ±500 yr B.P. and the last glacial maximum at 18000 ±1000 yr B.P. on radiocarbon time scale, equivalent to 21000 yr B.P. calendar scale (Figure 2-1). The reconstruction of the vegetation maps is based on a standard objective biomisation technique. With this, biomes reflect defined vegetation communities against climate conditions expressed and calculated by plant functional types (PFTs) (Steffen et al. 1992).
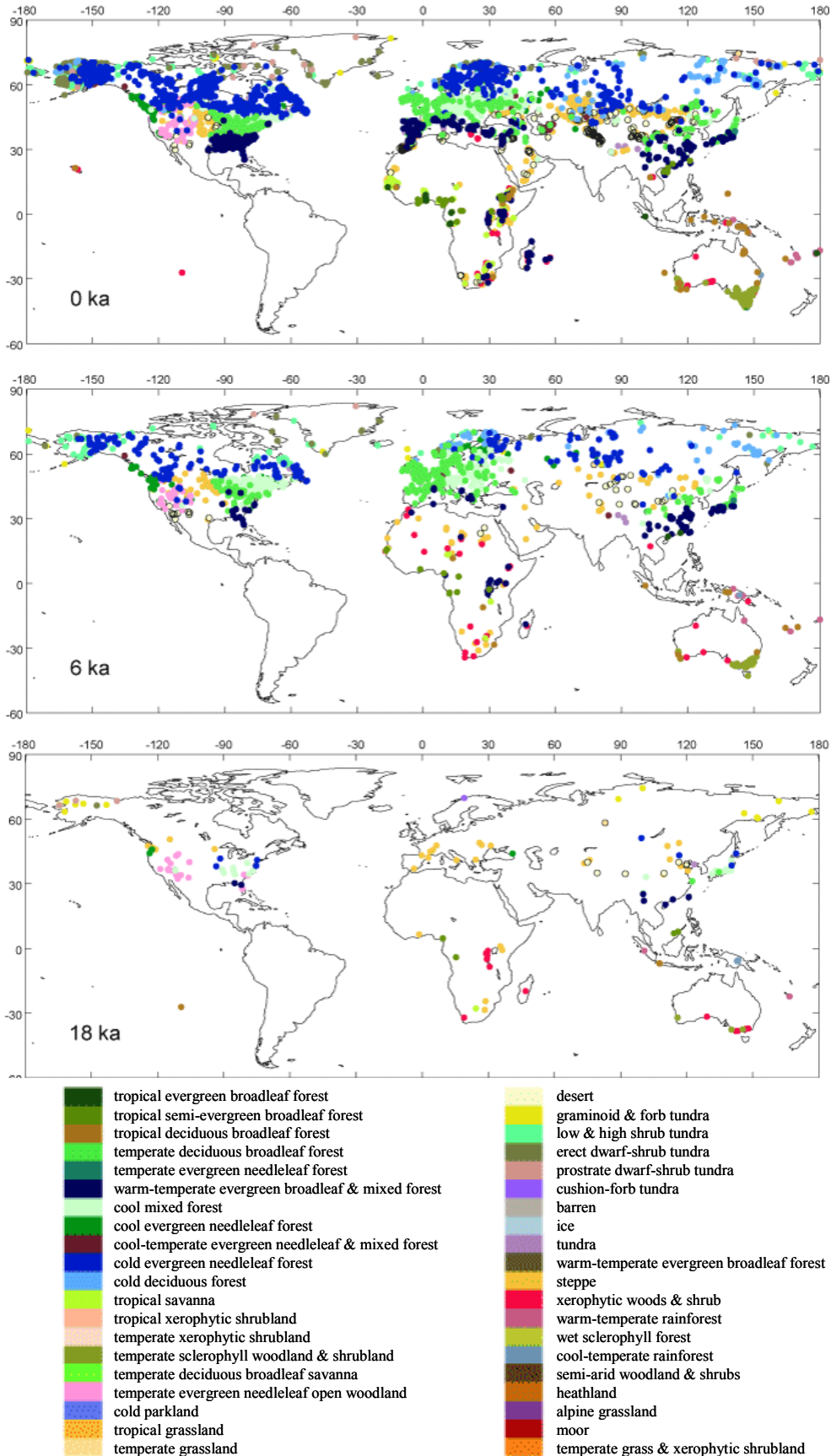
Figure 2-1: The Biome6000 data points for the sampling time slices (Prentice et al. 2000).

The taxa represented in the pollen or plant samples are allocated to one or more PFTs on the basis of life form, leaf form, phenology and bioclimatic tolerance in turn with an expected bioclimatic distribution. Combinations of characteristic PFTs define biomes. Because of the low taxonomic resolution of the pollen, some taxa can be classified into more than one PFT and those PFTs, which are known to occur in too many biomes, are excluded to provide more precise information to sever. The affinity from taxon assemblages to PFT and therefore from PFT to biome is calculated as the sum of pollen values for taxa which occur in that biome. In cases where the assemblage has equal affinity for more than one biome, occurring when one biome is defined by a subset of PFTs that characterise another one, the assemblage is allocated to the biome defined by the subset. Within the data sets the quality of a dating control at each time period is listed using the COHMAP dating control schemes as described in Yu and Harrison (1995).

The published version of the Biome6000 database (Version 3: Prentice et al. 2000) is based on maps produced on a region-by-region basis over a number of years. The regional data are fused together and the biome names are standardised, using names mostly consistent with the BIOME4 equilibrium biogeography vegetation model (Kaplan et al. 2003). For this database the following region-by-region data sets are used: Europe (Prentice et al. 2000), Africa (Jolly et al. 1998; Elenga et al. 2000), South-East Asia and the Pacific (SEAPAC; Pickett et al. 2004), Eastern and Boreal North America (Williams et al. 2000), Western North America (Thompson and Anderson 2000), Alaska and West Beringia (Edwards et al. 2000), Former Soviet Union and Mongolia (Tarasov et al. 1998; 2000), China (Yu et al. 1998; 2000; Harrison et al. 2001), Japan (Takahara et al. 2000), and Latin America and the Indian subcontinent (in progress).

Moreover, a second data set from the Pan-Arctic INitiative (PAIN) represents the sites north of 55 °N (Bigelow et al. 2003). The work of the PAIN project is focused on the terrestrial vegetation in the context of climate changes in the arctic region. Here, particularly the boundary between forest and tundra is further delimited and the former classified tundra biome is split into five new biome types (Low and high shrub tundra,

erect dwarf-shrub tundra, prostrate dwarf-shrub tundra, cushion forb, lichen and moss tundra, and graminoid and forb tundra) for more detailed reconstructions in the most northern regions. The attempt of PAIN follows the directives of the Biome6000 project and applies the standard biomisation procedure and the same time slices of modern (0 ka), mid-Holocene (6 ka ± 500a) and the last glacial maximum (18ka ± 1000a). The main advantage of the recently most elaborated compilation of palaeovegetation data in the Arctic is the compatible biome classification with the BIOME4 vegetation model, which is developed in part within the PAIN project. This enables a direct comparison between field observations and model simulations without an intermediate step for interpretation.

On basis of the related description of temperate and boreal biome types between Biome6000 and PAIN data, the two sets can be merged into one with the exception of the improved tundra types, which are adopted from PAIN. The latest version 4.2 of the Biome6000 data set (updated: 21/08/2006) already contains the PAIN data for download.

2.1.2   The BIOME4 model

The BIOME4 global vegetation model (Kaplan et al., 2003) is an equilibrium terrestrial biosphere model developed from the previous BIOME3 model of Haxeltine and Prentice (1996). The enhancement of the BIOME4 model implies the addition of five new PFTs, a new module to calculate isotopic discrimination dividing grass types into a C3 or C4 photosynthetic pathways and the re-parameterisation of the original PFTs. The additional PFTs lead to more precise representation of vegetation types in the Arctic and the arid Subtropics and can be associated with the PAIN classification more easily. The basic principal of the BIOME model is the calculation of ecosystems by vegetation compositions, so called biomes, from different composition of different

Tropical evergreen broadleaf forest
Tropical semi-deciduous broadleaf forest
Tropical deciduous broadleaf forest & woodland
Temperate deciduous broadleaf forest
Temperate evergreen needleleaf forest
Warm-temp. evergreen broadleaf mixed forest
Cool mixed forest
Cool evergreen needleleaf forest
Cool-temp. evergreen needleleaf mixed forest
Cold evergreen needlefeaf forest
Cold deciduous forest
Tropical savanna
Tropical xerophytic shrubland

Temperate xerophytic shrubland
Temperate sclerophyll woodland and shrubland
Temperate deciduous broadleaf savanna
Temperate evergreen needleleaf open woodland
Tropical grassland
Temperate grassland
Desert
Graminoid and forb tundra
Low and high shrub tundra
Erect dwarf shrub tundra
Prostrate dwarf shrub tundra
Cushion forb tundra
Barren

Figure 2-2: Standard modern (0 ka) potential vegetation map simulated by the BIOME4 model.

PFTs. These biomes arise from the combination of PFTs. Competition between PFTs is treated as a function of relative net primary productivity (NPP). The distribution of PFTs is described in terms of tolerance thresholds for cold, heat, chilling, sunshine and moisture requirements. Cold tolerance is expressed in terms of the minimum temperature (T_{min}). The chilling requirement is formulated in terms of the maximum mean temperature of the coldest month (MTCO). The heat requirement is expressed in terms of growing-degree-days (GDD) above a threshold of 5 °C for trees or 0 °C for non-woody plants. The distinction between cool and warm grass/shrub is based on mean temperature of the warmest month (MTWA). The sunshine is expressed in relative cloudiness. Moisture requirements are expressed in terms of limiting values of the ratio of actual to equilibrium evapotranspiration (α). BIOME4 simulates the global vegetation in 27 biomes (Figure 2-2), including five types of tundra vegetation, which

represents phenology, plant composition and climate regime out of the combination of 13 different PFTs which can deal additionally with variable C3/C4 plant PFTs.

The model requires monthly averages of temperature, precipitation, cloudiness and, for delimiting cold tolerance biomes, the yearly value of the minimum mean temperature. Subsidiary information about the soil physical properties like water holding capacity and percolation rates are part of the model input. For climate input values the BIOME4 model is tuned to the updated modern climatology database CLIMATE 2.1 by Leemans and Cramer (1991) and the standard input soil data derive from a global soil map from FAO (1995), Canadell et al. (1996), Haxeltine and Prentice (1996) and Jackson et al. (1996). For diagnostic purposes, BIOME4 runs using an anomaly procedure. The intra-climate-model differences are added to the BIOME4 climatology. The climate and soil input data sets are interpolated to the model resolution at a 0.5°grid. Note that the original cited CLIMATE 2.2 is not available anymore and the work has recently been discontinued (Cramer: http://www.pik-potsdam.de/~cramer/climate.html).

BIOME4 contains a coupled carbon and water flux model that simulates competition between PFTs as a function of relative net primary productivity (NPP). After certain

Table 2-1: Specific parameters for PFTs modified after Kaplan et al. (2003); egr = evergreen, sgr = summergreen, rgr = raingreen, $minC_{canopy}$ = minimum of canopy conductance, E_{max} = maximum of daily transpiration, $sw < rgr_l$ = raingreen leaves drop as soilwater availability below demand, $sw > rgr_l$ = raingreen leaves appear as soilwater availability above demand, $roots_{fr30}$ = roots fraction in top 30cm soil layer, $leaf_{long}$ = longivity of leaves in months, $GDD5_{out}$/$GDD0_{out}$ = number of growing degree days above 5/0 °C required for full leaf development, sap_{res} = sapwood respiration, $C4_{path}$ = possible C4 plant pathway of photosynthesis.

PFT specific parameters	phenology egr sgr rgr			$minC_{canopy}$	E_{max}	$sw < rgr_l$	$sw > rgr_l$	$roots_{fr30}$	$leaf_{long}$	$GDD5_{out}$	$GDD0_{out}$	sap_{res}	$C4_{path}$
tropical evergreen	x			0,5	10			0,69	18			1	
tropical raingreen			x	0,5	10	0,5	0,6	0,7	9			1	
temperate broadleaved evergreen	x			0,2	4,8			0,67	18			1	
temperate deciduous summergreen		x		0,8	10			0,65	7	200		1	
cool & temperate evergreen conifer	x			0,2	4,8			0,52	30			1	
boreal evergreen	x			0,5	4,5			0,83	24			1	
boreal deciduous		x		0,8	10			0,83	24	200		1	
C3/C4 temperate grass			x	0,8	6,5	0,2	0,3	0,83	8		100	2	x
C4 tropical/warm-temperate grass			x	0,8	8	0,2	0,3	0,57	10			2	x
C3/C4 desert woody plant	x			0,1	1			0,53	12			1	x
tundra shrub type	x			0,8	1			0,93	8			1	
cold herbaceous type		x		0,8	1			0,93	8		25	2	
lichen/forb type	x			0,8	1			0,93	8			1	

bioclimatic limits (Table 2-1) have determined whether a PFT can exist, the according NPP is calculated. An optimisation algorithm calculates the maximum leaf area index (LAI) of each PFT and its associated NPP for each grid cell. Then the model ranks tree and non-tree PFTs in terms of NPP, LAI and mean annual soil moisture. Semi-empirical rules classify the output to the most successful and second-most successful PFT and their sustainable LAI and assign the grid cell to one of the 27 biomes. The coupled carbon and water flux scheme computes the LAI that maximizes NPP based on intramodel daily time-step simulation of several PFT-specific parameters like soil water balance, canopy conductance, photosynthesis, respiration (Table 2-1), and inferred disturbance regimes such as fire risk. In general, BIOME4 is calibrated for a present CO_2 concentration of 324 ppm.

The main advantage of the BIOME4 model for studies of the high Northern Hemisphere is its high resolution of boreal and arctic vegetation types. Five different tundra biomes from almost arctic desert to shrubby vegetation on transition to forest boundaries are distinguished (Figure 2-3). Dry tundra exists as separate biome and is clearly delimited from grass and other xerophytic vegetation types.
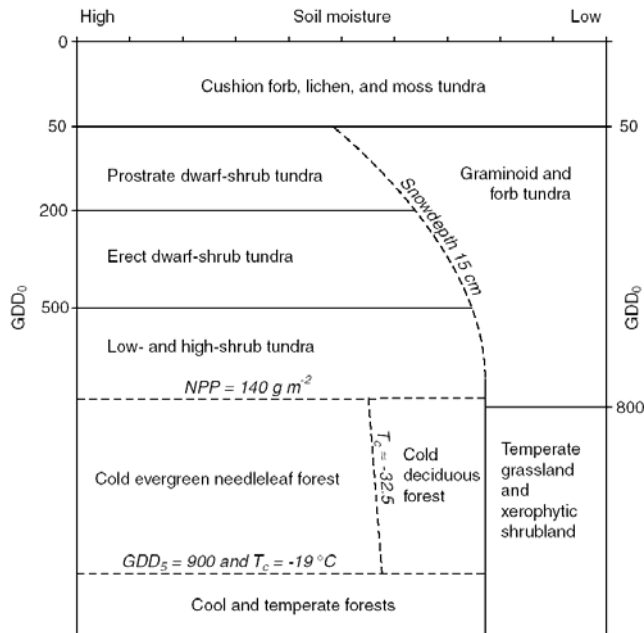

Figure 2-3: Climate space occupation of arctic and boreal biomes defined in BIOME4 (from Kaplan et al. 2003).

The BIOME models have mainly been used as diagnostic tools to simulate vegetation patterns consistent with a given climate simulation. These patterns can then be compared to other vegetation reconstructions or to observed palaeovegetation data such as in this study. However, at the time when dynamic vegetation models were still in progress and could not sufficiently achieve the requirements of coupled general circulation models (GCMs), essential studies of vegetation-climate feedback simulations used the BIOME model for the terrestrial compartment of climate system models (de Noblet et al., 1996; Claussen, 1997; Texier et al., 1997; Kubatzki & Claussen, 1998; Braconnot et al., 1999).

2.2 Climate system models

In the meteorological sense the climate is defined as statistical mean characteristics of atmospheric variables for a time period about 30 years (World Meteorological Organisation, Hantel et al. 1987). For the examinations of long-term climate the changes in the atmosphere are influenced by the oceans, the vegetation and the ice masses. This climate system consists of different subsystems regulating the climate dynamics (Peixoto and Oort 1992, Kraus 2000). Those units taken into account by modelling the climate system are the atmosphere, the hydrosphere like oceans, lakes, rivers and groundwater, the cryosphere like land-ice, sea-ice, snow and permafrost, the marine and terrestrial biosphere, the pedosphere and tectonical dynamics (e.g. Kraus 2000, Claussen 2003). Further earth system models add supplementary components like the antroposphere with aspects of economy and technical knowledge (Schellnhuber and Wenzel 1998, Schellnhuber 1999, Claussen 1998, 2001). But those components are not used in the present GCMs and therefore not considered in this study.

The general circulation models as described by Randall (2000) are currently the most complex global climate models, since they attempt to represent the main components of the climate system in three dimensions. They can be applied in multidisciplinary

studies of interaction and cycles in the earth climate system and are primarily used for the assembly and prediction of global events. Recent, past and future climate reconstructions on time scales of months to decades, such as the onset of El Nino, monsoons, and global warming estimates give valuable references for one of the most prevailing scientific discussion of climate change. Detailed knowledge of meteorology, oceanography, hydrology, photobiology and a wide spectrum of earth science have to amalgamate in numerical equations and be integrated forward in time. The soaring demand of computing resources and the level of scientific understanding of the climate system pose the limits of climate system model results.

The GCM varieties refer to structure, design, and of course the combination of different sub-model components. The model characteristics and parameterisations are basically and individual core aspects concerning grid resolution, flux correction, sea-ice modulation and land-surface condition. The experimental design and boundary conditions can be chosen in accordance with the aim of a study and include length of spin-up, length of simulation, solar radiation and climate relevant gas concentration. Due to the multiple options for model simulations every working group documents their configurations if not published in special reports commonly available online. Detailed descriptions of the composition of the used models are given in the related chapters.

2.3 Quantification of diagnostic BIOME4 model

The BIOME4 model produces a potential natural vegetation map as a standard output (Figure 2.2). As this map refers to the previous BIOME3 model simulation (Haxeltine and Prentice, 1996), the BIOME4 map is mainly based on the BIOME3 assessment with the constructed global vegetation map developed by Melillo et al. (1993). Several other global and regional maps are introduced to the Mellilo map to receive a maximum amount of information to calibrate the vegetation reconstruction of the

 BIOME model. Apart from some discrepancies in the southwest of Alaska, Prairie of mid-continental North America, the northern Mongolian steppe, and some savanna areas in southeast India the validation of the BIOME map is graded as reliable (Haxeltine and Prentice, 1996; Kaplan et al. 2003). The BIOME4 potential natural vegetation map for modern time has not been compared to the observation data stored in the Biome6000 and PAIN data set, yet. As both, the observation data and the model data are the main diagnostic tools in this study, an assessment of their comparable quality is introduced as follows.

Table 2-2: Classification of vegetation

vegetation classifications		
biomes	megabiomes	vegetation groups
Tropical evergreen broadleaf forest Tropical semi-deciduous broadleaf forest Tropical deciduous broadleaf forest & woodland	tropical forest	forest
warm-temperate evergreen broadleaf mixed forest	warm-temperate forest	
temperate deciduous broadleaf forest temperate evergreen needleleaf forest cool mixed forest cool evergreen needleleaf forest cool-temperate evergreen needleleaf mixed forest	temperate forest	
cold evergreen needleleaf forest cold deciduous forest	boreal forest	
tropical savanna temperate sclerophyll wood and shrubland temperate deciduous broadleaf savanna temperate evergreen needleeaf open woodland	savanna	grass, shrubs and desert
tropical xerophytic shrubland temperate xerophytic shrubland tropical grassland temperate grassland	grass	
desert barren	desert	
graminoid & forb tundra low & high shrub tundra erect dwarf-shrub tundra prostrate dwarf-shrub tundra cushion-forb tundra	tundra	tundra

As all analyses are focused on the Northern Hemisphere containing temperate, boreal and arctic regions north of 40 °N, other data are neglected in this study. In total 6158 data points from the Biome6000/PAIN data set refer to this extratropical region. In the BIOME4 half grid resolution 27431 terrestrial grid cells are calculated when the prescribed modern ice sheets (Peltier 1994) are subtracted. Altogether 5457 data coordinates and grid cells can be compared with each other. Those sites not taken into account have either been dated with a weak reputation or they are located on spots along the coasts, on islands or in broad rivers and lakes where the BIOME4 land scheme prevents simulated vegetation for comparison. In case of more than one pollen site in a 0.5 grid cell, the vegetation type reconstructed most frequently is used with the assumption that this represents the dominant vegetation. If there are equal numbers of different biome types all sites are taken into account.

For the purpose of a quantitative comparison a simplified biome classification scheme, which groups individual biomes into major vegetation types (megabiomes) is adopted (Harrison and Prentice 2003), and summarised in Table 2-2. Thus, the estimate of
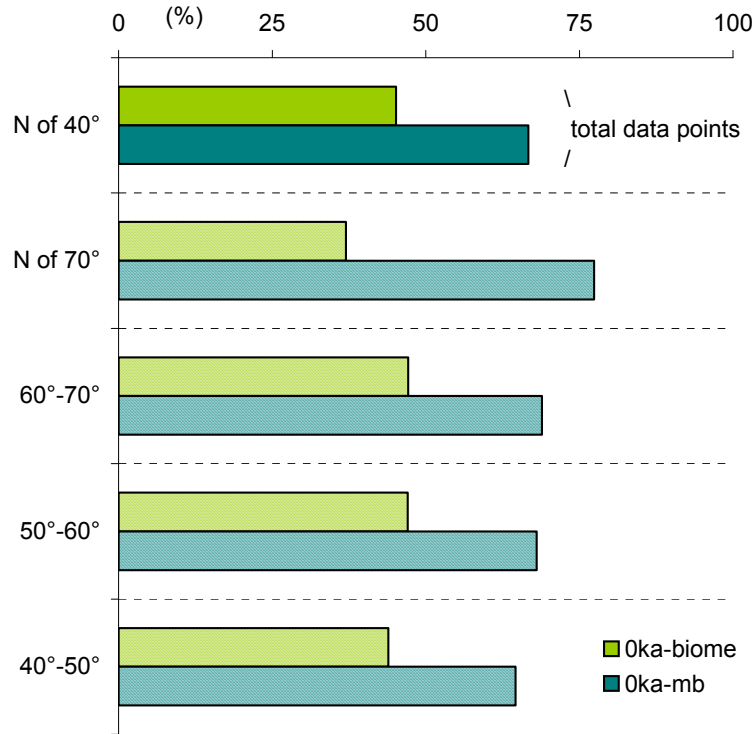

Figure 2-4: Matching agreement between observed and BIOME4 simulated modern vegetation in % for biomes (0ka-biome) and megabiomes (0ka-mb) of total 5457 data points, further divided into latitudinal bands.

agreement between the megabiomes of the data and the simulations are relatively conservative. But large climate signals peak in distinct vegetation changes, and can be diffused by comparing 24 biomes instead of seven megabiomes. The reduced number of biome types reasoned in neglecting the tropical vegetation types as not relevant for the extratropical investigation area.

In the study region north of 40 °N the BIOME4 simulation reaches an agreement of 45.2 % with the observations (Figure 2-4) for the biome classification. In the extratropical region this classification refers to 24 biomes instead of 27, as tropical biome types are excluded and the ice areas are prescribed. The best agreement is reached in the band between the 50th and 70th of northern latitude.

For the summarised vegetation classification of megabiomes in total 66.7 % matches, respectively 3639 of 5457 data points. In contrast to the biomes, the megabiomes agree especially in the polar region north of 70 °N, decreasing southwards. A statistical estimation of megabiomes with the Kappa statistics (Monserud 1990) for comparison of vegetation maps grades the agreement with k = 0.532 as fair close to good. The Kappa statistics is an objective and approved tool for comparison of categorical data like vegetation maps (Monserud and Leemans, 1992; Prentice et al. 1992; Claussen 1994, 1998; Foley et al. 1996; Haxeltine and Prentice 1996). Hereby the Kappa Statistics offers an index that compares the agreement against what might be expected by chance. The index renders the chance-corrected proportional agreement, and the values range from +1 for perfect agreement to 0 for the agreement expected by chance to -1 for complete disagreement.

The fact that more than a quarter of the BIOME4 predicted megabiomes disagree with the observations is an unexpected result. A visual comparison of the observation (Figure 2-5b) with the BIOME4 modern vegetation map (Figure 2-5a) shows that mismatches occur primarily in the regions of Beringia and Central Asia. These regions are particular figured out in Alaska (Figure 2-7) and Mongolia with South Siberia (Figure 2-8) in detail.

It appears that the forest-tundra difference in Alaska (180-130 °W; N of 50 °N) with 65.6 % matching is within the average range of 66.7 % of matching for the entire study area (Figure 2-6). In this case the high number of visual faults is related to the high

a)

b)
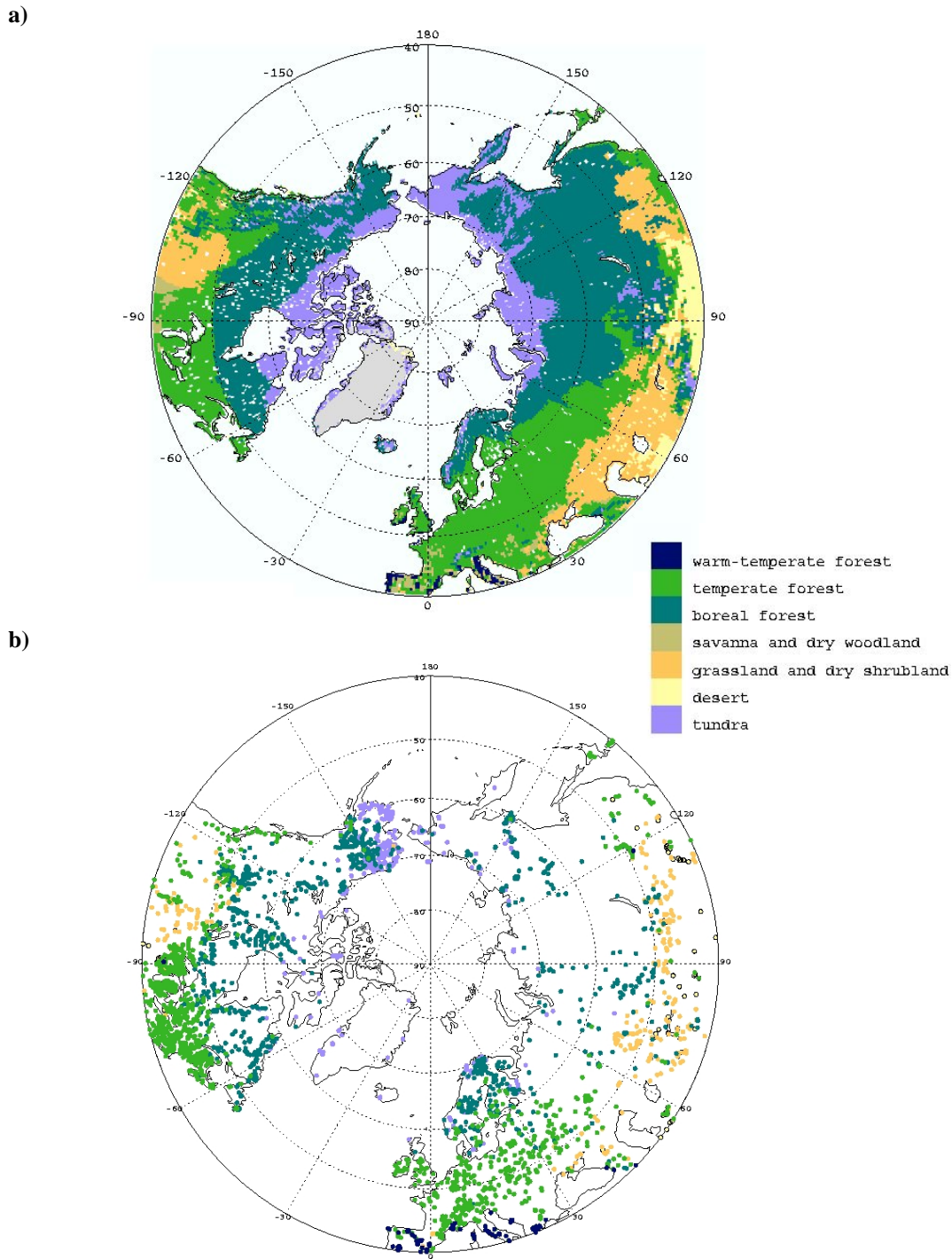
Figure 2-5: Vegetation maps of **a)** the BIOME4 standard modern (0 ka) simulation and of **b)** the observation data set for 0 ka showing megabiome classes.

number of total data in this particular area (210 faults of 610 data points). Presumably the low resolution of altitude favours forest against observed tundra and few data misclassifications explain the local differences.

In the description of the BIOME4 model the authors mentioned a model bias towards the simulation of boreal forest instead of tundra for southern and western Alaska. Assisting comparison with MODIS remote sensing satellite data for land cover albedo by the Moderate Resolution Imaging Spectroradiometer MODIS (Schaaf et al., 2002; Figure 2-7c) and maps of the Global Land Cover 2000 Project (Latifovic et al., 2002; Figure2-8c) support the vegetation reconstruction from observed data.

In Central Asia (60-120 °E; 40-60 °N) the simulated distribution of forest versus steppe megabiomes matches only 155 out of 440 data points, which means 35.2 % agreement (Figure 2-6). And further refining of the vegetation from megabiomes into biomes increases the mismatching noticeably. This excessive mismatching of simulated forest in the area with observed grassland and dry shrubland along the 50th latitude (Figure 2-8b) cannot be explained by the climate baseline of the climatology from Leemans and Cramer. Even though the meteorological information for this region
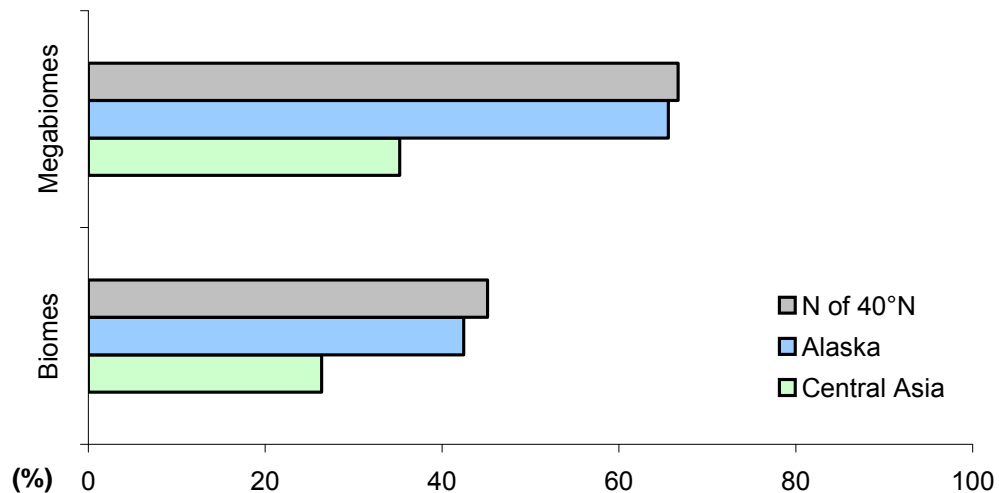
Figure 2-6: Matching agreement between observed and BIOME4 simulated modern vegetation in % for biomes and megabiomes for the spatial regions of Alaska (180-130°W; N of 50°N) and Central Asia (60-120°E; 40-60°N) compared to the mean result for N of 40 °N.

is rare, the temperature and precipitation for the calculation of the BIOME4 model would favour non-woody vegetation types. This bias was already mentioned by Haxeltine and Prentice (1996) in their description of the BIOME3 model. They pointed out, that the prevalence of forests in the model may be caused by assumed higher soil water availability especially for Mongolia. The land cover map of Northern Eurasia developed in the Global Land Cover 2000 Project (Bartalev et al. 2003; Figure 2-8c) also suggests less forest in this particular area than predicted by BIOME4. This strengthens the credibility of the observed data set but on the other hand calls for a more precise survey of the BIOME4 diagnostic simulations in this sensitive region.

a)

■	warm-temperate forest
■	temperate forest
■	boreal forest
■	savanna and dry woodland
■	grassland and dry shrubland
■	desert & baren
■	tundra

b)

c)

Figure 2-7: Comparison of **a)** BIOME4 simulation with **b)** differ observation data points (faults only) and **c)** remote sensing reconstructions of MODIS (Schaaf et al., 2002) for Alaska. Grey and white areas represent barren.

a)

b)

warm-temperate forest
temperate forest
boreal forest
savanna and dry woodland
grassland and dry shrubland
desert & baren
tundra

c)

Figure 2-8: Comparison of **a)** BIOME4 simulation with **b)** differ observation data points (faults only) and **c)** remote sensing reconstructions of Glob2000 (Bartalev et al. 2003) for southern Central Asia. http://www.pik-potsdam.de/ members/cramer/climate.html

3. Synergistic feedbacks between ocean and vegetation

(Wohlfahrt et al. 2004)

3.1 Introduction

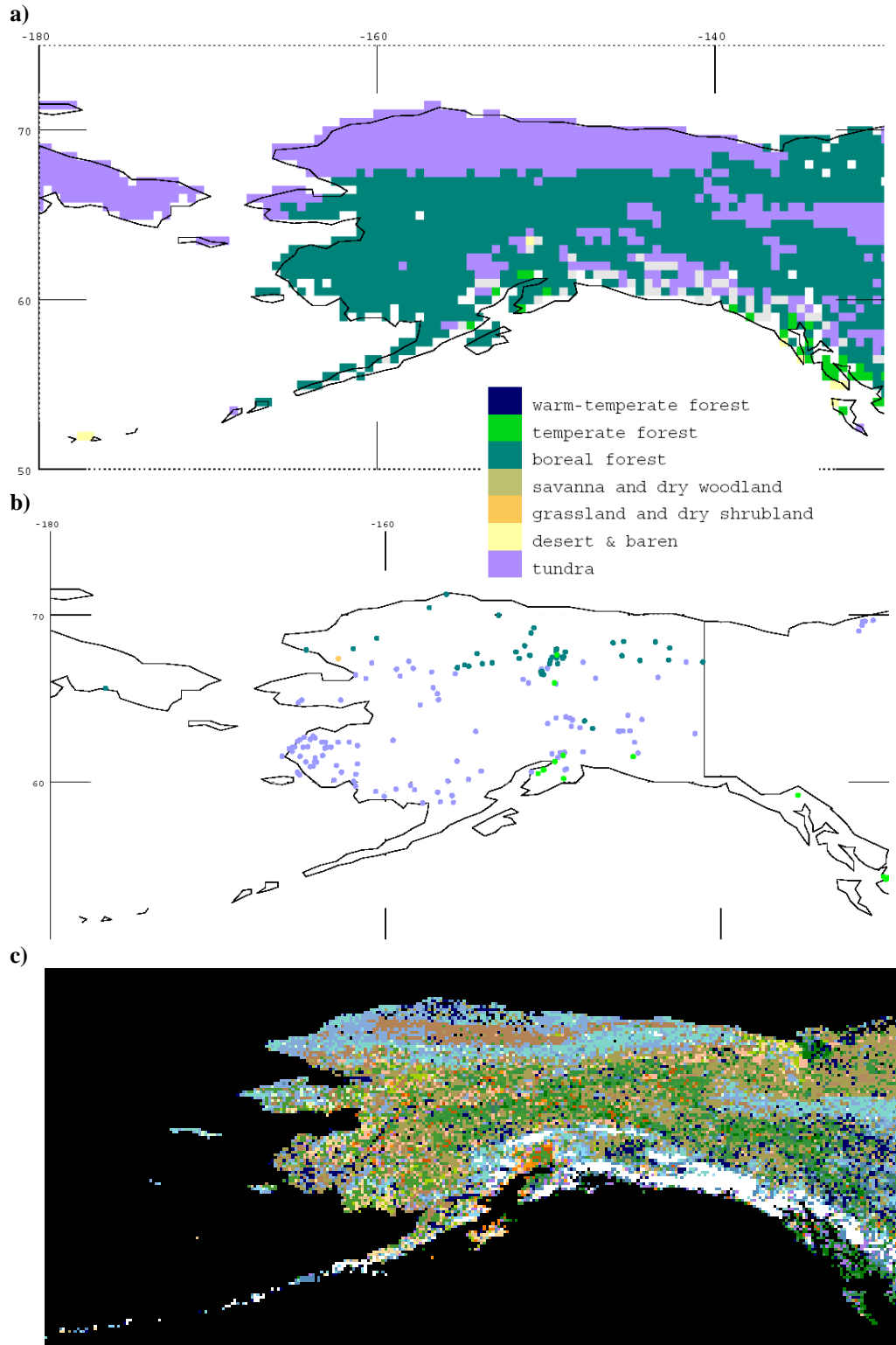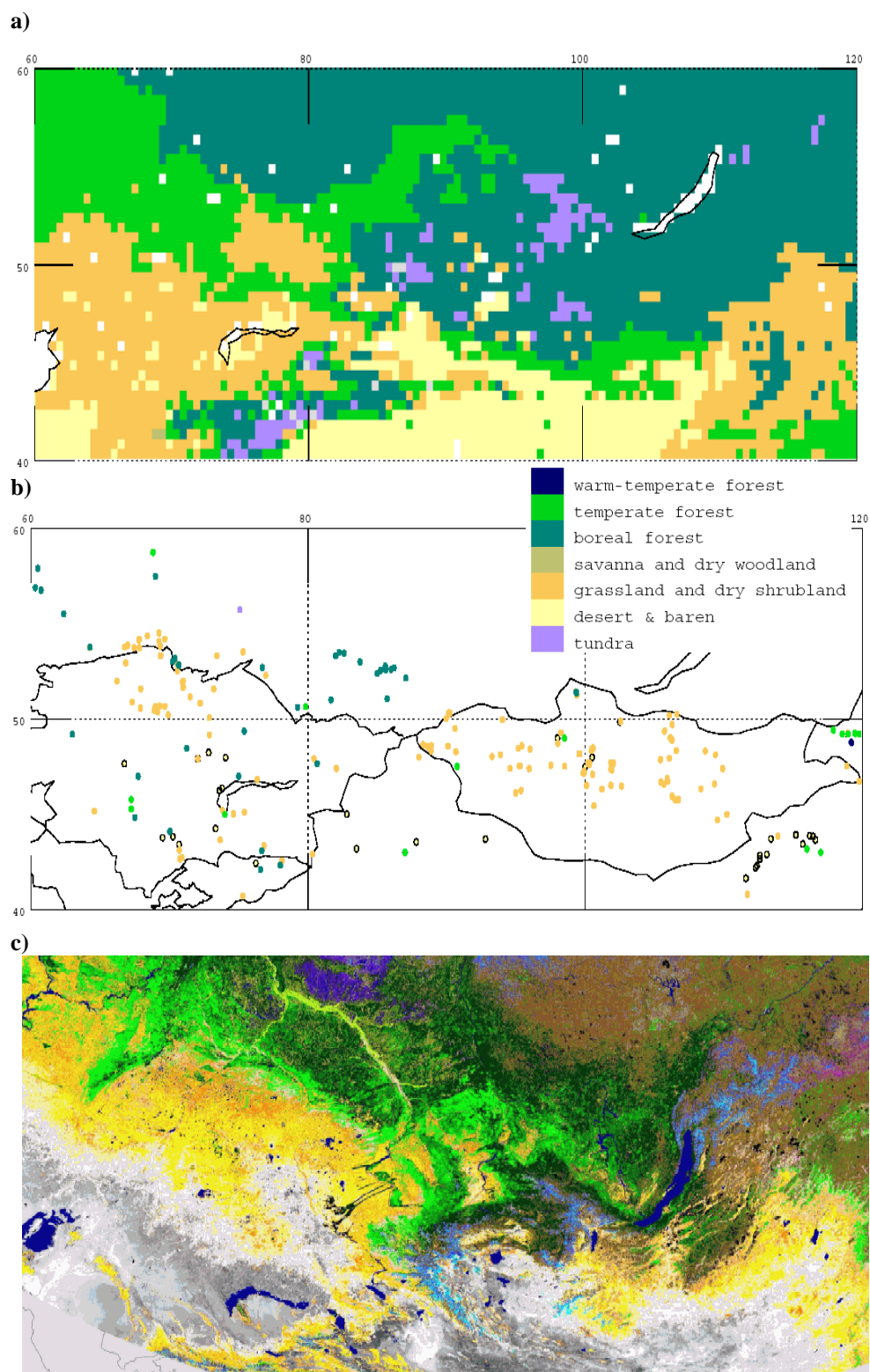Much of our understanding of the importance of ocean and land-surface feedbacks on Arctic climates has resulted from the analysis of palaeoclimate simulations (see e.g., Foley et al. 1994, de Noblet et al. 1996, Gallimore and Kutzbach 1996, TEMPO-Members et al. 1996, Claussen and Gayler 1997, Texier et al. 1997, Broström et al. 1998, Ganopolski et al. 1998, Kubatzki and Claussen 1998, Levis et al. 1999, Vavrus 1999, Hewitt et al. 2001). These simulations have shown that ocean feedbacks and vegetation feedbacks both amplify the response to changes in orbital forcing during the mid-Holocene, and to ice-age boundary conditions (including the impact of lower atmospheric CO_2 concentrations), and that synergy between ocean and land-surface feedbacks may cause a further amplification of the high latitude response. These conclusions appear to be robust across a range of experimental designs and different kinds of model, including a low-resolution but coupled ocean-atmosphere-vegetation model (Ganopolski et al. 1998), further analysed by (Claussen 2001). However, there is less agreement between the simulations about the relative magnitude of the two feedbacks, the strength of the synergy between them, and the degree to which the expression of the response to ocean- and land-surface feedbacks varies regionally. Thus, a further analysis of the role of ocean and land-surface feedbacks and synergy is desirable.

This analysis presents a pre-existing series of mid–Holocene experiments (Braconnot et al. 1999) with the Institute Pierre Simone Laplace (IPSL) coupled ocean–atmosphere general circulation model (Braconnot et al. 2000b), with only the atmospheric component of that model, and with both the atmosphere and the coupled ocean-atmosphere models asynchronously coupled to the BIOME1 equilibrium

vegetation model (Prentice et al. 1992). Comparison of these simulations allows to diagnose the relative importance of direct orbital forcing, ocean feedbacks, vegetation feedbacks, and synergies between the ocean and vegetation in explaining observed regional environmental changes in the mid- to high-latitudes of the northern hemisphere during the mid–Holocene (6 ka). The choice of the mid-Holocene is motivated partly because 6 ka has been a major focus for palaeoclimate modelling (Joussaume and Taylor 1995; 2000) and partly because of the existence of a new synthesis of palaeoenvironmental evidence documenting vegetation changes in the mid- to high-latitudes at 6 ka compared to today (Bigelow et al. 2003).

Observed vegetation patterns at 6 ka as shown by these data were compared with the simulations in order to determine the realism of each of the experiments and thus to assess whether the model-based estimates of the magnitude of individual feedbacks are realistic. To facilitate comparison with the palaeoenvironmental data, output from each climate experiment was used to drive an offline equilibrium biogeography model. The most recent version of the BIOME model (BIOME4: Kaplan et al. 2003) was preferred over BIOME1 because it has a better discrimination of high-latitude vegetation types, and because it uses a vegetation classification that is compatible with the classification used by Bigelow et al. (2003).

3.2   Methods to separate and evaluate feedbacks

The coupled ocean-atmosphere model

The atmospheric component of the coupled IPSLCM1 ocean-atmosphere general circulation model (AOGCM) is version 5.3 of the Laboratoire de Météorologie Dynamique (LMD) atmosphere general circulation model (Sadourny and Laval 1984; Masson and Joussaume 1997). The grid resolution is 64 points in longitude, 50 points in the sine of latitude, and 11 vertical sigma levels. The model includes the land-surface scheme SECHIBA (Ducoudré et al. 1993). There are eight vegetation types in

the SECHIBA scheme. The distribution of these vegetation types is prescribed either from observations as in the control run or from the output of vegetation model (i.e. BIOME1). When the climate model is asynchronously coupled to the equilibrium biome model, BIOME1 is used to prescribe the vegetation distribution. Thus, vegetation characteristics modulate the fluxes of momentum, latent and sensible heat, and evaporation between the surface and the atmosphere. SECHIBA computes the appropriate set of land-surface parameters (e.g. seasonally-varying albedo, roughness length, canopy resistance) for each grid cell as a function of vegetation type and vegetation phenology using parameter values formulated explicitly for the 17 vegetation types recognized in BIOME1 to force SECHIBA (Texier et al. 1997).

The oceanic component of the coupled model is the general circulation model OPA developed at the Laboratoire d'Océanographie Dynamique et de Climatologie (LODYC) (Madec et al. 1998). The horizontal resolution is 92 points by 76 points. The horizontal mesh is orthogonal and curvilinear on the sphere. The northern point of convergence is shifted over Asia to overcome the singularity at the North Pole (Madec and Imbard 1996). There are 31 vertical levels, with 10 levels in the upper 100 meters. The turbulent diffusion is isopycnal-diapycnal, with a limitation of the isopycnal slopes to 1 % (Guilyardi et al. 1999). The isopycnal diffusion coefficient is 2000 m^2s^{-1}, with no background horizontal diffusion. Momentum and heat fluxes are computed separately for sea ice and ocean (Braconnot et al. 2000b).

The sea ice model is a diagnostic prescribed sea-ice model (Braconnot et al. 1997), where an ocean grid box is assumed to be frozen when the sea-surface temperature (SST) falls below the freezing point of sea water. The heat fluxes from the ocean to the bottom of the sea ice are prescribed as -2 Wm^{-2} in the Arctic (Maycut and Untersteiner 1971). Once frozen, the sea-surface temperature can only warm by heat advection and diffusion. The surface temperature and albedo of the sea-ice fraction are computed using a one-layer thermodynamic model and making the assumption that sea ice is 3 m thick. The temperature at the bottom of the sea ice is prescribed as 271.2 K. The grid resolution in the ocean is greater than in the atmosphere, so the area covered by sea ice

represents a fraction in an atmospheric grid box. Freshwater fluxes to the ocean are simulated from 46 major rivers. The outflow of these rivers contributes directly to the ocean model grid at the location of the corresponding river mouth.

The equilibrium biogeography models

Models of the BIOME family are equilibrium biogeography models, which simulate the distribution of major vegetation types (biomes) as a function of the seasonal cycle of temperature, precipitation, sunshine and soil moisture conditions. The climate data used to run the model can either be derived from observations or, as here, from the output of climate model simulations.

For diagnostic purposes, BIOME4 was run using an anomaly procedure and not directly from the climate model output as in the BIOME1 simulations. The use of an anomaly procedure facilitates comparison with observations because it reduces the impact of model biases, which are assumed to be similar in both the control run and the experiments (Harrison et al. 1998). In the anomaly procedure, differences in the 20-year climate averages of monthly mean precipitation, temperature and sunshine between each of the 6 ka experiments and the control experiment were linearly interpolated to the 0.5° grid of the BIOME4 model and then added to a modern climatology (CLIMATE 2.1). Soil properties were specified from a data set derived from the FAO global soils (FAO 1995). BIOME4 is calibrated for a modern CO_2 concentration of 324.6 ppm representing the mean value for the interval covered by the CLIMATE 2.1 data set. The CO_2 concentration was left unchanged in these experiments to parallel the situation in the climate experiments. Thus, both the climate experiments and the vegetation response to the simulated climate changes show only the impact of orbital changes.

Control Simulation

The control simulation (0 ka control) was made using the coupled AOGCM with prescribed modern vegetation from climatology (Braconnot et al. 1999), and with modern orbital parameters for 1950 A.D. and vernal equinox fixed on 21st March. The atmospheric CO_2 concentration was set to 345 ppm. A value not equivalent to the actual situation but suggested by CLIMAP (1981) as a near present day value in order with sea surface temperature (SST) prescription and therefore commonly defined for climate model scenarios like PMIP. The simulation was run for 150 years in coupled mode. The atmospheric conditions used to initiate the coupled integration were those of January 1st of the 16th year of a pre-existing atmosphere-only simulation forced with the mean seasonal cycle of SST and sea-ice cover specified from Reynolds (1988). The ocean model was spun up with annual mean forcing of wind stress, heat fluxes, and water fluxes. Stable surface conditions in the upper ocean, with a global means SST of 17.8 °C, were achieved after 20 years of the coupled integration. The length of the simulation is not sufficient to bring the deep ocean to equilibrium, but allows studying changes in the seasonal cycle, which mainly affect the upper ocean. However, the drift at depth is small and similar in all simulations. The Arctic sea-ice cover built during Northern Hemisphere (NH) winter is underestimated by about 13 %, with an area of 11.7 km x 10^6 compared to the 13.5 km x 10^6 reported by (Gloersen and Campbell 1991).

Simulations of the 6 ka climate

To examine the response of the climate system to changes in orbital parameters at 6 ka four experiments from Braconnot et al. (1999) were used (Figure 3-1). The first experiment is a coupled AOGCM simulation (AO 6 ka) in which only the orbital parameters were changed to those of 6 ka (Berger 1978). This simulation was run for 150 years. The second experiment (A 6 ka) was made using the atmospheric component of the model alone. The A 6 ka simulation was then run for 20 years with sea surface temperature (SST) and sea ice cover (SIC) specified daily by the data extracted from years 80 to 100 of the control simulation (AO 0 ka control).

Comparison of this experiment and the AO 6 ka experiment allows assessing the contribution of the oceanic feedback at 6 ka. The third experiment (AOV 6 ka) was a coupled ocean-atmosphere simulation in which vegetation distribution at 6 ka was specified from the last of three iterations from the BIOME1 simulation, started with the 20 years average climate from the year 80 to 100 of the AO 6 ka experiment. This experiment was run for 50 years. The atmospheric CO_2 concentration was set to the same value as in the control simulation (345 ppm) in all of the 6 ka experiments. This prescription is not realistic since the CO_2 level at 6 ka was ca 270 ppm (e.g. Petit et al. 1999) but allows focusing on the response to changes in orbital forcing. The final experiment (AV 6 ka) was made using the atmospheric component of the model alone; in this experiment, vegetation distribution at 6 ka was specified from the BIOME1
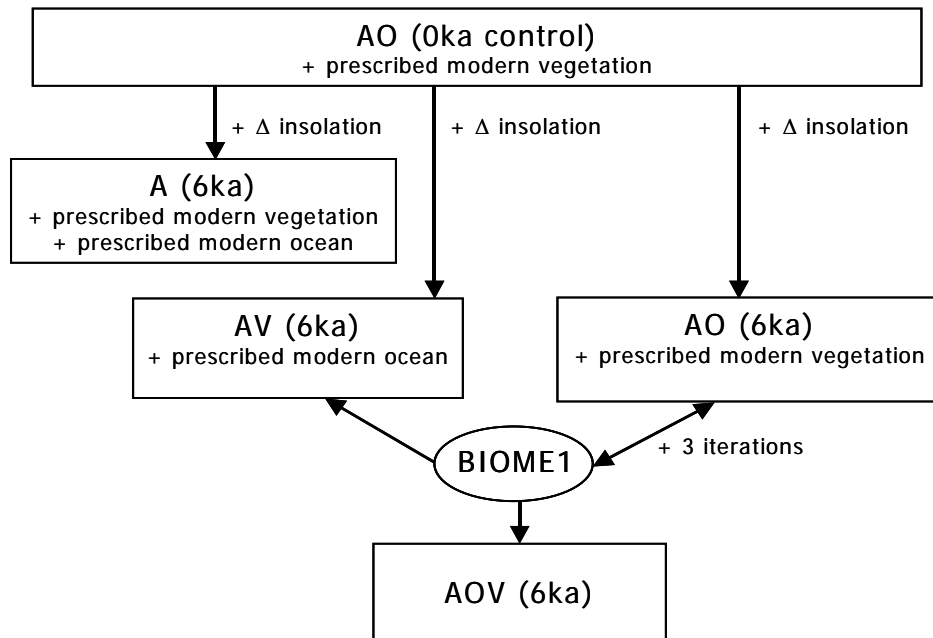
Figure 3-1: Flowchart showing the experimental set-up for the control and 6 ka

simulation used for the AOV 6 ka experiment. Daily SST and SIC were specified from the control simulation, as in the A 6 ka experiment. The AV 6 ka experiment was then run for 20 years. Comparison of this experiment with the A 6 ka experiment allows assessing the contribution of the vegetation feedback at 6 ka as a very preliminary study. As no iterations has been done in this fourth experiment. Since the vegetation in the AV 6 ka experiment, however, is derived from the AO 6 ka experiment, it is

impossible to separate out a pure vegetation feedback signal from these experiments as done by Ganopolski et al. (1998) and Claussen (2001) for the mid-Holocene or Kubatzki and Claussen (1998) for the last glacial maximum (LGM), and by Kubatzki et al. (2000) for the last interglacial interval, using the factor separation technique from Stein and Alpert (1993). Nevertheless, there is a significantly different response in the AV 6 ka experiment that is attributable to vegetation and it seems thus worthwhile to compare these experiments.

Analyses of the simulations were based on 20-year averages. The 20-year averages were derived from years 80 to 100 of the control 0 ka and AO 6 ka experiments, and the last 20 years of the A 6 ka, AV 6 ka and AOV 6 ka experiments. The present results are based on the modern calendar. Use of celestial calendar months might provide a more accurate representation of Holocene climate changes (Kutzbach and Gallimore 1988); (Joussaume and Braconnot 1997) but adoption of this calendar would not affect the conclusions of the analyses.

Analytical protocol for the derivation of the feedback and synergy components of the simulated 6 ka climatic changes

The relative importance of ocean and vegetation feedback and synergy on the seasonal cycle of temperature and precipitation over the continents north of 40 °N was assessed by comparing the simulated mean climate based on the 20-year averages, from each of the 6 ka climate simulations (Berger 2001) as follows:

$$[1] \quad (A6ka - ctr) = \Delta A_f$$

$$[2] \quad (AO6ka - ctr) - (A6ka - ctr) = \Delta O_f$$

$$[3] \quad (AV6ka - ctr) - (A6ka - ctr) = \Delta V_f$$

$$[4] \quad (AOV6ka - ctr) - (A6ka - ctr) - ((AO6ka - ctr) - (A6ka - ctr)) - ((AV6ka - ctr) - (A6ka - ctr)) = \Delta S_f$$

With *ctr* for the modern control run, atmosphere (A), ocean (O), vegetation (V) feedbacks and synergy (S) and the index $_f$ as the sum of all components.

Palaeovegetation data for 6 ka

The Pan–Arctic Initiative (PAIN) has made reconstructions of vegetation patterns at 6 $\pm$0.5 ka across the high northern latitudes (north of 55°N) based on pollen records from individual sites using a standard procedure (Bigelow et al. 2003). This reconstruction represents the most extensive compilation of palaeovegetation data from the high northern latitudes currently available, and has the merit of using a classification scheme that was designed to be compatible with the scheme used in BIOME4. There are 493 sites in the PAIN 6 ka reconstruction. Reconstructions of vegetation patterns to the south of the PAIN window have been made as part of the Palaeovegetation Mapping Project (Biome6000: Prentice and Webb III 1998; Prentice et al. 2000). There are reconstructions from 757 sites between 40 and 55 °N in the Biome6000 data set (Prentice et al. 1996, Tarasov et al. 1998, Edwards et al. 2000, Williams et al. 2000). Altogether there are 1250 sites in the combined data set (Figure 3-6f) but 245 of these sites are not used in the data-model comparisons: 125 of these sites are poorly dated and 147 sites lie along the coast, on islands or in inland lake areas where the BIOME4 model has sea, lakes and/or rivers and does thus not simulate vegetation for comparison. Three sites that, according to the original vegetation reconstruction, were misclassified as tundra (Prentice et al. 2000) have also been omitted from the comparison.

These data are used to evaluate the 6 ka palaeoclimate simulations by visual comparison. A more quantitative evaluation of the simulations is made by counting the number of matches between observed and simulated vegetation for the 0.5° grid cell within which each data point is located. In order to simplify this comparison, a classification into major biomes proposed by Harrison and Prentice (2003) is adopted and summarized in Table 3-1.

3.3   Results of the feedback analyses

The seasonal cycle of air temperature

The atmospheric response (equation *[1]*, p. 29) to orbital forcing produces a warming of the mid- and high-latitude continents of 1.15°C during the summer (June, July, August = JJA) and a cooling during the rest of the year (Figure 3-2; Table 3-1). The cooling is largest during winter (-0.61°C) and spring (-0.66°C). As a result, there is no change in mean annual temperature compared to today.

Ocean feedbacks (equation *[2]*, p. 29) amplify the response to 6 ka orbital forcing in spring (-0.11°C) and summer (0.14°C) and counteract the direct response to orbital

Table 3-1: Summary of seasonal changes in temperature (T, in °C) and precipitation (P, in mm/day) by latitude zones.

Region	Season	A 6ka		AO 6ka		AV 6ka		AOV 6ka	
		T	P	T	P	T	P	T	P
N of 40°N	DJF	-0.61	-0.01	-0.24	0.03	-0.31	-0.01	0.57	0.08
	MAM	-0.66	-0.03	-0.77	-0.02	0.29	-0.01	0.44	0.05
	JJA	1.15	-0.01	1.30	-0.01	1.50	-0.04	2.13	-0.05
	SON	-0.28	-0.01	0.51	0.06	-0.10	-0.02	1.00	0.09
	annual	-0.10	-0.02	0.20	0.02	0.34	-0.02	1.04	0.04
N of 70°N	DJF	0.00	-0.01	0.39	0.02	-0.33	-0.02	0.92	0.06
	MAM	-0.24	-0.01	-0.54	-0.01	0.16	0.02	0.07	0.04
	JJA	0.71	0.02	0.97	0.04	0.79	-0.01	1.29	-0.01
	SON	0.05	0.00	0.89	0.09	0.08	0.00	1.21	0.08
	annual	0.13	0.00	0.43	0.04	0.18	0.00	0.87	0.04
60-70°N	DJF	-0.61	-0.02	-0.41	0.03	-0.46	-0.01	0.24	0.05
	MAM	-0.61	-0.05	-0.92	-0.02	0.52	0.00	0.47	0.07
	JJA	1.24	-0.01	1.25	0.01	1.56	0.03	2.09	0.07
	SON	-0.46	-0.01	0.33	0.09	-0.27	0.02	0.76	0.14
	annual	-0.11	-0.02	0.06	0.03	0.33	0.01	0.89	0.08
50-60°N	DJF	-0.93	-0.02	-0.61	0.01	0.07	-0.02	0.77	0.11
	MAM	-0.92	-0.05	-0.94	-0.02	0.74	-0.01	1.06	0.09
	JJA	1.44	0.00	1.53	0.00	1.97	-0.05	2.83	-0.07
	SON	-0.68	-0.01	0.14	0.04	-0.32	-0.01	0.73	0.11
	annual	-0.27	-0.02	0.03	0.01	0.61	-0.02	1.35	0.06
40-50°N	DJF	-1.12	0.01	-0.49	0.06	-0.53	0.00	0.29	0.14
	MAM	-1.04	0.00	-0.67	-0.03	-0.37	-0.08	0.22	-0.01
	JJA	1.34	-0.05	1.57	-0.11	1.90	-0.16	2.62	-0.23
	SON	0.01	-0.06	0.67	-0.02	0.13	-0.11	1.33	0.01
	annual	-0.20	-0.03	0.27	-0.03	0.28	-0.80	1.11	-0.02

forcing in autumn and winter (Figure 3-3). This response largely reflects the time lag (1-2 months) introduced by the thermal inertia of the oceans (Le Clainche 2000). The warming caused by ocean feedbacks in the autumn is large (+0.79°C), resulting in conditions +0.51°C warmer in the AO 6 ka simulation than in the 0 ka control simulation. The winter warming caused by ocean feedbacks is smaller (+0.37°C): as a result winters remain slightly colder than at present (-0.24°C) in the coupled ocean-atmosphere simulation (although warmer than in the atmosphere-only simulation). As a result of the ocean feedbacks, mean annual temperature over the high northern latitudes is +0.30°C warmer in the AO 6 ka experiment than in the A 6 ka simulation and +0.20°C warmer than in the control.

Vegetation feedback (equation *[3]*, p. 29) results in enhanced warming in all seasons (Figure 3-3) compared to the atmospheric response to orbital forcing. The largest changes due to vegetation feedback occur in spring (+0.95°C), the smallest (+0.17°C) in autumn. This reflects the fact, that changes in vegetation and particularly in the
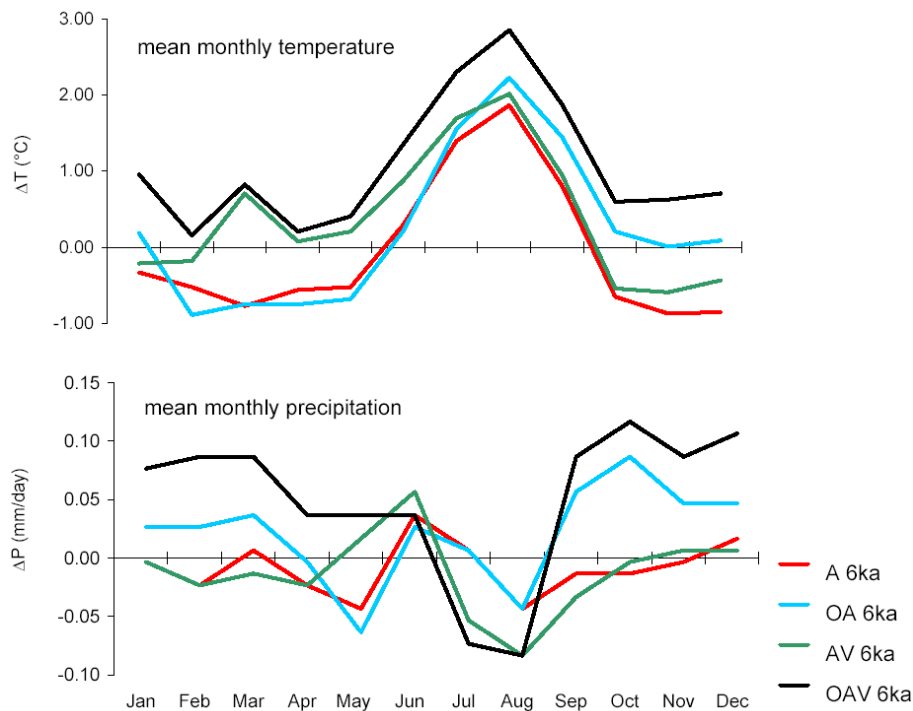
Figure 3-2: Changes in the seasonal cycle of temperature (ΔT, in °C) and precipitation (ΔP, in mm/day) as shown in each of the 6 ka experiments compared to the control AO experiment.

simulated extension of forest cover modify snow albedo and affect the timing of snow melt. As a result of the vegetation-induced enhancement, simulated temperatures in the AV 6 ka experiment are warmer than today in spring and summer (Figure 3-2; Table 3-1). Thus, vegetation feedbacks amplify orbital forcing in summer and offset the orbital-induced cooling in spring, but have little impact during the remaining seasons.

Synergy, according to equation *[4]* (p. 29), computed from the ocean and vegetation feedbacks indicates warming in all seasons (Figure 3-3). The magnitude of the warming caused by this synergy is largest in winter (+0.52°C) and in summer (+0.49°C). Indeed, in these two seasons the warming due to synergy is as large as the warming due to the combination of ocean and vegetation feedbacks when considered separately. The combined effect of ocean and vegetation feedbacks considered independently is to warm winter by 0.66°C and summer by 0.48°C.
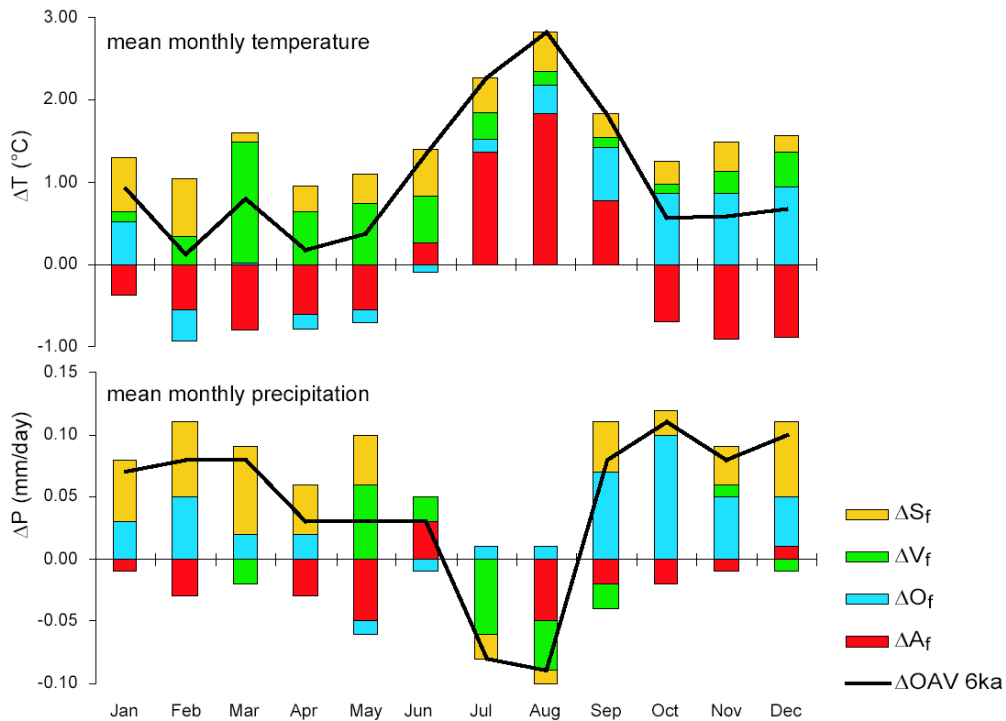
Figure 3-3: The relative contribution of the atmospheric response (ΔA_f), ocean (ΔO_f) and vegetation (ΔV_f) feedbacks, and the synergy (ΔS_f) between these feedbacks, to the changes in the seasonal cycle of temperature (ΔT, in °C) and precipitation (ΔP, in mm/day) at 6 ka as simulated in the AOV experiment (ΔAOV 6ka).

The combined effects of orbital forcing, ocean feedback, vegetation feedback and the synergy between the ocean and vegetation feedbacks produce temperatures ca 0.5°C warmer than present during the winter and spring, ca 2°C warmer than present during summer, and ca 1°C warmer than present during autumn in the AOV 6 ka simulation (Figure 3-2; Table 3-1). The importance of the contribution of the various effects to the overall warming varies from season to season: Summer warming is dominated by the direct response to orbital forcing, spring warming is dominated by the impact of vegetation feedback, autumn warming is dominated by the impact of ocean feedback, and winter warming is dominated by the synergy between the ocean and the vegetation feedbacks (Figure 3-4).

The seasonal cycle of precipitation

The direct response to orbital forcing results in a decrease of precipitation in the mid- and high northern latitudes during all seasons (Figure 3-2; Table 3-1). The largest changes, however, occur in spring (-0.03 mm/day). Ocean feedback leads to increased precipitation in the autumn, winter and spring (Figure 3-3), offsetting the orbital-induced tendency towards aridity (Le Clainche 2000), but has little effect in summer. As a result, mean annual precipitation is higher (0.04 mm/day) in the AO 6 ka simulation than in the A 6 ka simulation. Vegetation feedback increases precipitation
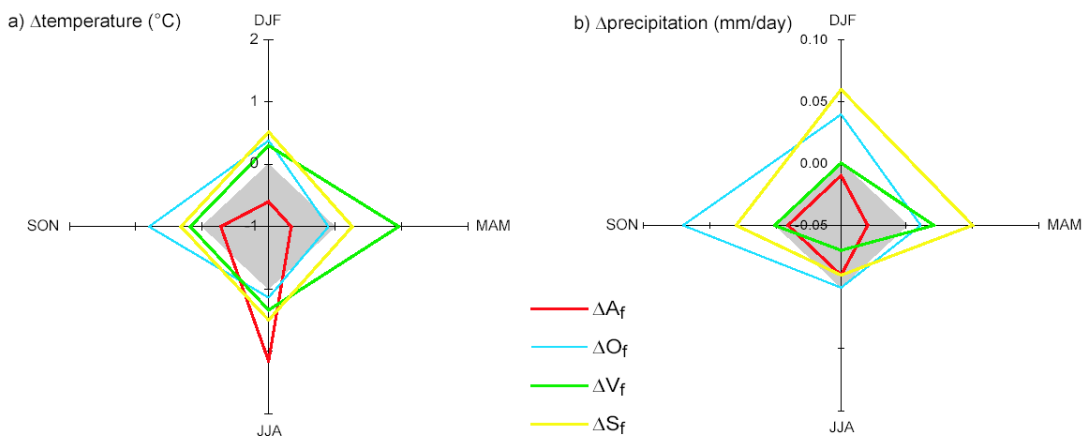
Figure 3-4: Seasonal contribution of the atmospheric response (ΔA_f), ocean feedback (ΔO_f), vegetation feedback (ΔV_f), and the synergy (ΔS_f) between ocean and vegetation feedbacks to **a)** the overall year-round warming (°C) and **b)** the seasonal changes in precipitation (mm/day) shown in the AOV 6 ka experiment. The outer boundary of the grey area represents the simulated seasonal values of temperature and precipitation in the control simulation.

in spring (+0.02 mm/day) and reduces precipitation in summer (-0.03 mm/day) but has no discernible effect on autumn and winter precipitation (Table 3-1). Vegetation feedback thus partially offset orbital-induced drying in spring and augment orbital-induced drying in summer (Figure 3-4b). As a result, mean annual rainfall in the AV 6 ka simulation is -0.02 mm/day less than today but similar to the mean annual rainfall as a result of orbital-forcing alone. The synergy between ocean and vegetation feedbacks has a large positive impact on precipitation in autumn (+0.03 mm/day), winter (+0.06 mm/day) and spring (+0.05 mm/day) and a smaller negative impact on summer precipitation (-0.01 mm/day) (Figure 3-4b). As a result, the seasonal contrast in precipitation is much larger in the AOV 6 ka simulation (Figure 3-2; Table 3-1) than today, with drier summer conditions and more precipitation during the remainder of the year.

Regional temperature and precipitation responses to changes in orbital forcing and feedbacks

The simulated temperature changes in response to orbital forcing, ocean and vegetation feedbacks, and the synergies between these feedbacks are not zonally uniform across the high northern latitudes (Figure 3-5; Table 3-1). The strength of the orbital-induced winter cooling is maximal in the mid–latitudes (40–50°N). The winter warming caused by vegetation feedback is also large in this latitude band (+0.59°C) although maximal (+0.99) between 50–60°N. Winter warming as a result of ocean feedback is relatively large (+0.39°C) along the Arctic coast (N of 70°N) but even larger (+0.63°C) between 40–50°N. The impact of the synergy between ocean and vegetation feedbacks on winter warming is largest in the far north. As a result, the latitudinal pattern of winter warming in the AOV 6 ka simulation has two maxima (Figure 3-5), with a warming of +0.92°C occurring in the high northern latitudes along the Arctic coast and a secondary maximum between 50–60°N (+0.77°C).

The situation in summer is simpler (Figure 3-5; Table 3-1). Direct orbital forcing, vegetation feedback, and the synergistic effects of ocean and vegetation feedbacks all

produce maximum warming in the latitude band between 50–60 °N. The contribution of the ocean to summer warming is small (+0.27°C), but intensified at high northern latitudes. As a result, the maximum summer warming in the AOV 6 ka experiment (+2.83°C) occurs between 50–60°N.

The simulated precipitation changes in response to orbital forcing, ocean and vegetation feedbacks, and the synergies between these feedbacks are also not zonally uniform (Figure 3-5; Table 3-1). Precipitation changes in response to orbital forcing alone (A 6 ka) are negligible in the far north. However, precipitation is decreased further south compared to present. Between 50–70°N, the overall decrease in mean annual precipitation (-0.02 mm/day) results from changes during winter and spring while in the temperate zone (40–50°N) the overall decrease (-0.03 mm/day) occurs largely as a result of decreased rainfall during the summer and autumn. Ocean
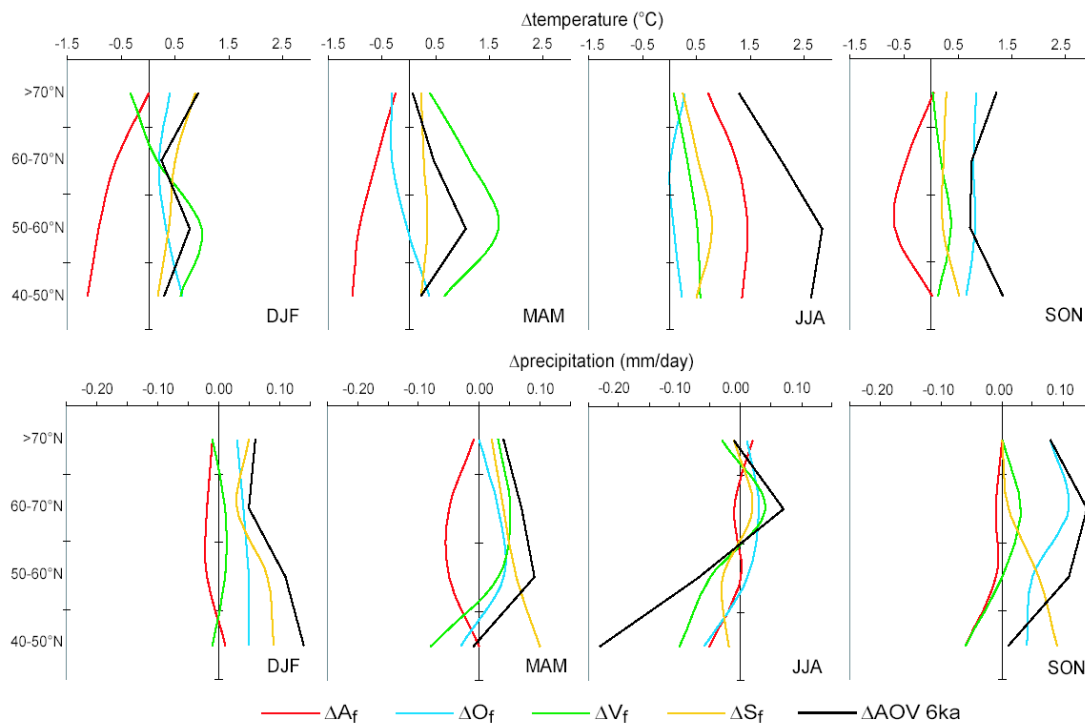
Figure 3-5: The relative contribution of the atmospheric response (ΔA_f), ocean (ΔO_f) and vegetation (ΔV_f) feedbacks, and the synergy (ΔS_f) between these feedbacks, to the changes in the seasonal cycle of temperature (°C) and precipitation (mm/day) at 6 ka as simulated in the AOV experiment for different latitudinal bands. The change in the AOV 6 ka experiment (black line) compared to the modern control is shown for comparison.

feedback enhances precipitation everywhere north of 50°N and in most seasons, with the largest changes in autumn. However, although the ocean feedback enhances autumn and winter rainfall in the temperate zone, this tendency is offset by decreased rainfall during the spring and summer. Thus, the impact of the ocean feedback is to create wetter conditions over most of the region while amplifying spring and summer drought (MAM: -0.03 mm/day, JJA: -0.06 mm/day) in the temperate zone (40–50°N).

The impacts of vegetation feedback on precipitation are spatially strongly differentiated (Figure 3-5). In the far north, vegetation feedback enhances precipitation in spring (+0.03 mm/day) but decreases precipitation in summer (-0.02 mm/day); as a result, there is little change in annual mean precipitation. Between 60–70°N, vegetation feedback enhances precipitation in all seasons leading to an increase in mean annual precipitation (+0.03 mm/day). To the south (50–60°N), seasonal changes in precipitation as a consequence of vegetation feedback offset each other and there is no overall change of mean annual precipitation.

The largest changes resulting from vegetation feedback occur in the temperate zone where precipitation is decreased in all seasons, specifically during the spring (-0.07 mm/day), summer (-0.10 mm/day) and autumn (-0.06 mm/day). These changes are caused by the large extent of grassland simulated in response to the pronounced spring and summer drought in the AO 6 ka experiment and used as input in the AV 6 ka experiment.

Synergy between ocean and vegetation has a positive impact on precipitation at all latitudes in autumn, winter and spring. However, in the summer months, this synergy tends to produce a small reduction in precipitation across most latitude bands.

Despite the apparent complexity of the changes in precipitation in response to individual components, the overall result of orbital forcing, ocean and vegetation feedbacks, and the synergy between these feedbacks (as shown in the AOV 6 ka simulation), is relatively straightforward (Figure 3-5; Table 3-1). Autumn and winter precipitation are increased at all latitudes, spring precipitation is also increased except

in the extreme south, summer precipitation is increased between 60–70°N but is decreased elsewhere and substantially decreased south of 60°N.

Changes in vegetation patterns in response to the simulated climate changes

The changes in vegetation patterns in response to simulated climate changes were derived using the BIOME4 model with the anomaly procedure described above. So for each of the 6 ka experiments a BIOME4 vegetation map is calculated for comparison.

There are large virtual changes in vegetation distribution in response to the orbital-induced changes in climate simulated by the atmosphere-only model (Table 3-2). About 30 % of the area north of the 40 °N has a different vegetation type compared to the modern situation.

The changes affect three major aspects of northern–hemisphere vegetation patterns: the

Table 3-2: Areas of major biomes (in 10^6 km^2) in the modern BIOME4 simulation and as a result of each of the 6 ka experiments.

	Modern	A 6ka	AO 6ka	AV 6ka	AOV 6ka
Key individual biomes					
Cold evergreen needleleaf forest	13.39	12.59	12.56	11.04	10.02
Cold deciduous forest	4.00	4.75	4.13	4.23	3.39
Temperate deciduous broadleaf forest	2.40	3.15	2.96	3.04	3.46
Temperate grassland	3.14	6.01	6.43	9.39	11.25
Major biomes					
Warm–temperate forest	12.12	10.64	10.65	9.61	10.03
Temperate forest	0.25	0.21	0.21	0.23	0.23
Boreal forest	17.39	17.33	16.69	15.28	13.41
Savanna and dry woodland	0.75	0.76	0.86	0.68	0.93
Grassland and dry shrubland	5.21	8.43	8.91	12.20	14.21
Desert	1.70	1.63	1.61	1.63	1.53
Dry tundra	0.23	0.22	0.18	0.15	0.13
Tundra	6.77	5.19	5.31	4.63	3.95
Summary					
All tundra	7.00	5.41	5.49	4.79	4.07
All forest	29.76	28.18	27.55	25.12	23.67

location of the tundra-forest boundary, the northern limits of temperate and cool forests, and the extent of grassland and shrubland in the interior of the continents. These features of the northern-hemisphere vegetation distribution are governed by different aspects of climate within the model. The limit between tundra and forest is controlled by accumulated temperatures during the growing season, the northern limits of temperate and cool forests by minimum temperature in winter, and the extent of grassland versus forest by growing-season aridity (Woodward 1987; Prentice et al. 1992; Kaplan et al. 2003).

In response to orbital forcing, the tundra-forest boundary is shifted northward across much of the Arctic and the overall area of tundra is reduced by 22.7 % compared to modern. This change is a result of the simulated summer warming and longer growing season in the A 6 ka experiment. The northward shift is most pronounced in eastern and central Siberia, and in central and eastern Canada, where the high-latitude summer warming is greatest. There is no discernible change in the tundra-forest boundary in Beringia, because the high-latitude summer warming is negligible there.

The northern limits of temperate and cool forests are further north than today, particularly in Europe and western Siberia and in eastern North America. The regions affected lie in the zone of maximum winter warming between ca 50–60°N (Figure 3-5). The impact on Europe and western Siberia is larger than elsewhere because warm-air advection from the Atlantic produces a large increase in winter temperature across this region.

The largest vegetation changes shown in the A 6 ka simulation are associated with expansion of grassland vegetation increase by 91.6 % compared to today in the interior of Eurasia. According to these simulations, grassland replaced temperate and boreal forest in much of central and northern China, across central Asia and in the region north of the Caspian and Aral Seas. The expansion of grassland reflects the reduction in precipitation during spring, summer and autumn in the mid-latitudes, and particularly in the Asian sector where mean annual precipitation is reduced by 0.04 mm/day.

There are only small changes in vegetation distribution as a result of ocean contribution: only 12 % of the area north of the 40 °N has a different vegetation type in

the AO 6 ka simulation from the A 6 ka simulation. There is little discernible change in the position of the tundra–forest boundary, except in the central part of eastern Beringia where the area of tundra was slightly larger than it is today because ocean feedback produces a cooling (-0.49 °C) in this region. The comparatively small changes in the tundra-forest boundary reflect the fact that the major impact of ocean feedback in the high northern latitudes occurs during winter; the simulated cooling in spring and warming in summer are small and do not substantially affect the length of the growing season. The impact of the ocean on the northern limits of temperate forest is spatially heterogeneous: in eastern North America, the simulated winter warming results in a more northerly position of the northern limit of temperate deciduous broadleaf forest than today. In contrast, the northern limit of temperate deciduous broadleaf forest is further south than today in Europe as a consequence of the expansion of cool mixed forest. Changes in the extent of cold deciduous forest also reflect changes in winter temperature: the extend of cold deciduous forest is reduced in eastern Siberia because of the simulated warmer winters, while in Beringia, where simulated winters are considerably colder than today, the cold deciduous forest is more extensive in the AO 6 ka experiment. In the mid–continent, and particularly in the Asian sector, there is a further expansion of grassland in the AO 6 ka experiment (increase by 105 % compared to modern) compared to the A 6 ka experiment. This expansion reflects the fact that ocean feedback amplifies summer drought in the temperate zone (40–50°N).

Vegetation has a much larger impact on simulated vegetation patterns in the mid- and high Northern Hemisphere than the ocean. Over 43 % of the area north of 40 °N has a different vegetation type compared to the modern situation and ca 25 % of the area is different from the A 6 ka simulation. The tundra-forest boundary is further north than today in central Siberia and in Europe in the AV 6 ka simulation. However, there is no significant difference in the position of this limit compared to the A 6 ka simulation. This reflects the fact that vegetation feedback has no impact on summer and autumn temperatures at high northern latitudes (Figure 3-5). The simulated northern limits of temperate and cool forests, particularly in the European sector, are further north than they are today, and also further north than they would be in response to orbital forcing

alone. This situation illustrates that the impact of vegetation feedback on winter temperature is maximal between 50–60°N. However, the most noticeable impact of vegetation contribution is on the extent of grassland. Grasslands cover an area of $9.3*10^6$ km^2 in the AV 6 ka simulation, an increase by 199 % compared modern (Table 3-2), extending north of 60°N in central Asia and in central North America. The expansion of grassland vegetation in eastern North America creates a disjunction between the temperate and boreal forests in the AV 6 ka simulation. This expansion results form the strong decrease in summer precipitation south of 60°N as a consequence of vegetation feedback, which is further amplified in the temperate zone (40–50°N) by decreases in spring and autumn precipitation.

Vegetation changes occur over 52 % of the area north of 40 °N in response to the climate changes simulated in the AOV 6 ka simulation. Most of the additional change (compared to the AV 6 ka simulation) is due to a further expansion of grassland which increases by 258 % compared to modern. This expansion reflects the synergy between ocean and vegetation feedbacks, which suppresses precipitation in the region south of ca 60 °N and particularly in the Asian sector. The northern limit of the temperate deciduous broadleaf forest in Europe is at its most northerly position in all the simulations, reflecting the additive effect of orbital forcing, ocean and vegetation feedbacks, and the synergy between them on winter temperatures in Europe between 50–60 °N.

temperate deciduous broadleaf forest
temperate evergreen needleleaf forest
warm-temp. evergreen broadleaf & mixed forest
cool mixed forest
cool evergreen needleleaf forest
cool-temp. evergr. needleleaf & mixed forest
cold evergreen needleleaf forest
cold deciduous forest
temperate xerophytic shrubland
temperate sclerophyll woodland and shrubland
temperate deciduous broadleaf savanna

temperate evergreen needleleaf open woodland
temperate grassland
desert
graminoid and forb tundra
low and high shrub tundra
erect dwarf-shrub tundra
prostrate dwarf-shrub tundra
cushion-forb tundra
barren
ice

Figure 3-6: Vegetation patterns simulated by BIOME4 under **a)** modern climate conditions and as a response to changes in 6 ka climate by **b)** orbital forcing only (A 6 ka), **c)** orbital forcing and ocean feedbacks (AO 6 ka), **d)** orbital forcing and vegetation feedbacks (AV 6 ka) and **e)** orbital forcing, ocean and vegetation feedbacks and their synergy (AOV 6 ka). The simulated vegetation patterns can be directly compared with **f)** reconstructed vegetation data from Biome6000/PAIN.

Comparison of observed and simulated vegetation patterns at 6 ka

Palaeoenvironmetal reconstructions show that the tundra-forest boundary was north of its present position in some regions at 6 ka but the pattern of this shift was strongly asymmetrical around the pole, with the largest northward shift in central Siberia (ca 200 km), a smaller northward shift in Fennoscandia, little change in Beringia and a southward shift of ca 200 km in Keewatin and Labrador (Figure 3-6 and Bigelow et al. 2003). More extensive geographic changes are seen in the boundaries among forest types south of the Arctic tree line, including a northward displacement of temperate deciduous forest in eastern North America and especially in western Europe, and a more restricted distribution of cold evergreen needle-leaved forest towards the western edges of the continents (western Europe and eastern Beringia). Expansion of drought-tolerant vegetation, including temperate grasslands and xerophytic shrublands occurred in North America (Harrison et al. 2003). However, the pollen-based reconstructions of 6 ka vegetation show no expansion of drought-tolerant biomes in the continental interior of Eurasia (Figure 3-6 and Tarasov et al. 1998). This finding is consistent with independent evidence based on geomorphic and biostratigraphic records of changes in lake status that show little or no change in the regional water balance of central Eurasia between the mid-Holocene and present (Harrison et al. 1996).

The position of the tundra-forest boundary is relatively well placed in all of the 6 ka simulations (Figure 3-6). About 75 % of the sites north of 70°N are correctly predicted in the A 6 ka simulation. Vegetation feedback has no discernable impact on summer temperature at high latitudes. The incorporation of ocean feedback, which produces a slight summer warming at high northern latitudes, improves the simulation of high-latitude biomes. In both the AO 6 ka and AOV 6 ka simulations, 81 % of the sites north of 70°N are correctly predicted (Table 3-3).

The simulated occurrence of temperate and cool-temperate forests north of their present position at 6 ka, particularly in Europe, is supported by the data. Vegetation feedback appears to play an important role in the correct simulation of these boundaries: the position of both the temperate deciduous broadleaf forest and the cool mixed forest in Europe is more accurately determined by the AV 6 ka and AOV 6 ka simulations than by the A 6 ka simulation, while the southward displacement and

fragmentation of the temperate deciduous broadleaf forest shown in the AO 6 ka simulation is unrealistic.

The simulation of expanded grasslands in the mid-latitudes of Asia in response to 6 ka orbital forcing is not supported by the data, nor is the massive expansion of these grasslands caused by ocean and vegetation feedbacks and the synergy between them. Only 53 % of the 114 sites between 40–60°N in the Asian sector are correctly predicted in the A 6 ka simulation, and this number is reduced to 37 % in the AV 6 ka, and 36 % in the AOV 6 ka simulations. The simulation of expanded grasslands in mid–continental North America in response to orbital forcing is credible (Harrison et al. 2003). However, the expansion of grassland in eastern North America in the region north of the temperate forests, shown in both the AV 6 ka and the AOV 6 ka simulations, is unrealistic (Williams et al. 2000). As a result, the agreement between observed and simulated vegetation between 40–50 °N in eastern North America is reduced from 85 % in the A 6 ka simulation to 68 % in the AOV 6 ka simulation.

3.4   Discussion

Table 3-3: Comparison between observed and simulated 6 ka distributions of major biomes in %. The number of observed points used in each comparison is indicated. When there are several observed sites in a single model grid cell, all of the sites are compared independently with the simulated vegetation pattern.

Area used for comparison	A 6ka	AO 6ka	AV 6ka	AOV 6ka	No. of sites
all land N of 40°N	70.0	69.1	62.1	61.9	1005
N of 70°N	75.0	81.3	75.0	81.3	16
60–70°N	61.4	61.0	57.7	59.3	241
50–60°N	76.1	75.7	70.3	64.5	259
40–50°N	71.0	69.1	59.5	61.1	489

The mean annual, seasonal and all individual months in the AOV 6 ka experiment are warmer than today. Temperatures are at least +2.1 °C warmer in summer, and +0.6 °C warmer in winter. Winter minimum temperatures increase more than the maximum temperatures. Mean annual precipitation is increased, mainly due to large increases in winter (+0.08 mm/day). These changes are a direct response to orbital changes in the mid-Holocene, and of ocean and vegetation feedbacks. The atmosphere response to insolation changes leads to warming in summer and cooling and drying in other seasons. The ocean feedback counteracts the orbital-induced cooling and drying in autumn and winter. Vegetation feedback induces significant warming in spring and enhances summer drought. Synergies between ocean and vegetation feedbacks increase temperature all through the year, though the impact is largest in winter, and increases precipitation mainly in winter and spring. As a result of these changes in climate, the simulated vegetation cover over more than 50 % of the land area north of 40 °N is different from today.

According to the simulations, the atmospheric response to orbital forcing is the most important source for summer warming in the northern latitudes. The combined impact of the feedbacks, however, causes an additional warming equivalent to ca. 85 % of the atmospheric response (Table 3-4). Ocean feedback by itself is less important, contributing only 14 % of the additional warming due to feedback. Vegetation feedbacks, and the synergy between vegetation and ocean feedbacks, are responsible for 35 % and 51 % of the additional warming, respectively. The combination of feedbacks and synergy effectively reverse the orbital-forced winter cooling in these simulations into a 6 ka winter warming. Ocean feedback appears to play a more important role in winter warming than the vegetation feedback, although again the synergy between these feedbacks is more important than either alone.

According to the simulations, vegetation feedbacks considerably amplify the orbital-induced reduction in summer precipitation. The magnitude of this effect is more than three times the initial atmospheric response (Table 3-4). Although ocean feedback alone appears to have no impact on summer precipitation, the synergy between ocean

and vegetation feedbacks causes a reduction in precipitation of the same order of magnitude as the atmospheric response. Comparison with palaeovegetation data suggests that the strength of the vegetation feedback is unrealistic: there is no evidence for massive aridity in mid-continental Eurasia as shown in the IPSL-BIOME simulations. Vegetation feedback plays no role in the simulated increase in winter precipitation, which is overwhelmingly driven by ocean feedback.

Table 3-4: Comparison of changes (temperature in °C; precipitation in mm/d) due to orbital forcing, ocean and vegetation feedbacks and the synergy between them, as simulated by the IPSL AOGCM asynchronously coupled to BIOME1 and by the CLIMBER model, for the land area N of 40°N. Results from the CLIMBER model are derived from the simulations made by Ganopolski et al. (1998).

	IPSL–BIOME		CLIMBER	
	NH_{land} (N of 40°N)		NH_{land} (N of 40°N)	
	Temperature	Temperature	Temperature	Temperature
	Summer (JJA)	Winter (DJF)	Summer (JJA)	Winter (DJF)
A	1.2	-0.6	2.1	-0.6
AO	1.3	-0.2	1.6	-0.3
AV	1.5	-0.3	2.7	-0.5
AOV	2.1	0.6	3.2	0.8
O feedback	0.1	0.4	-0.5	0.3
V feedback	0.4	0.3	0.6	0.1
S (synergy)	0.5	0.5	0.9	1.0
	Precipitation	Precipitation	Precipitation	Precipitation
	Summer (JJA)	Winter (DJF)	Summer (JJA)	Winter (DJF)
A	-0.01	-0.01	0.18	-0.04
AO	-0.01	0.03	0.15	-0.03
AV	-0.04	-0.01	0.29	-0.03
AOV	-0.05	0.08	0.33	0.03
O feedback	0	0.04	-0.03	0.01
V feedback	-0.03	0	0.11	0.01
S (synergy)	-0.01	0.06	0.07	0.05

Note: Differences in the model setup and experimental design mean that the two simulations are not strictly comparable. CLIMBER is a fully coupled AOV model of intermediate complexity. The IPSL-BIOME results are obtained with asynchronously coupling, and the A and AV simulations incorporate ocean effects (unlike CLIMBER). The CLIMBER simulations are run with $[CO_2]$ at 280 ppm, whereas the IPSL-BIOME simulations were run with $[CO_2]$ at 345 ppm.

The role of ocean and vegetation feedbacks on Arctic climate has also been investigated by Ganopolski et al. (1998) using a series of experiments with the CLIMBER model. The two models are very different in structure: CLIMBER is a climate system model of intermediate complexity (EMIC) with a 2.5-dimensional dynamic statistical atmosphere model, whereas the IPSL model is an ocean-atmosphere-general-circulation-model. However, the vegetation in CLIMBER is dynamically integrated with the other components, whereas in the IPSL experiments an asynchronous coupling between the vegetation and the AOGCM was employed. Furthermore differences in the boundary conditions of the two simulations compound a precisely comparison: Ganopolski et al. (1998) used a pre-industrial CO_2 level (280 ppm) in their experiments whereas a quasi-modern CO_2 level (345 ppm) was set in the IPSL simulations. Nevertheless, comparison of the results from the two series of experiments yields some first insights.

The CLIMBER simulation, in agreement with the results from the IPSL simulations, shows that ocean and vegetation feedbacks modify the orbital-induced pattern of summer warming and winter cooling (compared to present) and results in a warming around the year in the high-latitudes. The magnitude of the warming is larger in the CLIMBER experiment, although the relative magnitude of the summer (+3.2 °C) and winter (+0.8 °C) warming is comparable to the summer/winter warming obtained in the IPSL AOV 6 ka simulation (+2.1 °C in summer and +0.6 °C in winter). However, in the CLIMBER simulation ocean feedback appears to have a negative impact on summer temperature and the positive impact of vegetation feedback is almost double that shown in the IPSL simulations (Table 3-4). The impact of the ocean feedback on winter warming in the CLIMBER simulations is of a comparable magnitude to its impact in the IPSL simulations. Vegetation feedback appears to be a less important cause of winter warming in the CLIMBER simulation than in the IPSL simulations. Vegetation feedback has a smaller impact on winter temperatures than ocean feedback in both models, but the magnitude of the vegetation feedback is smaller in the CLIMBER (0.1°C) than in the IPSL model (0.3°C).

The CLIMBER simulation shows an increase in summer precipitation in the high northern latitudes in response to orbital forcing (Table 3-4). This increase is reduced somewhat by ocean feedback, but amplified by vegetation feedback and synergy between the vegetation and ocean feedbacks. The simulated changes are thus completely different from those obtained with IPSL-BIOME1, which shows summer drying resulting from the atmospheric response to orbital forcing and further amplified by vegetation feedback and synergy. The increased precipitation in the CLIMBER simulations is concentrated in the mid- to high-latitudes of Eurasia (see Figure 2C and 2D in Ganopolski et al. 1998), and appears to be associated with the simulated expansion of the Afro–Asian monsoon.

Both sets of experiments show an increase in high latitude winter precipitation, although the increase is larger in the IPSL-BIOME simulation (Table 3-4). The simulations disagree about the cause of this increase. In the IPSL-BIOME simulations, the increase in rainfall is driven by ocean feedback and ocean-vegetation synergy. Vegetation feedback has no impact on winter precipitation. In the CLIMBER simulations, both ocean and vegetation feedbacks have a small impact on winter precipitation, but the positive anomaly reflects the synergy between ocean and vegetation feedbacks.

3.5   Re-assessment of BIOME4 model

With respect to the results of the quantification of the BIOME4 model from Chapter 2.3 the results shown in Chapter 3 need to be re-assessed. The limited spatial quality of the BIOME4 model in the modern standard diagnostic mode has to be considered in some aspects. This affects the prediction of the vegetation distribution in mid-continental Eurasia.

An overestimation of temperate and boreal forest biomes distinguished to xerophytic grassland due to an assumed soil water bias in the BIOME4 model underlies the poor reputation of simulation compared to observations in this region. However, this failing is restricted to a region along the 50th northern latitude between 60 °E and 120 °E. Hence, those analytic errors are located prevalent further south of the discussed area with the massive aridity signal – as this is occurring north of the 60th latitude, reaching Central-Siberia (Figure 3-6).

Nevertheless, the given weak results for the agreement between simulations and palaeopollen data in Chapter 3.3 of 53 % for A 6ka, 37 % for AV 6ka and 36 % for AOV 6ka in the Asian sector between 100–140°E and 40–60°N have to be correlated with the critical match of 35 % in Central Eurasia (60–120°E and 40–60°N) for the modern 0ka basic BIOME4 simulation compared to the modern pollen map. Both conspicuous regions are not congruent but overlap in the area between 100 °E and 120 °E. While the mid-Holocene simulated drying signal is heading northward, the differences in the modern BIOME4 simulation is situated in more geomorphologic structured regions. But the fact that the BIOME model overestimates forests against grass in this particular region keeps a potentially reinforcing of the xerophytic vegetation distribution.

In both cases the reconstruction by pollen observation tends to be more realistic, as they are confirmed by modern vegetation maps and palaeo data like sea-water level. However, the number of palaeobotanic observations in Kazakhstan, Siberia and Mongolia is few and only patchy dispensed.

In principal, the basic approach to compare vegetation reconstructions of simulated with observed biome types is a promising method to evaluate climate models, except for this spatial region the appraisal has to be seen under reserve.

4.   Evaluation of GCMs with vegetation reconstruction

4.1 Introduction

In the year 2000 the Palaeoclimate Modelling Intercomparison Project (PMIP: Joussaume and Taylor 2000 and PMIP2: Harrison et al. 2002) as an initiative of the World Climate Research Programme (WCRP; JSC/CLIVAR working group on Coupled Models) and the International Geosphere and Biosphere Programme (IGBP; PAGES) was carried out. In order to drive the equilibrium global vegetation model BIOME4 the output of seven simulations from six different atmosphere-ocean general circulation models (AOGCMs) collaborated in PMIP are used.

In a first phase (Chapter 4.3) the response of the coupled ocean-atmosphere system to mid-Holocene (6 ka) orbital forcing is evaluated. The major goals of PMIP are to determine the ability of models to reproduce climate states that are different from those of today and to increase the understanding of large-scale features of simulated climate with respect to future predictions of climate changes. This evaluation compares the simulations from the models NCAR-CSM1.2 (Otto-Bliesner 1999), ECBILT (Weber 2001; Weber and Oerlemans 2003), HADCM2 (Hewitt and Mitchell 1998), ECHAM3 (Voss and Mikolajewicz 2001), IPSL-CM1 (Braconnot et al. 1999, 2000a) and MRI-CGCM1 (Kitoh and Murakami 2002). Apart from different boundary conditions other discrepancies impede a simplified comparison. The CSM model has run a second simulation, which differs with respect to the specification of the atmospheric CO_2 concentration, likewise the ECHAM3 simulation. The IPSL-CM1 simulation is the same simulation analysed in Chapter 3 of this study although the simulation has been run for a longer time period. The results are published by Wohlfahrt et al. (2008).

In a second phase (Chapter 4.4) comparable simulations with an improved atmosphere-ocean model (ECHAM5-MPIOM: Schurgers et al. 2007) out of the first phase

(ECHAM3), additionally coupled to a dynamic global vegetation model, were utilized to assess the developments by vegetation reconstruction with the BIOME4 model.

Once the different responses of different AOGCMs to mid-Holocene conditions have been determined (Chapter 4.3) and the feedbacks of dynamic vegetation have been isolated (Chapter 3.3), the results from the coupled AOVGCM can be analysed (Chapter 4.4). The validation is completed with a variability test of BIOME4 simulated vegetation distribution for the modern control run.

The simulated vegetation response integrates several aspects of climate, including changes in the seasonal cycles of temperature and moisture balance, and thus provides a relatively simple diagnostic of simulated climate changes. This approach also facilitates a comparison with palaeovegetation data. Here, as in Chapter 3, the simulated vegetation patterns north of 40 °N are compared with pollen-based vegetation reconstructions derived by combining the PAIN and Biome6000 data sets.

4.2 Methods

4.2.1   Climate model simulations

Evaluation of GCMs climate effects on vegetation changes (phase I)

The ECHAM3/LSG model was run in periodic synchronous coupling mode; this scheme consists of alternating synchronous (15 months) and ocean-only integrations (48 months) and was used to reduce computer time (Voss and Mikolajewicz 2001). All other models were run in fully coupled (i.e. synchronous) mode throughout the simulations. All the model groups adopted the definitions for modern and 6 ka insolation due to changes in the earth's orbit (Berger 1978) as proposed in PMIP. Atmospheric CO_2 concentration $[CO_2]$ at 6 ka was lower than today and marginally lower than in pre-industrial times (Raynaud et al. 1993). For this analysis it is assumed that the impact of changes in $[CO_2]$ on models with prescribed ocean conditions is

negligible (Hewitt and Mitchell 1998). Five out of the seven AOGCM simulations examined here adopted the same $[CO_2]$ for the control and 6 ka experiments (Table 4-1). Three of those used a value of 345 ppm $[CO_2]$ for both experiments. The HADCM2 simulation used a slightly lower level for both experiments. Two simulations reduced the CO_2 concentration from control value of 355 ppm (CSM1.2Δ) respectively 345 ppm to a 6 ka value of 280 ppm.

The impacts of differences in the specification of $[CO_2]$ between the various simulations are likely to be small compared to the impact of differences in model formulation (Table 4-2). However, there are considerable differences between the models in the treatment of model sub-components known to be important for high-latitude climates (Table 4-2). Changes in the extent of Arctic sea-ice, for example, have large impacts on the regional climates of the northern Extratropics (Kutzbach and Guetter 1986; Mitchell et al. 1988; Kutzbach et al. 1993), and differences in sea-ice parameterisation result in large differences in sea-ice extent in response to a given forcing (Hewitt et al. 2001; Vavrus and Harrison 2003). Most of the coupled models analysed here use a simple thermodynamic treatment of sea-ice based on the formulation by Semtner (1976) (Table 4-2). However, they differ in the number of ice layers. Furthermore, the CSM1.2, HADCM2 and MRI models also incorporate an explicit treatment of leads (channels) in the ice and some aspects of ice dynamics through allowing advection by ocean currents. Northern high-latitude climates are also known to be affected by changes in the amount of snow and the nature of the vegetation cover (Bonan et al. 1992; Douville and Royer 1996; Levis et al. 2000; Brovkin et al. 2003). Again, the models analysed here have land-surface schemes of varying complexity. Thus, the treatment of soil moisture ranges from simple single-bucket schemes (e.g. ECBILT) to multi-layer soils with separate calculation of moisture balance and soil temperature (e.g. CSM1.2, HADCM2, ECHAM3). Some of the models do not allow vegetation cover to modulate water- and energy-fluxes at the land surface (ECBILT, MRI) whereas the more complex land-surface schemes (e.g. LSM 1.0: Bonan 1998; SECHIBA: Ducoudré et al. 1993) distinguish multiple

Table 4-1: The experimental design and boundary conditions used by each of the AOGCMs for the control and 6ka climate simulations. The PMIP insolation for 6 ka is described by Berger (1978).

Model code	Spin-up		Simulation length (yr)	Averaging period (yr)	Insolation	[CO_2]	
	Control	6 ka	0 ka ; 6 ka	0 ka ; 6 ka		Control	6 ka
CSM1.2	0 accelerated	From control yr 275	400 ; 50	50 ; 50	PMIP	280	280
CSM1.2Δ	0 accelerated	From control yr 275	400 ; 50	50 ; 50	PMIP	355	280
ECBILT	coupled 3000 yrs	500 yrs	500 ; 500	50 ; 50	PMIP	345	345
HADCM2	510 yrs	60 yrs	210 ; 210	130 ; 150	PMIP	323	323
ECHAM	700 yrs	700 yrs	1000 ; 1000	300 ; 300	PMIP	345	280
IPSL-CM1	initial state: yr 10 surface restoring to climatological SSTs; 40 yr spin-up	Started from yr 20 of post-spin-up control; 40 yr spin-up	150 ; 150	70 ; 70	PMIP	345	345
MRI CGCM1	0 accelerated	50 yrs accelerated	210 ; 210	50 ; 60	PMIP	345	345

vegetation types. All of the models have a prognostic snow module, but again vary in how snow cover is estimated.

The models also have different spatial resolutions (Table 4-2), ranging from the relatively low-resolution ECBILT model (64 x 32 grid cells for both the atmosphere and the ocean) to the higher-resolution HADCM2 (96 x 73 grid cells for both atmosphere and ocean). Some of the models (CSM, IPSL, ECHAM and MRI) have higher resolution in the ocean than in the atmosphere. Differences in spatial resolution could be important in determining how well individual models resolve e.g. westerly storm tracks (Kageyama et al. 1999).

Table 4-2: Description of aspects of the coupled AOGCMs, including parameterisation of sea ice and land surface, relevant to the simulation of high-latitude climates

Model code	Model components	Resolution Atmosphere	Resolution Ocean	Air/sea flux correction	Sea-ice	Land-surface	Reference
NCAR CSM1.2	CCM3/LSM/ NCOM1.4	96 x 48 T31 18 levels	102 x 116 (3.6° x 1.8°) 25 levels	none	thermodynamic three-layer model, dynamics using cavitating-fluid ice rheology (Weatherly et al. 1998)	vegetation modulates surface fluxes based on LSM, six-layer soil model for temp. and moisture (Bonan 1998)	Otto-Bliesner 1999
NCAR CSM1.2Δ	CCM3/LSM/ NCOM1.4	96 x 48 T31 18 levels	102 x 116 (3.6° x 1.8°) 25 levels	none	thermodynamic three-layer model, dynamics using cavitating-fluid ice rheology (Weatherly et al. 1998)	vegetation modulates surface fluxes based on LSM, six-layer soil model for temp. and moisture (Bonan 1998)	Otto-Bliesner unpublished
ECBILT	ECBILT	64 x 32 T21 3 levels	64 x 32 (5.6° x 5.6°) 12 levels	none except freshwater flux in Arctic ocean	thermodynamic zero-layer model	Single bucket model for soil moisture; no explicit vegetation	Weber 2001; Weber & Oerlemans 2003
HADCM2	HADCM2	96 x 73 (2.5° x 3.75°) T42 19 levels	96 x 73 20 levels	SST, SSS (Levitus 1982)	thermodynamic zero-layer model for sea-ice extent + concentration dynamics driven by ocean currents (Johns et al, 1997)	Albedo determined by vegetation and snow depth; vegetation modulates surface fluxes based on UKTR scheme 4-layer soil model for temp. and moisture (Warrilow et al.,1986)	Hewitt & Mitchell 1998
ECHAM	ECHAM3/LSG (periodic synchronously coupling)	64 x 32 T21 19 levels	64 x 64 (5.6° x 5.6°) 11 levels	SST, SSS (Woodruff et al. 1987; Levitus, 1982)	thermodynamic zero-layer model	Land albedo prescribed; fractional vegetation cover controls evapotranspiration and interception; 5-layer soil temp. model and single bucket model for moisture (DKM, 1993)	Voss & Mikolajewicz 2001
IPSL-CM1	LMD5.3/OPA	64 x 50 11 levels	92 x 76 (4° x 3°) 31 levels	none	diagnostic sea ice, forms when SST is below -2; depth of 3m assumed	Vegetation modulates surface fluxes based on SECHIBA (Decoudré 1993) with 8 land cover types	Braconnot et al. 1999, 2000
MRI CGCM1	MRI CGCM1	72 x 46 (4° x 5°) 15 levels	144 x 111 (2.5° x 0.5°-2°) 23 levels	SST, SSS (Levitus 1982)	thermodynamic zero-layer model; ice advection, extent and concentration via surface currents	No explicit vegetation; 4-layer soil model with explicit simulation of temp. and moisture snow	Kitoh & Murakami. 2002

Finally, the models differ in the techniques used to spin-up the simulations, the length of simulation and in the length of interval over which mean climate statistics are calculated (Table 4-1). All of the simulations are in quasi-equilibrium with the 6 ka forcing and the ensemble climate statistics are in each case based on a minimum of 50 years, which is sufficient to ensure that the values are representative of the mean state of the 6 ka climate.

Validation of GCM palaeoclimate improvement owing to dynamic vegetation (phase II)

In phase II the improved ECHAM model from phase I is used to assess changes and potential enhancements under comparable terms and treatments. The climate system model, which provides the climate baseline for this validation, consists of the general circulation models ECHAM5 for the atmosphere and MPI-OM for the ocean (Jungclaus et al. 2005). In addition this complex model is coupled to the Lund-Potsdam-Jena dynamic global vegetation model (LPJ) and has been used for transient palaeo-simulations (Schurgers et al. 2007).

The atmosphere model ECHAM5 (Roeckner et al. 2003) is a spectral model used with a resolution of T31 and 19 vertical levels in this study. The prognostic variables that are calculated and stored are vorticity, divergence, temperature, surface pressure, water vapour, cloud liquid water and cloud ice. Convection is calculated by a mass flux scheme based on a steady state equation for mass, heat, moisture, cloud water and momentum fluxes for up- and downdrafts. Surface fluxes from the boundary layer are computed from bulk relationship with transfer coefficients. The transpiration is limited by stomata resistance and bare soil evaporation depends on the availability of soil water. The land surface is represented by five soil layers with respect to temperature, and with a single bucket layer for water. Hydrological discharge is calculated at a 0.5° grid. Surface runoff and drainage depend on the heterogeneous distribution of field capacity.

The ocean model MPI-OM (Marsland et al., 2003) is used in this study with a resolution of 1.5° and 40 vertical levels. The grid poles are located on Greenland and Antarctica. The numerical scheme includes advection, time stepping, free surface or rigid lid and vertical salt or freshwater fluxes. The parameterisation contains eddy fluxes, bottom boundary layer and mixed layer, isopycnal diffusion, and sunlight penetration. The incorporated sea ice sub-model operates with the same horizontal resolution and one layer of one ice category plus snow. The prognostic variables are ice thickness, ice concentration, ice velocity and snow depth.

The coupling procedure between the atmosphere and the ocean/sea ice is executed daily with heat and water conservations. Several variables are passed between the components, e.g. heat, freshwater, wind speed, solar radiation, sea surface temperature, ocean surface current, water fluxes, snowfall-sublimation and the ice variables, and no adjustments are prescribed. More detailed information about the two general circulation models is available in the model documentation on the web page of the Max Planck Institute for Meteorology http://www.mpimet.mpg.de/en/wissenschaft/modelle.

In order to analyse vegetation effects the model has been set up with additional coupled dynamic terrestrial vegetation by the LPJ-DGVM model (Sitch et al., 2003). The LPJ model combines mechanistic treatments of vegetation dynamics, carbon and water cycling. Terrestrial vegetation is described within ten plant functional types (PFTs), which are distinguished according to their phenology (evergreen, deciduous), physiology (C_3, C_4 photosynthesis), and morphology (tree, herbaceous). All PFTs have the possibility to exist in one grid cell. Population dynamics are updated annually and based on the productivity and also on mortality of each PFT. Mortality is computed as a function of PFT specific vigour and the occurrence of fire. This reduces the number of PFT individuals, and the success of new individuals is dependent on available ground for seeding. The photosynthesis and water balance for each grid cell is calculated daily and the net productivity is accumulated within a year and allocated to the plant tissues. There are four carbon pools for living biomass,

three for litter and two in the soil portion for the carbon exchange with the atmosphere. LPJ requires atmospheric CO_2 concentration, soil texture and monthly temperature, precipitation and sunshine fraction as downward short-wave radiation from ECHAM5-MPIOM.

As for the AOGCM simulations in phase I, the ECHAM-MPIOM / LPJ simulations run for modern (0 ka) and for mid-Holocene (6 ka) insolation conditions but with a stable CO_2 concentration of 280 ppm.

4.2.2   Analytic approach

In this comparison of the simulated and observed vegetation response to 6 ka climate changes, the signals previously identified in the analysis of simulations made with the IPSL AOGCM in Chapter 3 are focused. In the first phase comparison with other AOGCM simulations allows to determine whether these signals are robust or specific to the IPSL AOGCM. The simulated changes are compared with palaeovegetation reconstructions to decide whether the signals are realistic, and whether some models produce more realistic patterns than others. To quantify the degree of agreement between simulated and observed vegetation patterns, the reconstructed vegetation at each pollen site is compared to the simulated vegetation in the 0.5° BIOME grid cell.

In the second phase this approach is applied to evaluate the modifications of the advanced ECHAM-MPIOM model in combination with a coupled dynamic vegetation model (LPJ) compared to the previous version. Considering that the climate signals are relatively large and result in major changes in vegetation, a simplified biome classification scheme is adopted that groups individual biomes into major vegetation types (Harrison and Prentice 2003) for a quantitative comparison. Thus, the estimate of mismatches between the data and the simulations are relatively conservative.

4.3 Evaluation of coupled ocean - atmosphere simulations

(Wohlfahrt et al. 2008)

4.3.1   Results

As a consequence of simulated changes in climate between today and the mid-Holocene, all of the models produce changes in vegetation patterns compared to today (Figure 4-1). All models show a reduction of the high-latitude tundra vegetation and mid-continental spread of dry vegetation types in Eurasia. However, there are differences in the nature and magnitude of regional vegetation changes between the simulations. For example, the CSM1.2Δ simulation produces a contraction of xerophytic vegetation in the western part of central North America that is not shown by the other models. Similarly, the IPSL-CM1 model produces a much larger northward migration of temperate deciduous forest than other models, such that the cool mixed forest belt in eastern North America is barely represented in this simulation.

4.3.1.1   Impact of averaging period length on simulated vegetation patterns

Differences between the models could reflect differences in the number of years averaged to construct the mean climate statistics used to drive the BIOME4 simulations. To assess how far this might be the case, BIOME4 simulations based on a 20-year average from the IPSL-CM1 simulation (from year 80 to 100: IPSL-CM1$_{20}$) are compared to a 70-year average (from year 80 to 150: IPSL-CM1$_{70}$) from the same simulation (Table 4-3). The direction of change in vegetation is the same in both cases, although the magnitude of change in climate and the derived change in vegetation varies. Thus, both BIOME4 simulations show an increase in forest area at the expense of tundra, but the longer simulations show a smaller expansion of forest, indicating the fact that the simulated mean summer warming is smaller. The

difference in tundra area between the IPSL-CM1$_{20}$ and IPSL-CM1$_{70}$ runs is 2.57*10^5 km^2 (equivalent to 20.5 % of the change between 0 and 6 ka in the IPSL-CM1$_{70}$). Both BIOME4 simulations show an increase in xerophytic vegetation, but again the longer simulations show a smaller increase. The difference in the area of xerophytic vegetation between the IPSL-CM1$_{20}$ and IPSL-CM1$_{70}$ run is 10.36*10^5 km^2 (equivalent to 37 % of the change between 0 and 6 ka in the IPSL-CM1$_{70}$ simulation). The difference in the area of xerophytic vegetation between the two runs is greater in Eurasia than North America, due to the simulation of a larger decrease in precipitation in Eurasia than in North America. There are no differences in the extent of temperate forests between the two versions. This reflects the fact that the simulated temperature changes over eastern North America and Europe are very similar in the IPSL-CM1$_{20}$ and IPSL-CM1$_{70}$ runs.

Table 4-3: Difference in vegetation area (Δarea, in 10^5 km^2), temperature (ΔT, in °C) and precipitation (ΔP, in mm/d) between the 70 year and the 20 year simulation of the IPSL.CM1 model.

Region		IPSL-CM1$_{70}$	IPSL-CM1$_{20}$
N of 40° N			
	Δarea tundra	-12.53	-15.1
	Δarea forest	-15.59	-22.13
	ΔT mean summer (JJA)	1.27	1.36
North America 90-120° W, 40-55° N			
	Δarea xerophytic vegetation	4.36	5.2
	ΔP mean summer (JJA)	0.00	0.02
90-120° W, 40-55° N			
	Δarea temperate deciduous broadleaf forest	3.68	3.68
	ΔT mean winter (DJF)	-0.26	-0.22
Eurasia 70-140° E, 40-60 °N			
	Δarea xerophytic vegetation	14.90	21.17
	ΔP mean summer (JJA)	-0.16	-0.21
Europe 10° W-30° E, 40-60° N			
	Δarea temperate deciduous broadleaf forest	-0.78	-0.78
	ΔT mean winter (DJF)	-0.31	-0.35

temperate deciduous broadleaf forest
temperate evergreen needleleaf forest
warm-temperate evergreen broadleaf & mixed forest
cool mixed forest
cool evergreen needleleaf forest
cool-temperate evergreen needleleaf & mixed forest
cold evergreen needleleaf forest
cold deciduous forest
tropical xerophytic shrubland
temperate xerophytic shrubland
temperate sclerophyll woodland and shrubland
temperate deciduous broadleaf savanna

temperate evergreen needleleaf open woodland
tropical grassland
temperate grassland
desert
graminoid and forb tundra
low and high shrub tundra
erect dwarf-shrub tundra
prostrate dwarf-shrub tundra
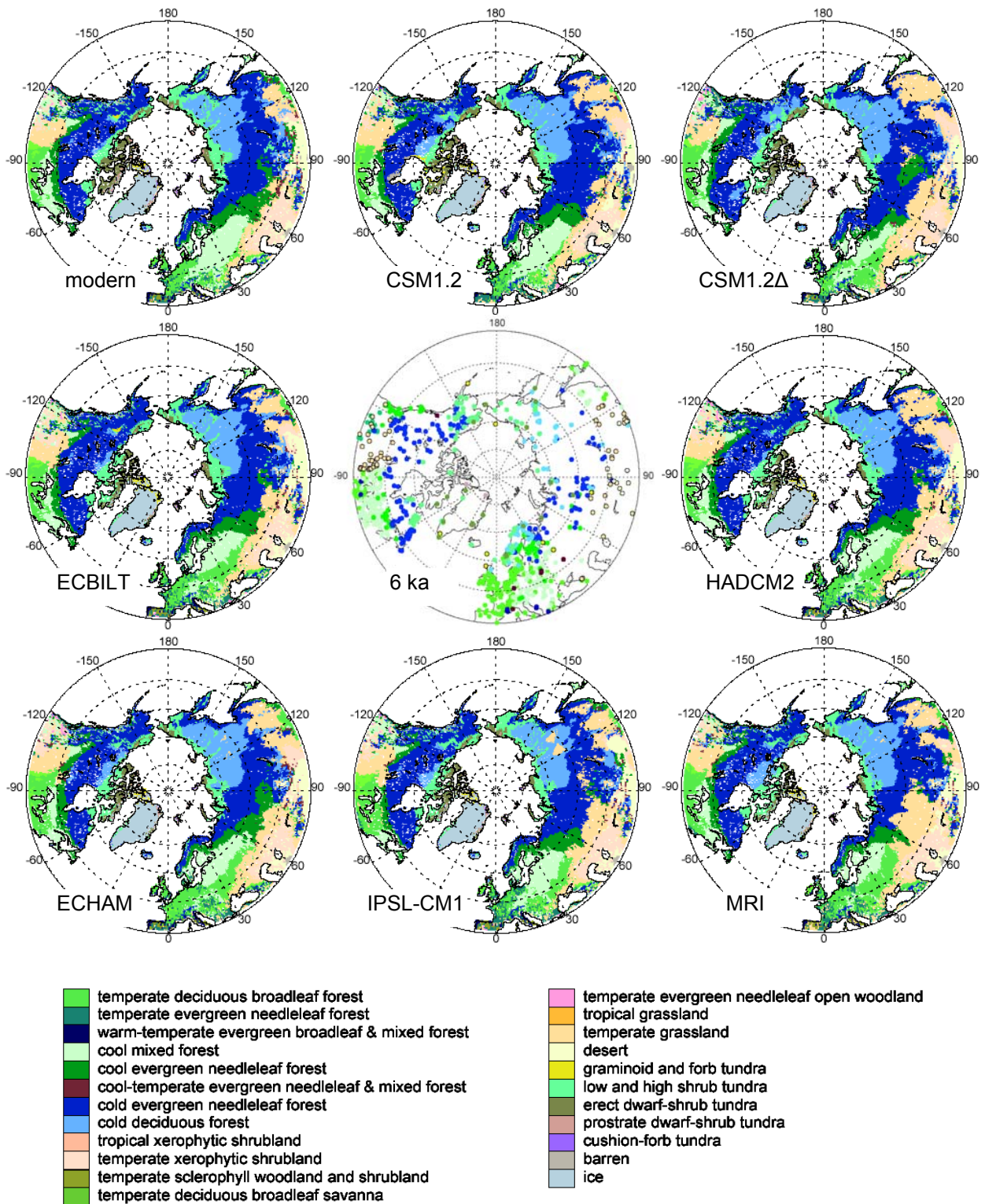cushion-forb tundra
barren
ice

Figure 4-1: Vegetation patterns at 6 ka as simulated by BIOME4 driven by output from 7 AOGCM simulations. The modern vegetation map (upper left), simulated by BIOME4 driven by a modern climatology (CLIMATE 2.1; Cramer), and the pollen based reconstructions of 6 ka vegetation (centre) with merged data from 40 °N – 55 °N derived from Biome6000 (Prentice et al. 2000) and N of 55 °N derived from PAIN (Bigelow et al. 2003), are shown for comparison.

These comparisons show that the length of the averaging period does not appear to affect the direction of the simulated vegetation changes. However, the magnitude of the changes is affected, and appears to be less extreme in the longer simulation. This can be explained by a more accurate representation of the mean climate in the 70 year averaged simulation by filtering out the impact of interannual to decadal variability. In the following, the differences between IPSL-CM1$_{20}$ and IPSL-CM1$_{70}$ are used to determine whether inter-model differences in simulated biomes are likely to be important.

4.3.1.2 Shifts in the tundra-taiga boundary

All of the models produce a northward shift in the position of the tundra-taiga boundary (Figure 4-1). This shift results in a decrease in the area of tundra by between $9*10^5$ km^2 and $34.9*10^5$ km^2 depending on the model, compared to present (Figure 4-2 and Table 4-4). The decrease in tundra area is markedly asymmetric, with
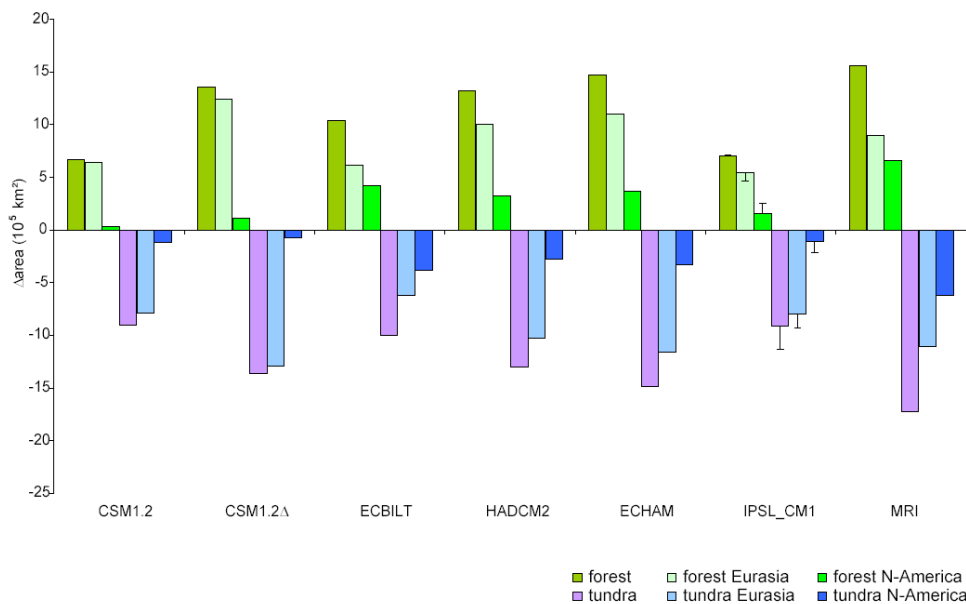

Figure 4-2: Simulated changes in the area of tundra and forest north of 60° N. The changes are also shown for Eurasia (10° W to 170° W) and North America (170° W to 10° W) separately. The error bars show the deviation between the IPSL-CM1$_{20}$ and IPSL-CM1$_{70}$ simulation.

most of the reduction occurring in Eurasia with 6.2–12.8*10^5 km^2 (6.5–13.6 %) and a smaller reduction in North America with 0.7 – 6.2*10^5 km^2 (1.4–11.9 %). The shift of forest into areas that are tundra today results in an increase in the total area of forest north of 60 °N (Figure 4-2). Using the difference between the IPSL-CM1$_{20}$ and IPSL-CM1$_{70}$ results as a guideline, the differences in the size of the reduction in tundra area between the models are relatively small. Only the MRI simulation produces changes that appear to be larger than the other models.
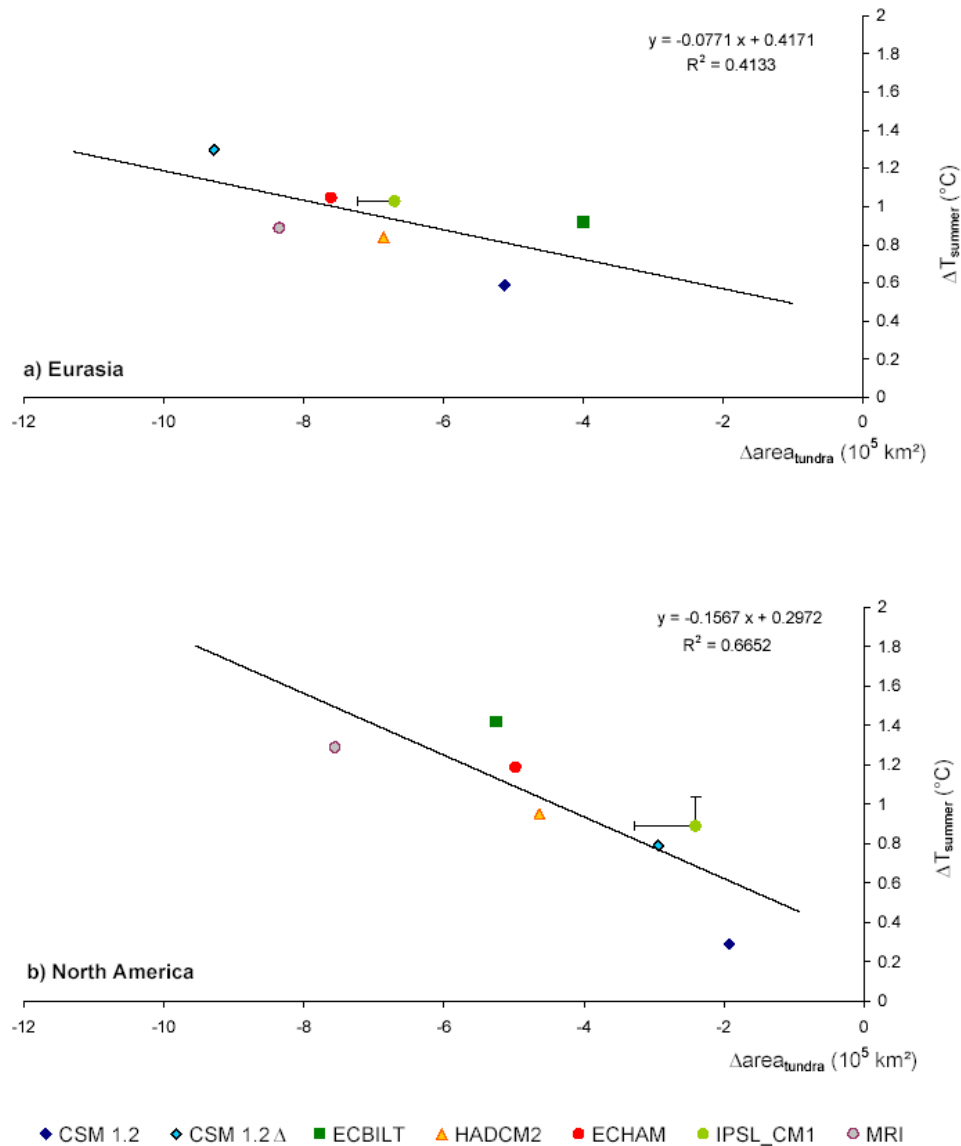
Figure 4-3: Comparison of simulated changes of tundra and changes in mean summer temperature (June, July, August, September). Comparisons are made for **a)** Eurasia (10° W–170° W) and **b)** North America (170° W–10° W). The southern boundary for these comparisons is at 65° N in Eurasia and 55° N in North America to take into account the different location of the taiga-tundra boundary. The error bars show the deviation between IPSL-CM1$_{20}$ and IPSL-CM1$_{70}$ simulation.

The decreased extent of tundra at 6 ka is a consequence of changes in the length of the growing season: simulated GDD is much higher at 6 ka than today. The increase in GDD is driven by higher temperatures during the summer and autumn. The change in summer and autumn (June through September, Figure 4-3) temperatures explains 42 % of the inter-model variation in the change in tundra area in Eurasia, and 67 % of the variation in the change in tundra in North America. The increase in summer temperatures is a direct consequence of the orbital forced increase in high latitude
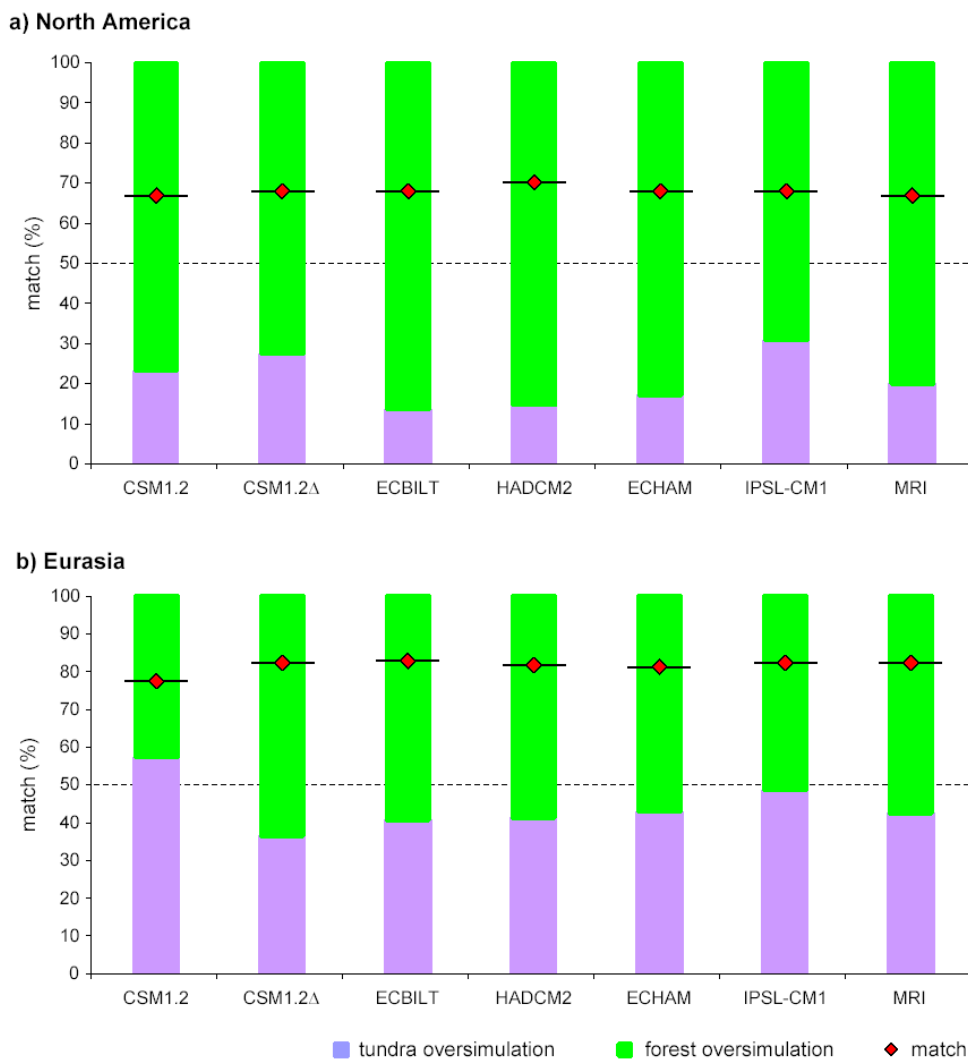
Figure 4-4: Comparison of observed and simulated changes in the tundra-taiga boundary in **a)** North America (170° W - 10° W, N of 55° N) and **b)** Eurasia (10° W - 170° W, N of 65° N). The red diamonds show the overall match (%) between observed and simulated changes for each model. The stacked bars show the relative proportion of the mismatches that are due to simulation of forest in areas where the observed vegetation was tundra (forest oversimulation) or the simulation of tundra in areas where the observed vegetation was forest (tundra oversimulation).

insolation. The prolongation of warm conditions into the autumn is caused by ocean feedbacks.

The northward shift of the tundra-taiga boundary and the asymmetry of this shift, with largest changes in Europe and Central Siberia, are qualitatively in agreement with palaeoenvironmental observations. Quantitative comparisons between the simulated vegetation changes and the combined PAIN-Biome6000 data set (Figure 4-4) show that the models produce a relatively good match (67–70 %) with observations in North America. Analyses of the mismatched sites show that the models consistently predict more forest than reconstructed by observations. Most of the errors occur in eastern Canada, where the observations suggest that tundra was located further south than today at 6 ka but the simulations show a northward shift in forest. The failure to simulate southward expansion of tundra probably reflects the fact that the models do not include the relict Laurentide ice sheet which persisted in Quebec as late as 5000 yrs B.P. and resulted in a local cooling (Clark et al. 2000; Marshall et al. 2000). The quantitative match to observations in Eurasia is better (77–83 %) than in North America. Furthermore, there is no consistent pattern to the individual mismatches: neither forest nor tundra is consistently over-represented in the simulations.

4.3.1.3   Mid-continental expansion of xerophytic vegetation

All of the models produce an expansion of xerophytic vegetation (e.g. tropical/temperate shrubland, tropical/temperate grassland, temperate sclerophyll woodlands/savannahs, and desert) in the mid-continental regions of the northern hemisphere (Figure 4-1). The area of xerophytic vegetation in the mid-latitudes increases by 15.4 to $35.4*10^5$ km^2 (Table 4-4), with most of the increase (11.1 to $19.9*10^5$ km^2) in Eurasia (70-140 °E, 40-60 °N), in particular east of 100 °E (5.3 to $12.8*10^5$ km^2). The expansion of xerophytic vegetation in Eurasia resulted in a decrease in the area of temperate and boreal forests (Figure 4-5). The largest changes

in the area of mid-latitude xerophytic vegetation are shown by the MRI and HADCM2 model and the CSM1.2Δ simulation. Most of the models show an expansion of xerophytic vegetation in North America, but this expansion was relatively small (0.8 to $4.4*10^5$ km^2) and confined to the western part of the continent.

Surprisingly the two simulations with largest overall increase in xerophytic vegetation show smallest changes in western North America. The CSM model simulation in which [CO_2] was lowered at 6 ka, however, shows a small decrease in xerophytic vegetation. With this exception, the inter-model differences in the magnitude of the expansion of xerophytic vegetation are small. Using the difference between the IPSL-CM1$_{20}$ and IPSL-CM1$_{70}$ results as a guideline; all models produce a similar expansion of dry xerophytic vegetation in the mid-continents.

The increased extent of xerophytic vegetation at 6 ka is a consequence of changes in plant-available moisture during the growing season (Figure 4-6). In earlier analyses of the expansion of xerophytic vegetation in the IPSL simulation (Wohlfahrt et al. 2004), the decrease in plant-available moisture appeared to be driven by a decrease in
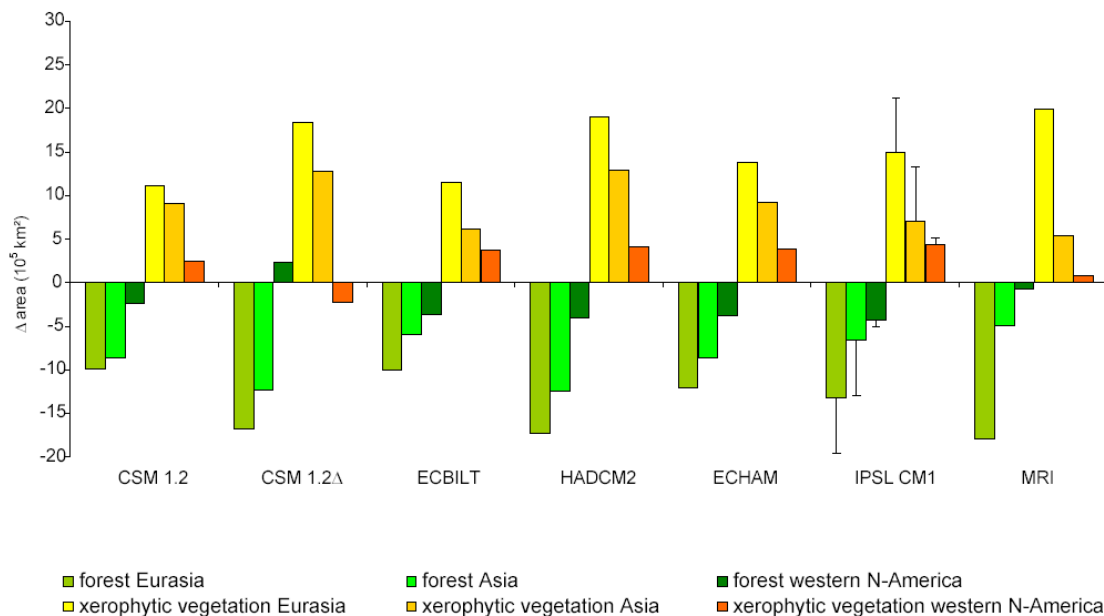

Figure 4-5: Simulated changes in xerophytic vegetation and forest in 105 km² for mid-continental Eurasia (70-140 °E, 40-60 °N), the core region Asia (100-140 °E, 40-60 °N) and western North America (90-120 °W, 40-55 °N). The error bars show the deviation between the IPSL-CM120 and IPSL-CM170 simulation.

Table 4-4: Area of biomes and major biomes simulated by each of the AOGCMs in the northern hemisphere extratropics (north of 40° N) compared to the BIOME4 modern area in 10^5 km².

Biome name	modern	CSM1.2	CSM1.2Δ	ECBILT	HADCM2	ECHAM	IPSL-CM1$_{70}$	MRI
temperate deciduous broadleaf forest	24.03	23.9	32.31	33.6	33.57	42.17	29.85	40.29
temperate evergreen needleleaf forest	7.07	7.76	6.32	8.23	8.47	8.58	10.53	9.03
warm-temperate evergreen broadleaf mix forest	2.51	1.09	2.65	2.37	2.31	2.97	2.1	2.01
cool mixed forest	45.83	38.52	30.44	35.51	37.86	36.73	33.64	29.66
cool evergreen needleleaf forest	39.48	27.62	31.85	33.17	33.76	36.8	30.28	28.95
cool-temperate evergreen needleleaf mixed forest	4.82	2.45	2.09	3.47	3.17	4.14	3.15	3
cold evergreen needleleaf forest	133.85	134.83	133.67	134.04	126.03	111.73	129.84	121.6
cold deciduous forest	40	51.77	53.15	42.77	43.2	50.91	42.62	50.89
All forest	**297.61**	**287.95**	**292.49**	**293.16**	**288.37**	**294.03**	**282.02**	**285.43**
temperate xerophytic shrubland	20.68	17.88	22.07	21.5	24.17	23.99	22.31	22.31
temperate sclerophyll wood and shrubland	1.94	0.71	1.57	2.35	2.23	2.12	2.32	2.28
temperate deciduous broadleaf savanna	4.66	3.19	2.03	4.25	5.12	4.98	5.46	2.47
temperate evergreen needleleaf open woodla	0.87	1.01	1.74	0.95	1.29	1.1	0.99	0.44
temperate grassland	31.38	52.14	64.17	46.23	54.86	52.08	56.25	67.43
All xerophytic vegetation	**59.55**	**74.94**	**91.58**	**75.29**	**87.7**	**84.31**	**87.38**	**94.96**
graminoid and forb tundra	2.27	5.18	1.1	3.06	2.24	1.95	1.8	2.36
low and high shrub tundra	42.25	33.18	31.64	39.29	33.08	33	38.22	34.16
erect dwarf-shrub tundra	19.86	15.92	14.55	11.95	13.29	12.13	14.02	9.51
prostrate dwarf-shrub tundra	4.02	2.69	3.27	1.63	2.61	2.83	2.74	1.82
cushion-forb tundra	1.63	1.6	0.91	0.61	0.89	0.83	0.71	0.82
All tundra	**70.02**	**58.57**	**51.48**	**56.54**	**52.11**	**50.74**	**57.49**	**48.68**
desert	14.63	13.47	7.43	17.33	14.54	13.89	16.04	13.64
barren	2.41	9.28	1.23	1.88	1.48	1.23	1.28	1.5

precipitation during the spring, summer and autumn (Figure 4-6, lower panels). Inter-model differences in the change in area of xerophytic vegetation in western North America are strongly correlated with changes in summer precipitation ($R^2 = 0.83$).

In Eurasia, however, only ECBILT shows the same pattern of decreased precipitation during spring, summer and autumn as the IPSL model. Although most of the models show a decrease in spring precipitation, this is compensated by an increase in

precipitation during summer. The decrease in spring precipitation alone is not sufficient to explain the inter-model differences in the expansion of xerophytic vegetation. The relationship between changes in the area of xerophytic vegetation and changes in summer precipitation is weak ($R^2 = 0.06$). Conversely, there is a strong positive correlation ($R^2 = 0.80$) between the change in the area of xerophytic vegetation and summer (June through August) temperatures over Eurasia. There is a similar relationship between the change in xerophytic vegetation and summer temperatures over western North America ($R^2 = 0.70$). These results imply that the expansion of xerophytic vegetation is controlled by temperature-driven increases in evapotranspiration rather than a change in precipitation, although decreases in precipitation may contribute to the decrease in plant-moisture availability for individual models.
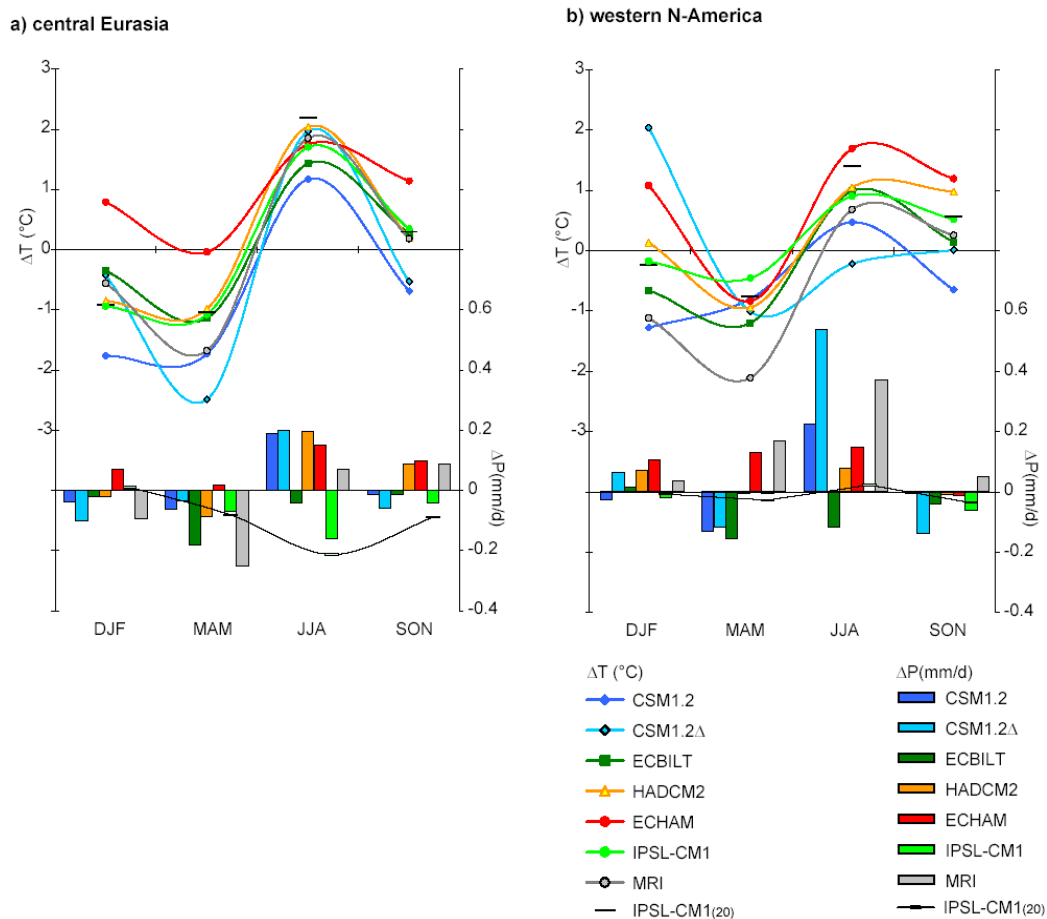

Figure 4-6: Changes in seasonal cycle of temperature and precipitation for **a)** Eurasia (70- 140 °E, 40-60 °N) and **b)** western North America (90-120 °W, 40-55 °N) as simulated by AOGCMs. For comparison the results of the IPSL-CM1[20] simulation are shown in black.

The expansion of xerophytic vegetation in western North America is qualitatively in agreement with palaeoenvironmental observations (Harrison et al. 2003). Quantitative comparisons with the combined PAIN-Biome6000 data set (Figure 4-7) show that the
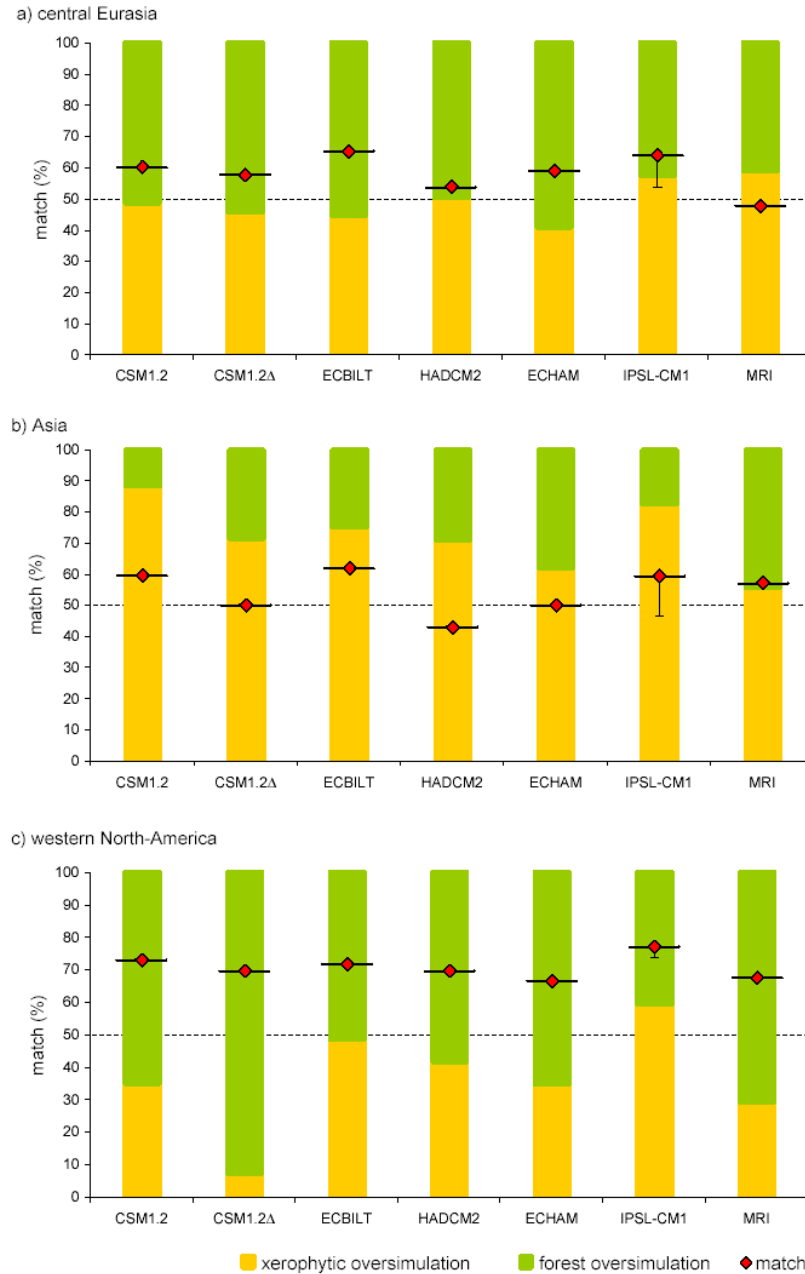

Figure 4-7: Comparison of observed and simulated changes in xerophytic and forest vegetation in the mid-continent regions of **a)** Central Eurasia (70-140 °E, 40-60 °N), **b)** of Central Asia (100-140 °E, 40-60 ° N) and **c)** North America (90-120 °W, 40-55 °N). The red diamonds show the overall match (%) between observation and simulated changes. The stacked bars show the relative proportion of mismatches that are due to simulation of forest in areas where the observations show xerophytic (forest oversimulation) or the simulation of xerophytic in areas where forest (xerophytic oversimulation) was observed. The error bar shows the deviation between the IPSL-CM1$_{20}$ and IPSL-CM1$_{70}$ simulation.

models produce a relatively good match (66–77 %) to observations. Analyses of the mismatched sites show that there is a tendency for the models to overestimate the amount of forest. There is a significantly poorer match between the simulated and observed vegetation patterns in Eurasia (48–65 %, Figure 4-7a). Focused on the Asian core region the match is further declining. Analyses of the mismatched sites show that the models consistently over-predict the extent of xerophytic vegetation in the Asian sector (Figure 4-7b).

4.3.1.4   Shifts in the temperate forests of eastern North America

All of the models produce a small northward expansion of the temperate deciduous broadleaf forests in eastern North America (Figure 4-1). The area of temperate deciduous broadleaf forest in the zone from 40° - 55° N increases by 0.7 to $3.7*10^5$ km^2 (16–80 %), generally at the expense of cold forest types (Figure 4-8a) although in the case of CSM1.2, CSM1.2Δ, ECBILT, and IPSL-CM1 the increase in temperate deciduous broadleaf forest also occurs as a result of the decrease in temperate and cool evergreen and mixed forest. The increase of temperate deciduous broadleaf forest and cool-temperate mixed forest in the HADCM2 is related to the decrease and northward shift of boreal forest. In the case of the CSM and IPSL simulations the decrease in cool-temperate mixed forest is larger than can be accounted for by the expansion of temperate deciduous broadleaf forest, and is partly due to encroachment by non-forest types. The expansion of temperate forests is a result of winter warming. However, because the changes are relatively small and occur in discrete patches (rather than as a shift of a zonal boundary across the region) it is difficult to show a strong statistical relationship between the simulated climate and biome changes.

The northward shift of the temperate deciduous broadleaf forest is consistent with observations (Figure 4-9a). Quantitative comparisons between the simulated vegetation changes and the combined PAIN-Biome6000 data set (Figure 4-10) show

that the match to observations varies considerably from model to model: the worst match (42.7 %) is produced by the IPSL simulation and the best match (75.5 %) by the CSM simulation. However, analyses of the mismatched sites (Figure 4-10a) show that all of the models tend to predict forest types characteristic of warmer conditions than observed. The observed expansion of temperate forests in the northern part of this region was probably limited by regional cooling due to the presence of the relict Laurentide ice sheet.
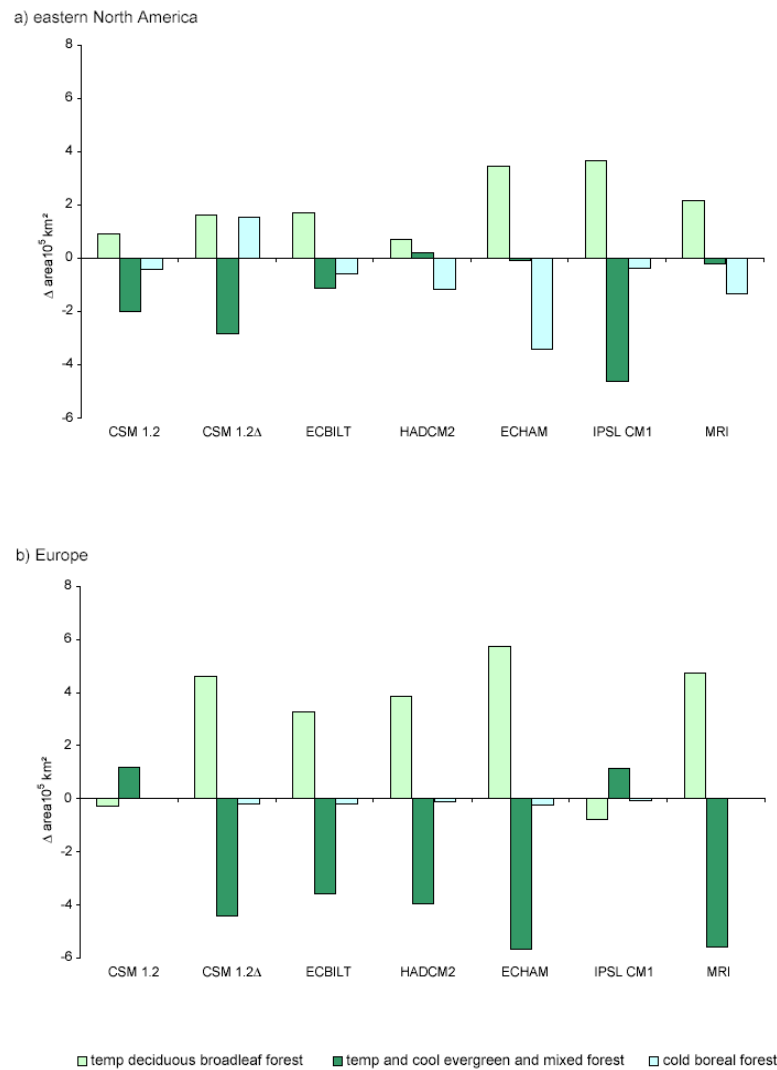
Figure 4-8: Simulated changes in the area of the main forest types in a) eastern North America (60-90 °W, 40-55 °N) and b) Europe (10 °W-30 °E, 40-60 °N). The changes in the temperate deciduous broadleaf forest are shown relative to changes in temperate and cool evergreen and mixed forest grouping the biomes types of temperate evergreen needleleaf forest, cool-temperate evergreen needleleaf mixed forest, cool mixed forest and cool evergreen needleleaf forest and cold boreal forest, combining cold evergreen needleleaf forest and cold deciduous forest. Differences between the two IPSL-CM simulations are negligible.

4.3.1.5 Shifts in the temperate forests of Europe

The simulated changes in temperate forest belts in Europe are not consistent and vary in strength and direction from model to model (Figure 4-1). Five of the models show an increase in temperate deciduous broadleaf forest, in response to the simulation of warmer winters. In the case of the ECBILT and MRI models, this warming appears to be highly localised and does not show up in regional averages. In contrast, two of the models (CSM and IPSL) produce a decrease in temperate deciduous broadleaf forest, in response to the simulation of colder winters.

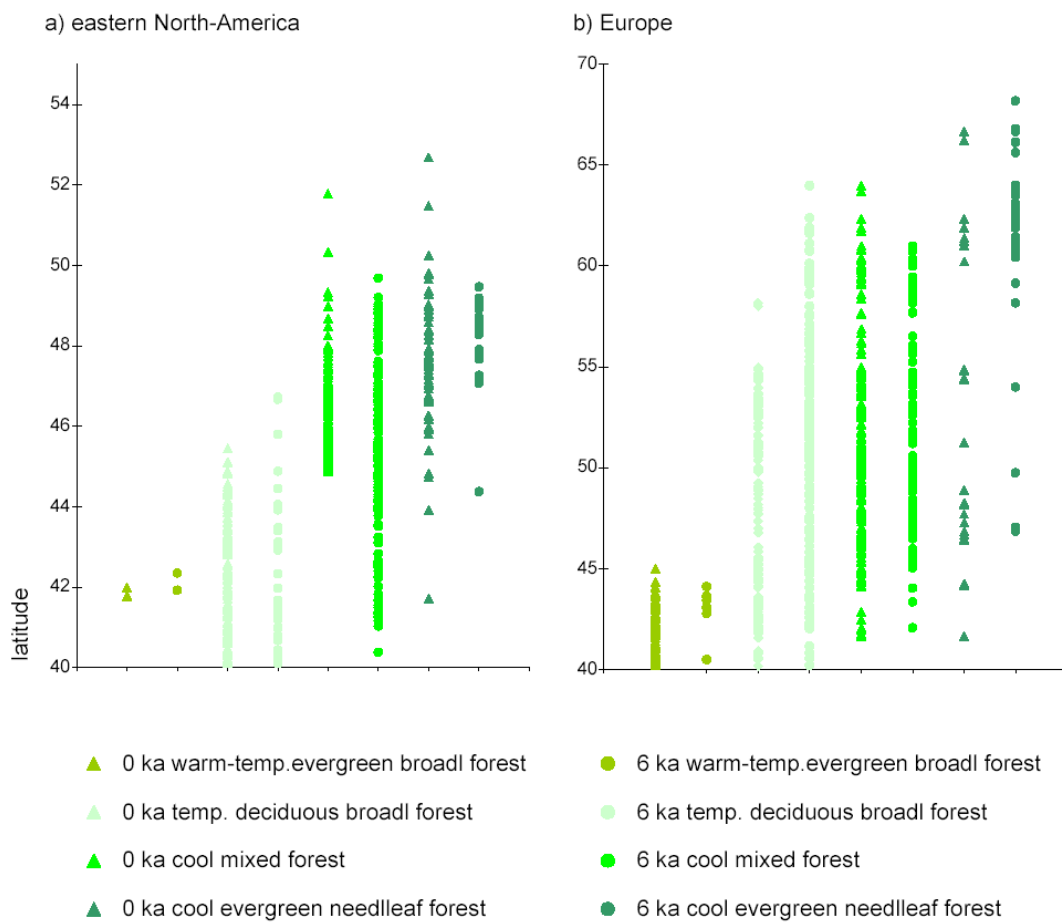**Figure 4-9:** Observed changes in the latitudinal distribution of warm-temperate evergreen broadleaf forest, temperate deciduous broadleaf forest, cool mixed forest and cool evergreen needleleaf forest 0 ka and 6 ka in **a)** eastern North America (60-90 °W, 40-55 °N) and **b)** Europe (10 °W-30 °E, 40-60 °N).

Observations show that the northern boundary of the temperate deciduous broadleaf forest in Europe was much further north at 6ka than it is today (Figure 4-9b). Thus, the models that produce a northward shift in the northern boundary of this forest type are qualitatively correct. However, quantitative comparison of the simulated changes
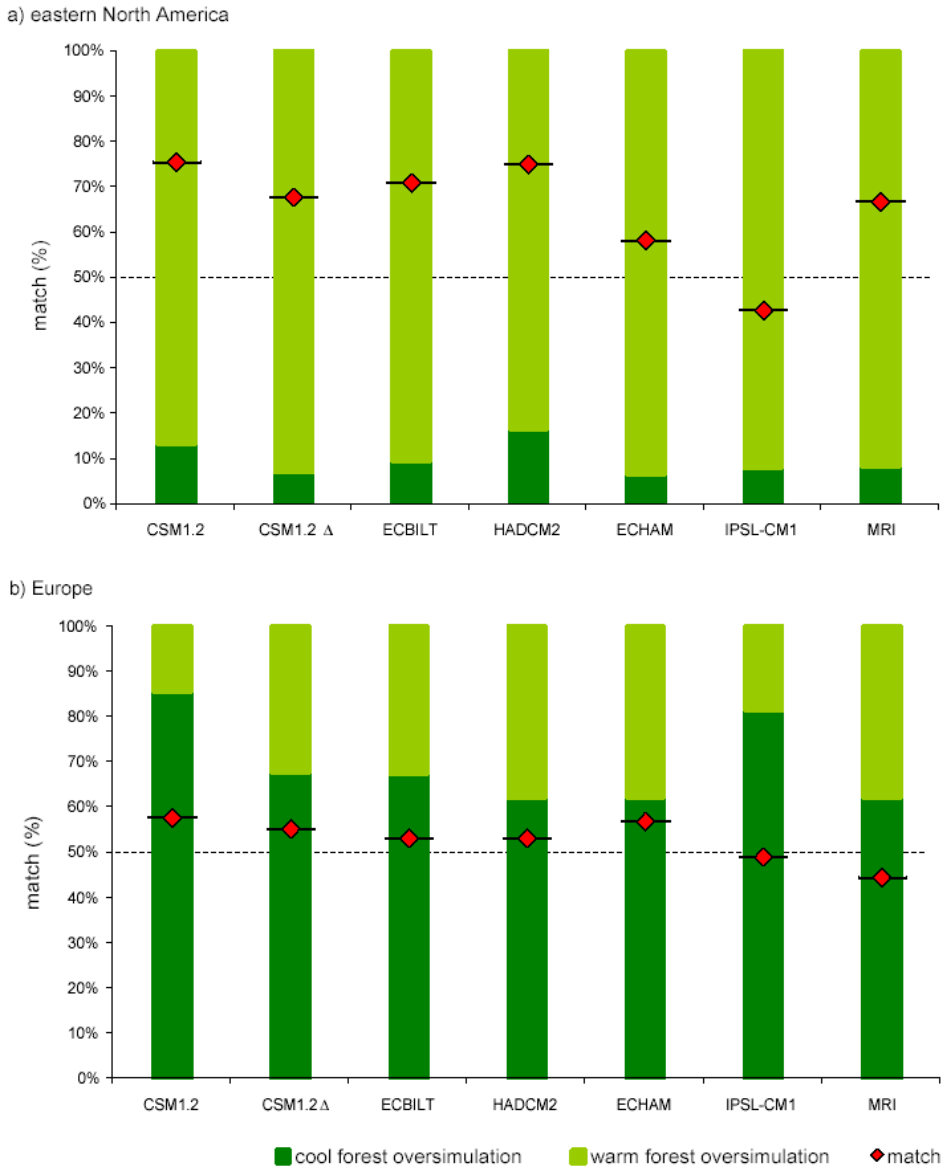
Figure 4-10: Comparison of simulated and observed vegetation in **a)** eastern North America (60-90 °W, 40-55 °N) and **b)** Europe (10 °W-30 °E, 40-60 °N). The red diamonds show the overall match (%) between observation and simulation for each model. The stacked bars show the relative proportion of the mismatched simulated vegetation types. In areas where the observations show temperate deciduous broadleaf or warm-temperate evergreen broadleaf forest and the simulations show cool mixed or cool evergreen needleleaf or cool-temperate evergreen needleleaf forests, the mismatches indicates "cool forest oversimulation". The "warm forest oversimulation" implies errors in the opposite direction (i.e. temperate forests being simulated where cool forests occurred). Differences between the two IPSL-CM simulations are negligible.

indicates that even these models only produce a moderate match (44-58 %) to the observations (Figure 4-10b). Furthermore, analyses of the mismatches show that these models consistently underpredict the amount of temperate deciduous broadleaf forest, and that they thus underpredict the magnitude of winter warming compared to the changes implied by the observations. IPSL and CSM, the two models that produce winter cooling, show the largest over-representation of cold forests at the expense of temperate deciduous broadleaf forest. The differences between model simulations and the large discrepancies between model and data suggest that coupled simulations do not produce a better simulation of the climate of western European region than PMIP AGCM simulations (Harrison et al. 1998; Guiot et al. 1999; Masson et al. 1999).

4.3.1.6 The impact of changing $[CO_2]$ on simulated vegetation patterns

The ECHAM 6 ka simulation differs from the ECHAM control simulation not only with respect to insolation forcing but also because the 6 ka CO_2 level was lowered from 345 ppm (control) to 280 ppm (6 ka). It seems unlikely that this difference in experimental design is important as a factor for inter-model differences. In fact, the ECHAM simulation show the same broad-scale changes as the other models and the magnitude of the changes in key areas lies within the range shown by the other models which have the same CO_2 level in the control and 6 ka experiment. This difference in experimental design raises the issue of how changing $[CO_2]$ might impact on the 6 ka simulations. This can be examined by comparing two simulations made with the CSM1.2 model. In the first set of simulations (CSM1.2), there is no change in $[CO_2]$ between the control and 6 ka simulations. In the second set of simulations (CSM1.2Δ) $[CO_2]$ is lowered from 355 ppm in the control to 280 ppm at 6 ka.

Comparison of these simulations shows that changing $[CO_2]$ has an impact on northern hemisphere vegetation patterns. The CSM1.2Δ simulation shows a larger decrease in tundra area than the CSM1.2 run, predominantly in Eurasia (Figure 4-2). This reflects the fact that the change in summer temperature (Figure 4-3) in the CSM1.2Δ run is approximately double the change in the CSM1.2 run. Since the climate response of summer warming and tundra decrease of ECHAM is representative for the group of GCMs considered here, inferior polar warmth by steady CO_2 concentration may be considered as a robust feature. In the mid-latitude continental regions, the CSM1.2Δ simulation produces a larger increase in xerophytic vegetation in Eurasia than the CSM1.2, but reduces the area of xerophytic vegetation in North America (Figure 4-5). This reduction in the area of xerophytic vegetation in North America results from large increase in summer precipitation and cooler summer temperatures (Figure 4-6). As this is a unique feature and no similarity to the other $[CO_2]$ lowering ECHAM simulation can be seen, this result can be meant as model specific. In eastern North America, the CSM1.2Δ simulation produces enhanced winter warming compared to the CSM1.2 simulation in the south, resulting in expansion of temperate deciduous broadleaf forest. Further north, however, the change in $[CO_2]$ results in colder winters and an expansion of the cool mixed forest belt that lies between (Figure 4-1). Consequently, the temperate deciduous broadleaf forest and the boreal forest are reduced. The $[CO_2]$ lowering produces a radical change in the signal over Europe. In CSM1.2 the winters are colder, resulting in a small reduction of temperate deciduous broadleaf forest. In CSM1.2Δ, the temperate deciduous broadleaf forest expands in response to winter warming. The ECHAM simulation corresponds to the general signal of increasing warmer forest. However the evident decrease of cold boreal forest in eastern North America unto the Hudson Bay means a clear overestimation of winter warming, shifting the complete band of temperate and cool evergreen & mixed forest northward.

Overall, the response to lowering $[CO_2]$ appears to depend on the relative importance of the direct atmospheric response and the ocean feedback in producing the change in regional climate. In those regions, where the atmospheric response is strong, lowering

[CO_2] produces colder (e.g. eastern North America) and drier (e.g. continental Eurasia) conditions as might be expected. However, when ocean feedback has a significant impact, the effect of lowering [CO_2] is to strengthen this signal.

4.3.2   Discussion

Analyses of a suite of AOGCM simulations of 6ka show that there are a number of robust changes in regional climate and vegetation in response to orbital forcing. These robust features include (a) the reduction of tundra in high northern latitudes, (b) the northward expansion of temperate forests in eastern North America, and (c) the expansion of xerophytic vegetation in mid-continental Eurasia.

All of the models produce a northward shift in the boundary between boreal forest and tundra. This shift is markedly asymmetric, with largest changes occurring in northern Eurasia and relatively small changes occurring over North America. The changes in tundra area are driven by warmer conditions during the growing season, partly driven by orbital forced changes in summer temperature and partly driven by warming in autumn because of ocean feedback. The marked asymmetry in the changes in the tundra-taiga boundary is not a feature of most atmosphere-only simulations (see e.g. TEMPO 1996). This suggests that changes in the Arctic Ocean play an important role in producing this asymmetry, a conclusion consistent with studies of the role of changes in sea ice on high-latitude climates (Vavrus and Harrison 2003). The simulated changes in high-latitude vegetation are in good agreement with observations: in Eurasia, for example, all the models produce a match between observed and simulated vegetation at between 77-83 % of the actual pollen sites and there is no systematic signal in the mismatches. With respect to the qualitative analyses of BIOME4 modern vegetation (Chapter 2.3) ensuing 70 %

global agreement to modern observation data these results can be assessed as very good.

All models produce a northward expansion of temperate forests at the expense of boreal forest in eastern North America, in response to winter warming. Comparison with observations shows that the northward expansion of temperate forests is realistic, but too large. It is hypothesised that this overestimate of the magnitude of vegetation changes is a result of the unrealistic prescription of inland ice cover in the simulations, and specifically the omission of the small remnant of the Laurentide ice sheet that persisted in Quebec until well after 6 ka. Although there is only one simulations of the 6ka climate by Renssen et al. (200?) which incorporate this ice sheet, suggesting only an insignificant effect, simulations of the early Holocene (ca 9 ka) climate made with and without presence of ice in eastern Canada show that this ice mass has a non-negligible sway on regional temperatures (Mitchell et al. 1988). The relict of the Laurentide ice sheet is not incorporated in the next 6ka PMIP2 (http://www-lsce.cea.fr/pmip/) simulations either. The analyses suggest that this will limit the usefulness of comparisons with pollen-based vegetation reconstructions from eastern North America (e.g. Williams et al. 2000) and propose that there is a need to run mid-Holocene experiments incorporating changes in ice cover in order to fully understand the evolution of North American climates during the Holocene.

All AOGCM simulations produce a significant expansion of xerophytic vegetation in the mid-continent of Eurasia. The robustness of this signal across the suite of simulations is a matter of concern because the simulated expansion is not consistent with data reconstructions. Unfortunately the BIOME4 model is burdened with a strong bias in a part of that region. The southern Altai mountain ridge and West Mongolia provide an inferior agreement between the model standard and the observations (Figure 2-8). Those weak agreements of the AOGCMs for Central Eurasia of 48 – 65 % involve an origin match of 54 % in the BIOME4 modern standard (Figure 2-6). The origin bias of BIOME4 modern leads to the simulation of forests instead of observed xerophytics. That means although the diagnostic BIOME4

model trends to favour forest in this region an over-estimation of dry vegetation types is given, enhancing the unrealistic reconstruction from climate models data.

Nevertheless, this problem of diminished validity is regionally restricted to the southern edge of the examined area; the crucial regions of aridity are located further north. Furthermore the bias is addressed to the poor representation of soil properties prescribed in the BIOME4 model which are constant for all simulations.

The diagnosis of the IPSL-CMI simulation, (Chapter 3) have shown that the expansion of xerophytic vegetation in mid-continental Eurasia is already present in atmosphere-only simulations, and is amplified by ocean feedback. When these simulated changes in vegetation are used to prescribe land-surface conditions in a second AOGCM simulation, they produce a further increase in aridity resulting in a considerable expansion of xerophytic vegetation and a further degradation of the match between simulated and observed vegetation patterns (Figure 4-11). A similar result would presumably be produced if simulated vegetation patterns from any of the AOGCM simulations were used to prescribe vegetation changes in 6ka experiments. Previous analyses of coupled AOGCM simulations have emphasised the role of ocean feedback in improving simulated regional climates (e.g. Kutzbach et al. 2001). However, as the analyses show, the incorporation of both ocean- and land-surface feedbacks has the potential to produce less realistic simulations of the climate.

The tendency for models to produce more arid conditions in central Eurasia than shown by palaeoenvironmental data was already apparent in analyses of earlier AGCM simulations (see e.g. Yu and Harrison 1996; Qin et al. 1998; Tarasov et al. 1998), but the cause of this difference was unclear. This study of AOGCMs suggests that the simulated increase in aridity is primarily a function of temperature-driven increases in evapotranspiration during the growing season. Simulated changes in precipitation are not consistent from model to model, with some models producing decreased precipitation during summer and others producing a marked increase in precipitation. Thus, given that the simulated response to 6ka orbital changes in mid-continental Eurasia is inaccurate although the BIOME4 diagnostics are weak, this

analyses suggest that the problem lies in the treatment of land-surface water and energy exchanges with the atmosphere. Simulated changes in atmospheric circulation patterns surely take a part in the incorrect prediction for this special region (Bonfils et al. 2004), transporting moisture into the furthest inland areas, but do not account directly for the vegetation reconstruction with the BIOME model.

This evaluation shows that some features of the response of the coupled ocean-atmosphere system to 6ka orbital forcing are not robust from model to model. Specifically, the models have different responses in the mid-continent of North America and over Europe. It is possible that these inter-model differences in response reflect differences between the control simulations. Analyses of the response of the northern African monsoon to 6 ka orbital forcing (Joussaume et al. 1999; Braconnot et al. 2002), for example, show that inter-model differences in the location of the simulated monsoon front in the control simulation partly determine the magnitude of the response to changes in orbital forcing.
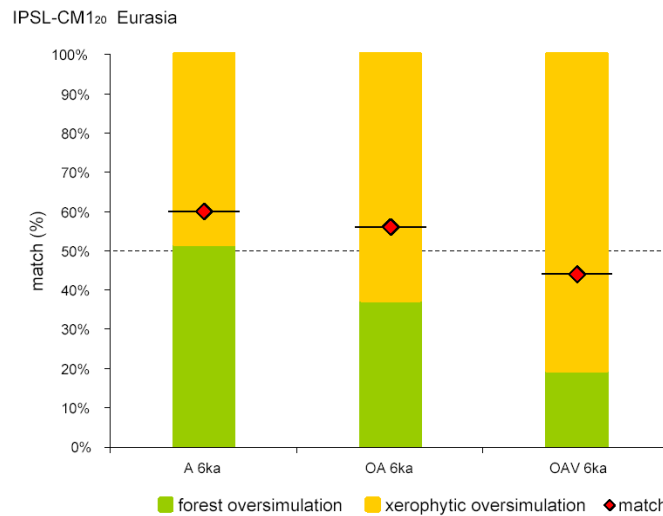
Figure 4-11: Comparison of observed vegetation changes in Eurasia (70-140 °E, 40-60 °N) and changes as simulated by the IPSL model with 20 years averages (IPSL-CM1$_{20}$) as a result of the atmosphere-only response (A 6ka), the coupled ocean-atmosphere response (OA 6ka), and the coupled ocean-atmosphere-vegetation response (OAV 6ka) to 6ka orbital forcing. The red diamonds show the overall match (%) between observation and simulated changes for each simulation. The stacked bars show the relative proportion of the mismatches that are due to simulation of forest in areas where the observed vegetation was xerophytic (forest oversimulation) or the simulation of xerophytic in areas where the observed vegetation was forest (xerophytic oversimulation).

The models differ in the degree to which they produce an increase in xerophytic vegetation in mid-continental North America, although only the CSM1.2Δ simulation fails to produce an increase. Harrison et al. (2003) have shown that mid-continental aridity is dynamically linked to the simulation of an enhanced monsoon in western North America: precipitation is suppressed in the regions characterised by subsidence around the monsoon core. This suggests that the differences in magnitude of the expansion of xerophytic vegetation is likely to be correlated with differences in the strength of the simulated monsoon expansion in North America and could help to explain the correlation between changes in the area of xerophytic vegetation and summer temperature.

The simulated changes in vegetation patterns over Europe differ from model to model: most models produce an increase in the extent of temperate forests but the IPSL-CMI and CSM models produce a decrease. In the previous analyses of the IPSL model, it could be demonstrated that ocean feedback enhanced the orbital-induced winter cooling over Europe shown in atmosphere-only simulations and that vegetation feedback was necessary to produce a more realistic northward expansion of temperate forests in this region. The current comparisons show that this conclusion needs to be revisited. In the absence of atmosphere-only simulations associated with the current AOGCM runs, it is not possible to say whether the differences between the models are already apparent in the atmospheric response to orbital forcing or are a consequence of differences in ocean feedbacks. However, even those models which show winter warming over Europe do not produce a warming large enough to reproduce the northward expansion of temperate forests shown by the observations. Thus, the conclusion that vegetation feedback is necessary to simulate mid-Holocene climate changes over Europe correctly is still likely to be true.

4.4 Evaluation of atmosphere –ocean –vegetation simulations

4.4.1   Results

4.4.1.1   Mean climate of climate system model

The GCMs simulations of ECHAM-MPIOM (AO) and ECHAM-MPIOM-LPJ (AOV) provide the diagnostic vegetation BIOME4 model with mean climate variables. The BIOME model simulates detailed vegetation distributions out of a combination of temperature, precipitation and cloudiness, so the results can be easily evaluated. As the BIOME model calculates with differences between a scenario run and the control run (anomaly procedure) to avoid model-specific noise effects, the climate changes with respect to changed boundary conditions, in this case the insolation, are separated and transformed into biome changes comparable with all other BIOME diagnosis. For that reason, BIOME4 simulations do not refer to the original state of the climate, produced by the climate system models and therefore a
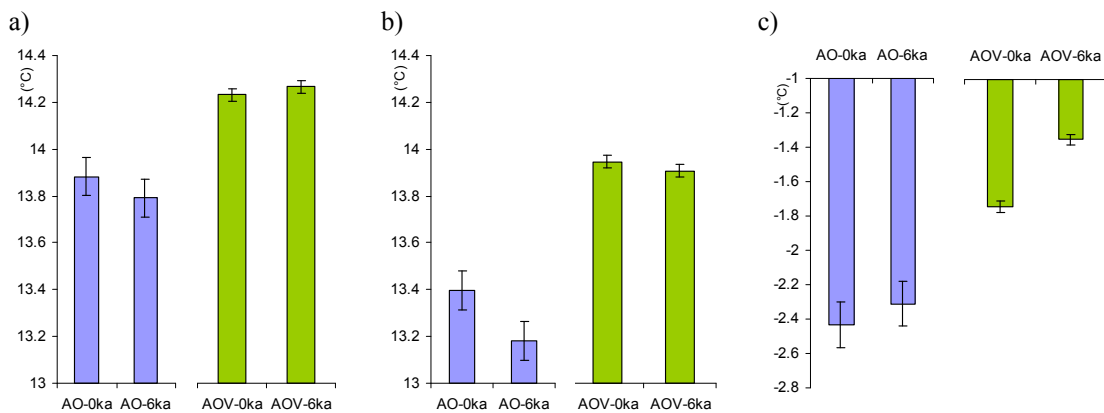

Figure 4-12: Comparison of the general mean temperature 2 m above ground computed by the AO (blue) and AOV (green) simulations for modern control and 6 ka. Separated for **a)** the entire globe except Antarctica, **b)** the global land mass and **c)** the land north of 40 °N. The error bars show the standard deviation derived from variability analyses for the modern control simulations.

brief outline of the basic climate input of the GCMs in the context of biome reconstructions is given.

For the climate input data the atmospheric simulation years 2247 – 2477 are averaged for the experimental set up: two runs with ECHAM-MPIOM for modern (AO-0ka) and mid-Holocene (AO-6ka) conditions and two with ECHAM-MPIOM-LPJ for modern (AOV-0ka) and mid-Holocene (AOV-6ka). The following analyses refer to bilinear interpolation from climate model T31 to BIOME model 0.5° grid resolution.

The computed global mean temperature (2 meter above ground) in the AO-0ka run is 13.88 °C and decreases by –0.09 °C in the AO-6ka run (Figure 4-12a). The AOV-0ka modern global mean temperature is +0.35 °C warmer than the AO-0ka run and increases further by +0.48 °C under the mid-Holocene conditions from AO-6ka to AOV-6ka. Regarding the global mean temperature over land only - respectively the land area prescribed in the BIOME4 model land mask excluding Antarctica, the mean temperature is reduced for all simulations. Without the grid cells of the ocean in both AO simulations (AO-0ka and AO 6ka) the temperature decrease for more than a half
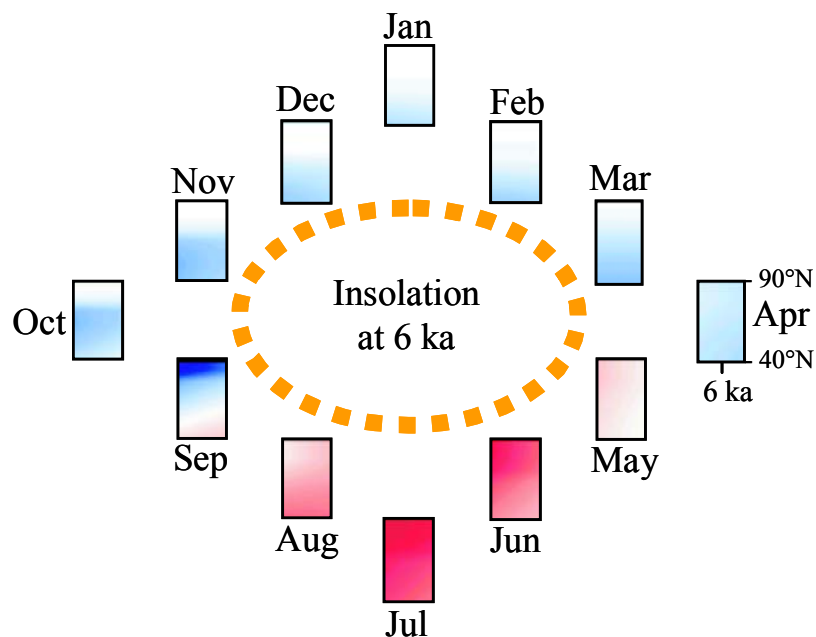

Figure 4-13: The annual receipt of insolation over the mid-Holocene period from 5.5 ka until 6.5 ka for the region north of 40 °N; modified from Bradley et al. 2002, Fig. 6-21.

°C. The AOV-0ka simulation decreases only about –0.29 °C, and –0.36 °C in the AOV-6ka run. Although in this case AOV-6ka is slightly colder than AOV-0ka, the difference to the AO runs is amplified and more pronounced for the 6 ka orbital forcing (Figure 4-12b). This already does emphasize the indirect positive feedbacks between ocean and vegetation. Restricting the land territory to the examination area of the Extratropics on the northern Hemisphere the mean temperatures of the simulations decrease for about 15.5 °C and reach freezing values (Figure 4-12c). Thus, the mid-Holocene orbital conditioned summer warming from May till August and cooling from September till April results in a mean warming over the year (Figure 4-13). Especially the AOV-6ka run increases the temperature by almost one degree (+0.96 °C) compared to the AO-6ka run, and by +0.4 °C compared to the AOV-0ka run. This increase from 0ka to 6ka for the simulations with dynamic vegetation is a significant signal with regard to standard deviation. Altogether the AOV model simulates a considerable warmer setting for the 0ka control run, which is ignored by the BIOME4 vegetation analyses in Chapter 4.4.1.3.

The mean annual temperature changes between AO-6ka and AO-0ka are located along the northern polar region, clearly spotted in the Barents Sea (Figure 4-15a left). There the Holocene conditions lead to an explicit heating of +4 °C and more. On the other hand the subtropical monsoon areas, notably the Sahel and West Sahara, are cooling due to increased cloudiness and annual precipitation (Figure 4-15b, c). The northern regions are not that affected by precipitation or cloudiness changes, but an enhanced drying signal along the equatorial Atlantic appears. This feature is confirmed by the AOV-6ka anomalies. Even though the African and Asian monsoon is more reinforced, northern Africa is clearly divided into east and west with explicit respect to the hot area of the Libyan Desert resulting in further warming. Moreover, the arctic sea shows increased temperatures as the entire extratropical northern Hemisphere does. This mean pattern of temperature development by the AOV-6ka run is already confirmed in the mainly orbital forced summer season (JJA, Figure 4-14). Note that at the region of the circum-Antarctic current shows an additional warming by +0.75 °C along the 60th latitude South in the Antarctic winter. Since the

AOV-6ka simulation produces a stronger annual warming than the AO-6ka run in this particular region (Figure 4-15a right) - far from any vegetation - it is not clear which effects of interactive vegetation lead to this signal.

Main differences between the two experimental sets prevail in the northern Hemisphere. The strong temperature increase over the Barents Sea in the AO simulation is not that distinct in the AOV run, although most of the sub-polar regions show an amplified warming, except the northern part of East Europe, probably influenced by the Barents Sea warming in the AO run. The increase of temperature in the Sahara is more amplified by the AOV simulation, even though in West Africa. And the 6ka signal along Kamchatka is reversed from cooling in the AO simulation to warming in the AOV simulation. The AOV model computes a decreased amount of precipitation over the East Pacific and the Central Atlantic, an area not affected by annual temperature changes. The differences of the annual mean fraction of sunshine between the two models are moderate compared to the changes between modern and 6ka. Only the dynamic vegetation induced modest enhanced cloudiness over large parts of Siberia and the monsoon regions of Africa and Asia are markable.

ΔAOV-6ka zonal temperature (°C)
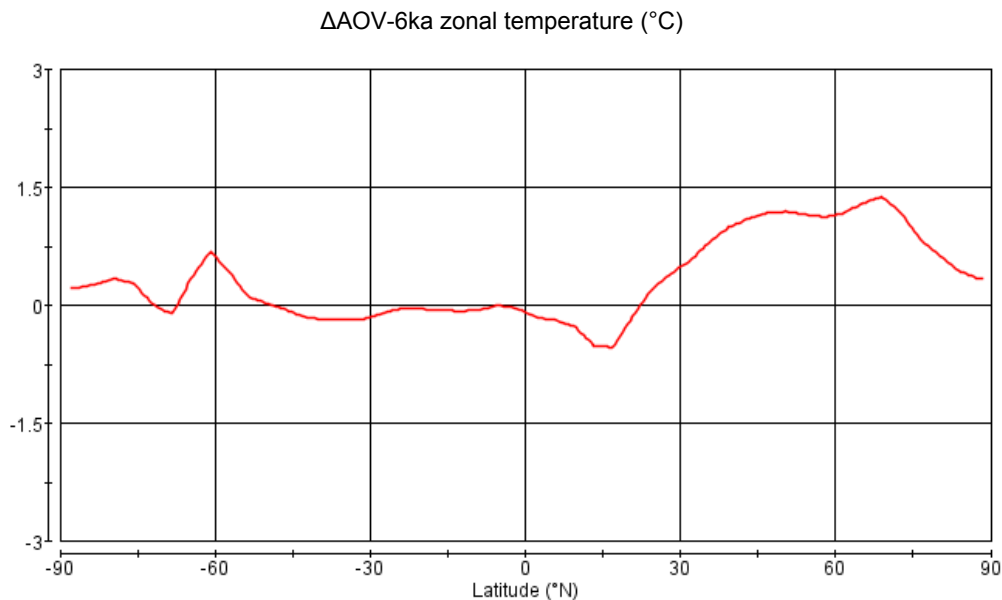
Figure 4-14: Changes of latitudinal mean temperature (°C) for AOV-6ka compared to AOV-0ka (ΔAOV-6ka) in the summer season (JJA).
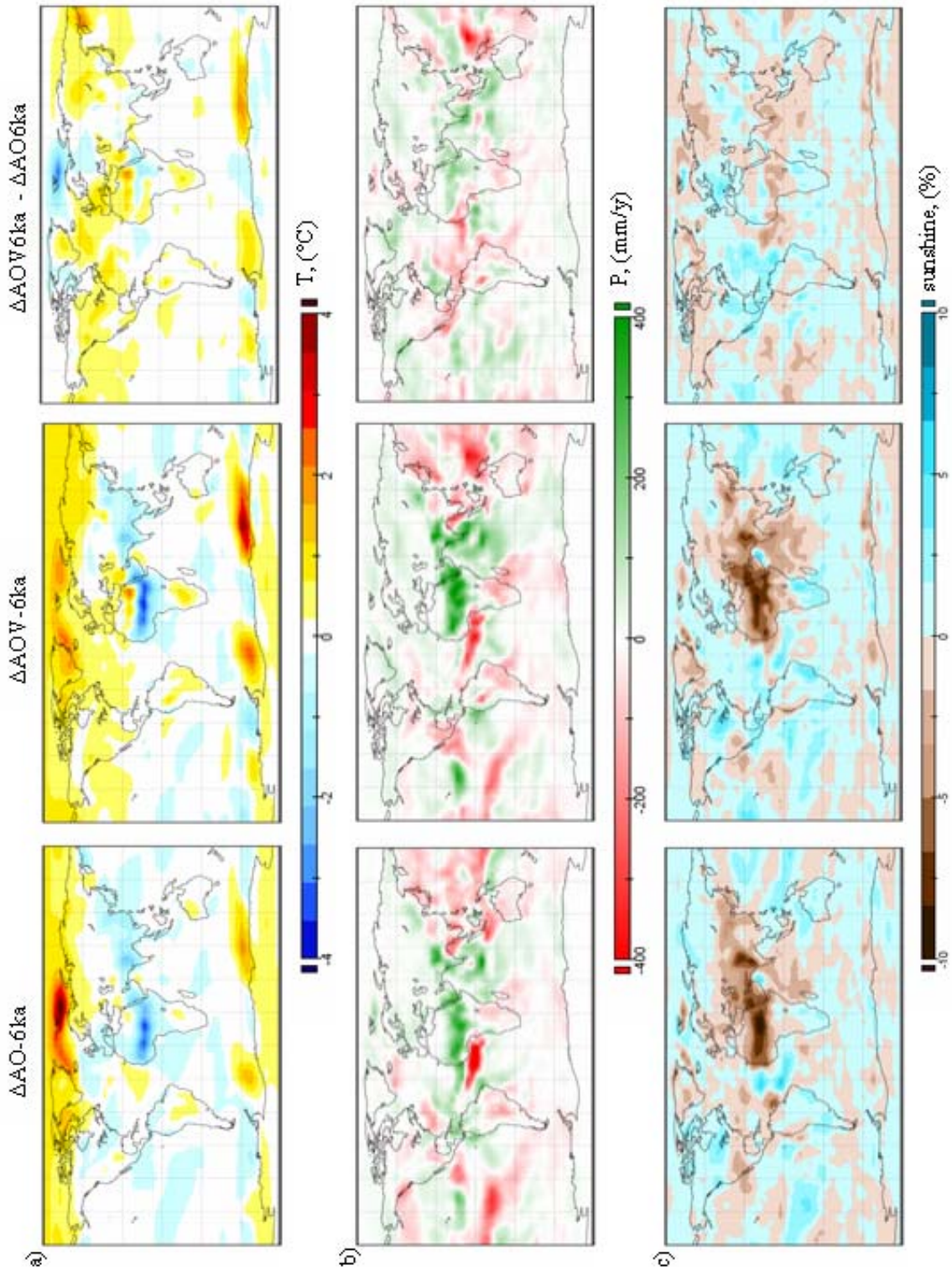
Figure 4-15: Comparison of the simulated changes between AO-6ka and AO-0ka (ΔAO-6ka, left), between AOV-6ka and AOV-0ka (ΔAOV-6ka, middle) and the differences between both changes (ΔAOV-6ka − ΔAO-6ka, right). Shown for the BIOME4 relevant climate variables of **a)** mean 2m temperature (°C), **b)** annual precipitation (mm/year) and **c)** the sunshine fraction (%).

4.4.1.2   Quantification of control analyses

As a baseline for the validation of ECHAM5-MPIOM simulations, with and without the interactive LPJ vegetation model, the standard control runs are taken to assess variations in the reconstruction of vegetation pattern. The intra-model variability of climate and the different simulation-time periods lead to differences in the input variables for the diagnostic BIOME4 simulation. This results to deviations in the resulting biome structure. Therefore a calculation of the variability for modern vegetation (0 ka) is used to define limits of minimum and maximum distribution of biome types, the standard deviation and correlations. Those indices are assigned to the modern standard BIOME4 values as adjustment and then referred to the original described simulation results.

All in all, 20 separate BIOME4 reconstructions are used for the analyses of climate indicated variations in plant distribution. Five sequent 50 year time periods of the AO simulation and the AOV simulation are averaged for monthly mean temperature, precipitation, and cloudiness and the yearly absolute minimum temperature. As the resolution of the ECHAM5-MPIOM climate simulations is T31, the climate variables are interpolated to the half grid resolution of the BIOME4 model. For technical reasons the common procedure is a bilinear interpolation to fit the climate and soil information in the calibrated BIOME4 standard simulation. In addition the same experiments are interpolated in a conservative grid-dividing way to get evidences about the climate model characteristics. Altogether four sets of five bilinear interpolated AO and five AOV model vegetation maps, plus five conservative interpolated AO and five AOV model vegetation maps are compared to determine the simulated biome variability.

So far the uncertainties of the biome distribution are usually not defined and this attempt with the BIOME4 model helps to diagnose sensitive vegetation types and significant changes.

Variability of vegetation area

For the assessment of the vegetation distribution in the northern Extratropics the global situation is considered. The global pattern reflects the general situation of which modelled vegetation communities are most sensitive to climate change. In all variability simulations the area of the entire forests is reduced compared to the BIOME4 standard simulation. Therefore the other vegetation groups of grass and tundra are increased (Figure 4-17a), wherein shrubs, desert and barren are counted for grass.

In general the global area that is recovered with differ vegetation, compared to the BIOME4 modern standard, is intensified in the AO model (Figure 4-16). Almost 25 % ($324*10^5$ km^2) of the global vegetation – divided into forest, grass and tundra – is affected. And for the biome classification this change is enlarged to 43 % reaching additional $66*10^5$ km^2 compared to the AOV simulations.
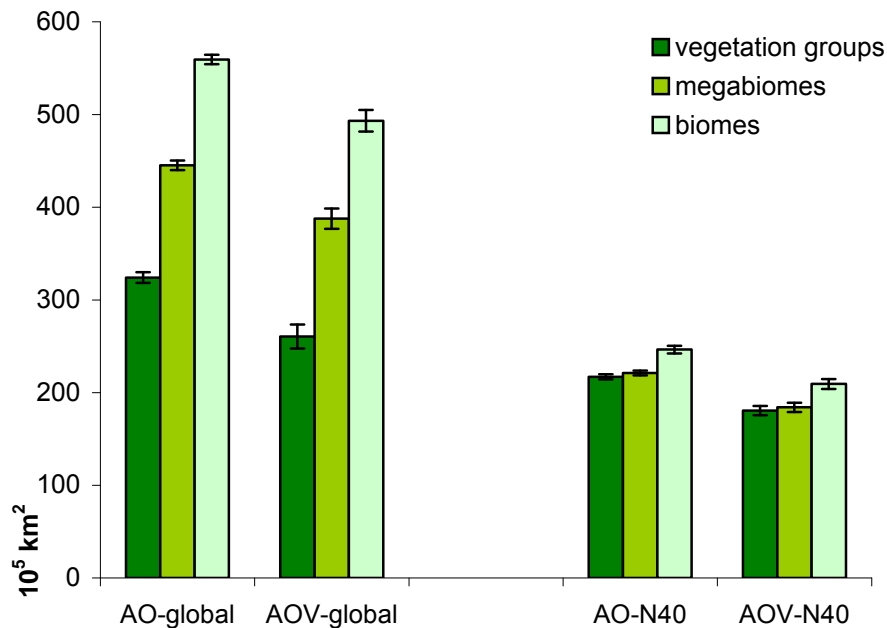
Figure 4-16: Total changes of vegetation area averaged over 5 runs for AO-6ka and AOV-6ka compared to BIOME4 modern standard for the classifications of vegetation groups, megabiomes and biomes in 10^5 km^2. Shown for global and the extratropical region north of 40 °N (N40).

North of 40 °N the intensified changes caused by high resolute classifications are clearly condensed. The relation of the changes for vegetation groups, towards biomes reveal a general difference of both models structure compared to the BIOME4 model standard, as the changes for the basic vegetation types are comparatively high (Figure 4-16 right).
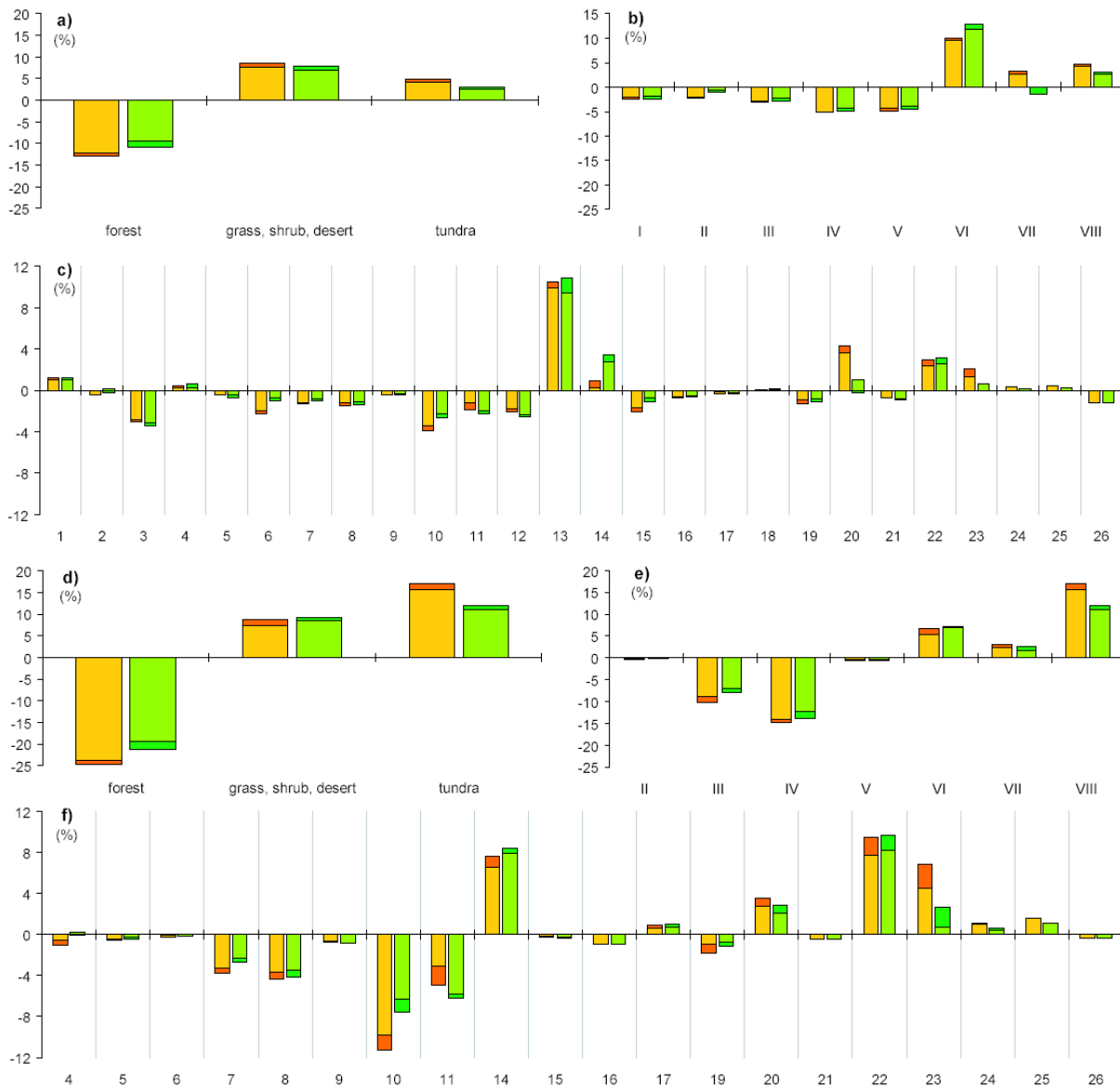
Figure 4-17: Differences of vegetation changes for 0 ka simulations compared to BIOME4 modern standard in (%). 1st bar = AO (orange) and 2nd bar = AOV (green). For each column the minimum and maximum values are shown. Global: **a)** vegetation groups, **b)** megabiomes and **c)** biomes, and north of 40 °N: **d)** vegetation groups, **e)** megabiomes and **f)** biomes. For legend numbers refer to Table 4-4.

The difference between the minimum and the maximum change (spread) within a set of simulations is used as an expression of variability limits. For the global vegetation distribution this spread is more pronounced in the AOV simulations. The spread of the general vegetation groups in the AOV simulation ranges from 0.4 % for tundra (Table 4-5) up to 1.5 % for forest in the bilinear interpolation compared to averaged 0.7 % in the AO simulations.

The AOV simulated forests are less reduced by ca. 3 % in contrast to the AO simulation (Figure 4-17a). This is mainly related to the warm-temperate forest and the

Table 4-5: Variation of changes of biome distribution related to (%) of BIOME4 standard area. The range between the maximum and the minimum value of the simulations is described as spread. The standard deviation relates to the five simulations each. The numbers in front of the vegetation classification are used as legend for Figure 4-17.

| biome variability	global				N of 40 °N			
	AO 0k		AOV 0k		AO 0k		AOV 0k	
	spread	deviation	spread	deviation	spread	deviation	spread	deviation
vegetation groups								
forest	0.7	0.2	1.5	0.5	0.9	0.3	1.7	0.6
grass, shrubs and desert	0.9	0.3	1.0	0.4	1.4	0.5	0.8	0.3
tundra	0.5	0.2	0.4	0.2	1.4	0.5	0.9	0.3
megabiomes								
I tropical forest	0.4	0.2	0.5	0.2	-	-	-	-
II warm-temperate forest	0.3	0.1	0.4	0.1	0.2	0.1	0.2	0.1
III temperate forest	0.3	0.1	0.5	0.2	1.3	0.5	0.9	0.3
IV boreal forest	0.2	0.1	0.7	0.2	0.6	0.2	1.6	0.6
V savanna	0.6	0.2	0.4	0.1	0.3	0.1	0.3	0.1
VI grass	0.6	0.2	0.9	0.4	1.2	0.4	0.4	0.1
VII desert	0.6	0.2	1.3	0.5	0.8	0.3	0.8	0.3
VIII tundra	0.5	0.2	0.4	0.2	1.4	0.5	0.9	0.3
biomes								
1 tropical evergreen broadleaf forest	0.2	0.1	0.2	0.1	-	-	-	-
2 tropical semi-deciduous broadleaf forest	0.1	0	0.3	0.1	-	-	-	-
3 tropical deciduous broadleaf forest & woodland	0.2	0.1	0.2	0.1	-	-	-	-
4 temperate deciduous broadleaf forest	0.2	0.1	0.3	0.1	0.5	0.2	0.3	0.1
5 temperate evergreen needleleaf forest	0.3	0.1	0.3	0.1	0.2	0.1	0.1	0
6 warm-temperate evergreen broadleaf mixed forest	0.3	0.1	0.4	0.1	0.2	0.1	0.2	0.1
7 cool mixed forest	0.1	0.1	0.2	0.1	0.4	0.2	0.3	0.2
8 cool evergreen needleleaf forest	0.2	0.1	0.2	0.1	0.7	0.3	0.7	0.2
9 cool-temperate evergreen needleleaf mixed forest	0	0	0	0	0.1	0	0.1	0
10 cold evergreen needleleaf forest	0.5	0.2	0.4	0.2	1.5	0.5	1.3	0.4
11 cold deciduous forest	0.6	0.2	0.2	0.1	1.8	0.6	0.4	0.2
12 tropical savanna	0.3	0.1	0.2	0.1	0	0	0	0
13 tropical xerophytic shrubland	0.6	0.2	1.5	0.6	0	0	0	0
14 temperate xerophytic shrubland	0.6	0.2	0.7	0.2	1.1	0.4	0.5	0.2
15 temperate sclerophyll wood & shrubland	0.3	0.1	0.4	0.1	0.1	0	0.1	0.1
16 temperate deciduous broadleaf savanna	0.1	0	0.1	0	0.0	0	0.0	0
17 temperate evergreen needleleaf open woodland	0.1	0	0.1	0	0.3	0.1	0.3	0.1
18 tropical grassland	0	0	0.1	0	0	0	0	0
19 temperate grassland	0.4	0.1	0.3	0.1	0.9	0.3	0.3	0.1
20 desert	0.6	0.2	1.3	0.5	0.8	0.3	0.8	0.3
21 graminoid & forb tundra	0	0	0.2	0.1	0	0	0.1	0
22 low & high shrub tundra	0.6	0.2	0.5	0.2	1.7	0.6	1.5	0.5
23 erect dwarf-shrub tundra	0.8	0.3	0.7	0.2	2.3	0.8	1.9	0.6
24 prostrate dwarf-shrub tundra	0.1	0	0.1	0	0.2	0.1	0.2	0.1
25 cushion-forb tundra	0	0	0	0	0.1	0	0	0
26 barren	0	0	0	0	0	0	0	0

boreal forest megabiomes (Figure 4-17b-II-IV), being more equivalent to the BIOME4 standard under the climate conditions with interactive vegetation. The AO simulations create dryer regions in the mid-continents preferred by grasses witch are more deserted, and a cooler arctic zone with expanded tundra regions.

By analysing the effect of bilinear and conservative interpolation no structural differences between the modes of data interpolation show up. Even if the bilinear runs of the AO model generate more forest and less grass than the conservative runs for the global situation, this pattern vanishes at the region north of 40 °N and is generally not valid for the AOV runs. Therefore the distinction by bilinear and conservative interpolation is neglected in the following analyses.

Variability of megabiomes

On the subject of the megabiome classification the spread of AOV runs show a higher variation for the global estimates, especially for the calculation of boreal forests and deserts (Table 4-5). This higher variability of AOV simulated boreal forests is associated with some less decreases (Figure 4-17b-IV) compared to BIOME4 standard. And the distinct higher variability for AOV simulated desert derives from an ambiguous signal from reduced to slightly increased area within the set of five runs (Figure 4-17b-VII).

Restricted to the area north of 40 °N the displacement of tree communities by non-woody plants (Figure 4-17d) illustrates the composite dryer and northern-cool conditions compared to BIOME4 standard. This reflects the limited development of temperate- and boreal forests in both models with fewer changes in the AOV version (Figure 4-17e-II-III). Especially the 5 % differ of change between AO and AOV tundra (Figure 4-17e-VIII) by a maximum spread of 1.4 % (Table 4-5) reflects clearly warmer polar conditions by additional dynamic vegetation. The zone of moisture ruled transition from forest to grass is prescribed as savannas, and in this case the two ECHAM5-MPIOM models left this particular megabiome unchanged in the amount

of area (Figure 4-17e-V) even the zone of savanna vegetation is partly shifted. This result indicates that the climate conditions of ECHAM-MPIOM simulate cooler and dryer environments but keeps the climatic gradients reliable and comparable with the initial situation of the BIOME4 standard.

Variability of biomes

Regarding the variability of global vegetation reconstruction in case of the high resolution of 26 biome types, the AOV simulations have high spreads in the prediction of tropical xerophytic shrubland and desert (Figure 4-17c 13+20, Table 4-5). It is apparent that this higher variability is connected with the increasing number and competition of vegetation classes. Globally however, the ca. 10 % increase of tropical xerophytic shrubland area represents a quarter of the total change of $493*10^5$ km^2 measured up to BIOME4 standard (Figure 4-16). The variability of desert is more than doubled for the AOV simulations compared to the AO runs, even though the area changes are minimized. These ambiguous values for AOV desert due to one exceptional result of the AOV runs.

North of 40 °N tropical xerophytic shrubland is not existent. The spread of desert is unique for both models, but amplified for the two boreal forest biomes; the low & high shrub tundra and the erect dwarf-shrub tundra (Table 4-5, Figure 4-17f 10-11-20-

Table 4-6: Mean correlation for the average of five bilinear interpolated simulations for the modern control runs of the ECHAM-MPIOM (AO-0ka) and the ECHAM-MPIOM-LPJ model (AOV-0ka) compared to the BIOME4 modern standard. Shown for the global vegetation and for the region north of 40 °N, with *n* equal the total area in km^2.

mean correlation		AO-0ka	AOV-0ka
global	*n = 129985539.31*		
	vegetation groups	0.878	0.920
	megabiomes	0.788	0.794
	biomes	0.855	0.854
N of 40° N	*n = 44420588.17*		
	vegetation groups	0.911	0.996
	megabiomes	0.723	0.821
	biomes	0.804	0.851

22-23). The generally higher global variability of the AOV model is not confirmed north of 40 °N as the spreads of the AO model are clearly increased.

Main differences of biome area changes between the two models arise in the opposing strength of the reduction of the two boreal forest types – cold evergreen needleleaf forest and cold deciduous forest – and the increase of erect dwarf-shrub tundra (Figure 4-17f 10-11-23). Beside these obvious results, the AOV runs simulate larger areas of temperate deciduous broadleaf forest, cool mixed forest, and cool evergreen needleleaf forest compared to AO runs resulting by lower reduction. Furthermore the area of temperate xerophytic shrubland is increasing (Figure 4-17f 4-7-8-14).

The mean correlation of predicted biome area between ECHAM-MPIOM and ECHAM-MPIOM-LPJ with the BIOME4 modern standard points out, that the AOV simulations are closer related to the global vegetation distribution of natural potential vegetation (ρ = 0.920) than the AO simulations (ρ = 0.878, Table 4-6). The high correlation is strongly affected by the high number of n = 129˙985˙539 km^2; equivalent to the entire global land mask in km^2, excepting the fixed area of glaciers, ice sheets and Antarctica.

Even better correlations are reached by the AOV simulations in the region north of 40 °N than those without interactive vegetation. As expected, the coarse structure of summarized vegetation groups implicates highest correlation referring to the land area of n = 44˙420˙588 km^2 (Table 4-6). For the classification of megabiomes the mean correlation with modern standard declines clearly. However, further partition into biome types improves the correlation again, especially for the AO simulations. The neglecting of tropical vegetation types intensifies the differences between the models and supports the reconstruction by the AOV model.

A comparison of the divergence of changes between each individual simulation gives evidence about the potentially strength of the differences in the simulations. The change of vegetation-groups measured against the overall averaged change in all AO

and AOV simulations shows a clear global division (Figure 4-18a). The AO runs strictly simulate less forest and more tundra than the AOV runs. The change for the group of grass (combined with shrub and desert) is not straightforward. In both sets one run reaches values within the range of the other model. This indicates that the area of grass could potentially simulated equal in both models. The higher global variability of the AOV simulations is emphasised by the dissimilar result of the simulation AOV-3 and AOV-4.

In the Extratropics the changes for the tundra and the forest group are model specific significant, less dispersed in strength and similar to the global trend (Figure 4-18b). Likely to the global estimation the differences in simulated grass area are not significant. However, in the region north of 40 °N the AOV model preferably predicts dry types of vegetation in contrast to the global trend.
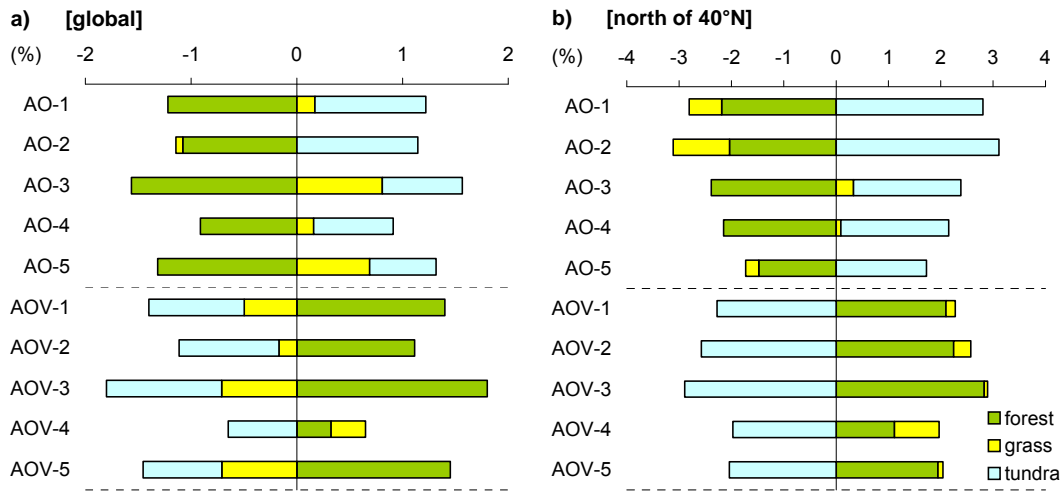
Figure 4-18: Differences of changes against the average change of all ten simulations by each single run for **a)** global and **b)** restricted to the extratropical region north of 40 °N for vegetation groups.

Variability of the data-model comparison

The estimation of the accuracy and quality of the simulations is based on the Biome6000/PAIN pollen data set. This enables a comparison of simulated grid-cell vegetation with the spatial corresponding data point. Altogether 5457 field sites are in

disposition to verify the potential modern vegetation in the region north of 40 °N. It points out that the biome reconstructions from the AOV simulations coincide better than those from the AO simulations (+3.1 %, Figure 4-19).

Examine the Extratropics in single latitudinal bands this result confirms as a robust signal. For the polar region north of 70 °N the coupled vegetation runs reach a consistency of 32.2 % to 35.6 % – an evident progress of +18 % compared to the AO runs. The apparent mismatches of the AO simulations arise from a consistent replacement of prostrate dwarf-shrub tundra where the observations declare the warmer preferring erect dwarf-shrub tundra biome. Obviously the AO and AOV experiments reveal an equal spread of differences between minimum and maximum agreement (3.4 %) besides the different matching. In the boreal band from 60 – 70 °N the AOV simulations reach a significant better match with respect to the standard deviation of 1.5 % (Table 4-7), whereas in the temperate region from 40 – 60 °N the

Figure 4-19: Estimation of simulation-observation agreement of the ECHAM5-MPIOM (AO-bil) and the ECHAM5-MPIOM-LPJ (AOV-bil) model showing the spread from minimum to maximum for t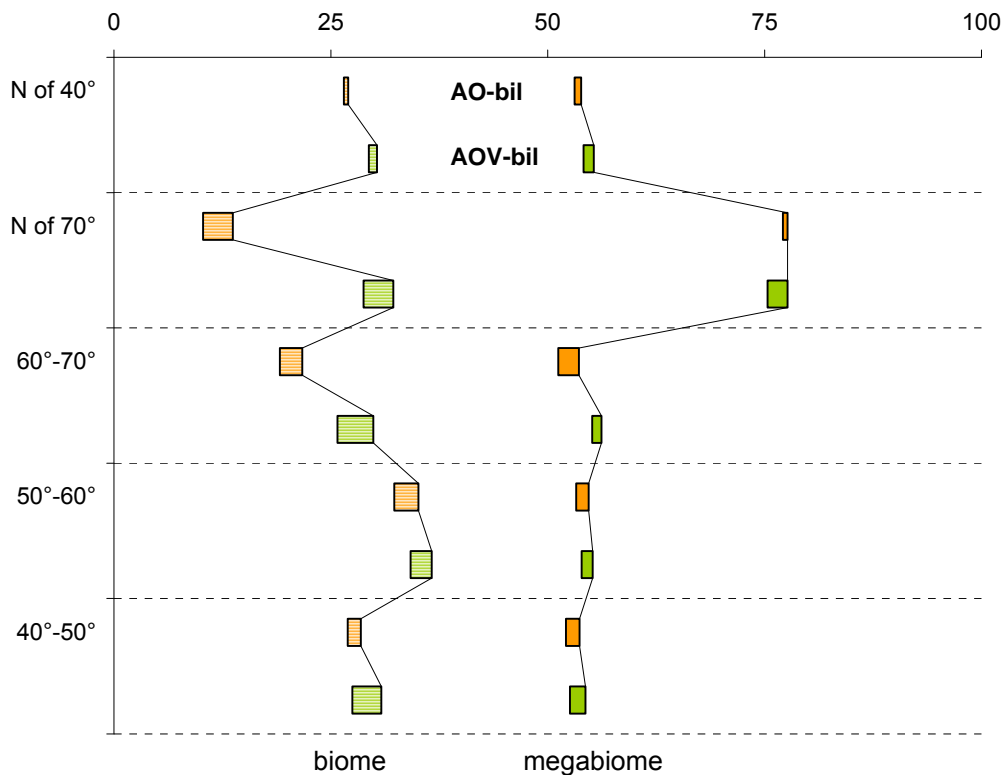he biome (striped) and megabiome classification in (%). Further separated into latitude bands. For visualization the maximum values are connected with a line.

better agreement of AOV simulated biomes is almost achieved by the AO simulations. However, the best results for biome comparison of all experiments are situated in the region from 50 – 60 °N. Only in this latitudinal band the spread and deviation of matches by the AOV simulations is narrowed. The comparatively low improvement of AOV against AO reconstructions for the entire study region compared to the single band qualities arise basically from the asymmetric distribution of the field data locations. A prevailing mass of 4003 data points are situated south of the 60th northern latitude which equivalents ¾ of all data.

For the aspect of megabiome classification the matches exceed 50 % agreement. Likewise the biomes are summarized, the results are compressed and adjusted but again the AOV reconstructions are superior (+1.5 %). In the polar region north of 70 °N especially high matches up to 77.4 % are reached. This contrasts the results from the biome classification and particular the AO runs improve about 64 % for the maximum and 67 % for the minimum limits, respectively. The reason for this exceptional increase consists in a tremendous intra-tundra misinterpretation for the biome classification and in addition to that, for the megabiome classification the

Table 4-7: Comparison of the standard deviation for biomes and megabiomes by the assessment of simulation with observed data agreement for the Extratropics within the experimental set of five runs each. Further divided into latitudinal bands and the overall Kappa statistics below.

Standard deviation of simulation-observation-estimation		AO-0ka	AOV-0ka
biomes	**N of 40° N**	**0.20**	**0.31**
	N of 70° N	1.41	1.59
	60°-70° N	1.14	1.54
	50°-60° N	1.02	0.90
	40°-50° N	0.65	1.22
megabiomes	**N of 40° N**	**0.33**	**0.39**
	N of 70° N	0.00	0.82
	60°-70° N	0.83	0.40
	50°-60° N	0.63	0.50
	40°-50° N	0.58	0.70
Kappa statistics		0.394	0.406

simulations predict solely tundra in all corresponding grid-cells. Therefore all observed tundra data points (113 out of 146) match with the simulation with one exceptional AOV run simulating three fault boreal forest grid-cells. The remaining 22.6 % of mismatches refer to tundra oversimulation located at boreal forest observations.

The average of the Kappa statistics (Monserud 1990) for the sets of five simulations ranges around $k = 0.4$ for the megabiome classification for both models (Table 4-7, bottom). This value can be assessed as a fair degree of quality. The Kappa statistics contain the complete comparable data set of each simulation. However, the bilinear AOV simulations associate slightly better with the Biome6000/PAIN data map.

Although there is a tendency of higher variability due to the coupling of atmosphere and ocean models with dynamic vegetation, the results of the AOV model are improved compared to the AO simulations with respect to the modern potential vegetation of the BIOME4 model and the Biome6000/PAIN observations. As these analyses are realised by the straight diagnostic of the climate models output and not by the common anomaly procedure, the results do not analogous the following validation of simulations for the mid-Holocene scenario (Chapter 4.4.1.3), but do refine statements about significant changes and supports the quality of the model evaluation.

4.4.1.3 Distribution of biome vegetation at 6 ka

A diagnostic simulation of vegetation characterises combinations of climate parameters. Vice versa complex climate changes produce lucid changes in vegetation distribution. In case of the following analyses, the ECHAM5-MPIOM-LPJ (AOV) climate system model is a new and improved version compared to the ECHAM3.2-LSG (ECHAM3) model, which was part of the evaluation in Chapter 4.3. The model results are different in their climate based reconstructions of vegetation but not in

Table 4-8: Simulated vegetation distribution in (%) for the global area ($129*10^5$ km^2) and for north of 40 °N ($44*10^5$ km^2). Results of three different vegetation classifications for the BIOME4 modern standard simulation (BIOME4-mod), the previous ECHAM3-LSG (ECHAM3), the ECHAM5-MPIOM (AO-6ka) and ECHAM-MPIOM-LPJ (AOV-6ka) simulations for the mid-Holocene.

biome area distribution	global				N of 40°N			
	B4-mod	ECHAM3	AO-6ka	AOV-6ka	B4-mod	ECHAM3	AO-6ka	AOV-6ka
vegetation groups								
forest	48.4	49.0	49.3	48.9	67.2	66.4	67.0	66.0
grass, shrubs and desert	44.7	45.7	45.3	45.7	17.3	22.5	21.9	23.0
tundra	6.9	5.3	5.4	5.4	15.5	11.1	11.1	11.0
megabiomes								
I tropical forest	16.4	16.7	17.5	17.4	-	-	-	-
II warm-temperate forest	12.9	13.6	12.1	12.0	0.6	0.7	0.7	0.6
III temperate forest	4.9	5.4	4.6	4.8	27.2	28.8	23.9	24.5
IV boreal forest	14.2	13.3	15.2	14.7	39.4	36.9	42.4	40.9
V savanna	10.8	9.7	10.2	10.5	1.7	1.8	1.5	2.1
VI grass	19.5	22.8	23.8	25.2	11.9	17.3	17.3	17.7
VII desert	14.4	13.3	11.3	10.0	3.8	3.3	3.1	3.1
VIII tundra	6.9	5.3	5.4	5.4	15.5	11.1	11.1	11.0
biomes								
1 tropical evergreen broadleaf forest	6.4	6.1	6.2	6.5	-	-	-	-
2 tropical semi-deciduous broadleaf forest	3.7	3.9	3.6	3.7	-	-	-	-
3 tropical deciduous broadleaf forest & woodland	6.3	6.7	7.7	7.3	-	-	-	-
4 temperate deciduous broadleaf forest	3.5	5.1	4.1	3.9	5.4	9.5	6.4	6.6
5 temperate evergreen needleleaf forest	1.8	2.0	1.9	1.8	1.5	1.9	1.6	1.3
6 warm-temperate evergreen broadleaf mixed forest	4.9	5.4	4.6	4.8	0.6	0.7	0.7	0.6
7 cool mixed forest	3.9	3.1	3.3	3.2	10.3	8.2	8.9	8.6
8 cool evergreen needleleaf forest	3.2	3	2.3	2.7	8.9	8.3	6.4	7.4
9 cool-temperate evergreen needleleaf mixed forest	0.5	0.5	0.4	0.4	1.1	0.9	0.7	0.6
10 cold evergreen needleleaf forest	10.9	9.2	11.1	11.0	30.3	25.3	30.8	30.6
11 cold deciduous forest	3.3	4.1	4.2	3.7	9.1	11.6	11.6	10.3
12 tropical savanna	6.6	5.8	6.0	6.4	0	0	0	0
13 tropical xerophytic shrubland	9.7	11.1	11.2	12.5	0.0	0.0	0	0.0
14 temperate xerophytic shrubland	5.9	5.9	7.0	6.8	4.7	5.5	5.8	5.4
15 temperate sclerophyll wood & shrubland	2.6	2.6	2.8	2.6	0.4	0.5	0.4	0.6
16 temperate deciduous broadleaf savanna	0.8	0.7	0.7	0.9	1.1	1.1	0.9	1.3
17 temperate evergreen needleleaf open woodland	0.8	0.6	0.8	0.8	0.2	0.2	0.2	0.2
18 tropical grassland	0.1	0.1	0.2	0.2	0	0	0	0
19 temperate grassland	3.7	5.7	5.4	5.6	7.1	11.8	11.5	12.3
20 desert	13.3	12.9	10.7	9.4	3.3	3.2	2.8	2.9
21 graminoid & forb tundra	1.1	0.9	1.0	0.9	0.5	0.4	0.6	0.5
22 low & high shrub tundra	3.6	3.0	3	2.9	9.5	7.3	7.6	7.3
23 erect dwarf-shrub tundra	1.7	1.1	1.1	1.2	4.3	2.6	2.3	2.6
24 prostrate dwarf-shrub tundra	0.3	0.3	0.2	0.2	0.9	0.6	0.4	0.5
25 cushion-forb tundra	0.2	0.1	0.1	0.1	0.4	0.2	0.1	0.2
26 barren	1.1	0.4	0.6	0.6	0.4	0.2	0.3	0.3

their tendencies of the mean signals. In agreement with the observations, the mid-Holocene boundary conditions cause certain features like the reduction of tundra, an increase of xerophytic grass types and the shifting of forest communities.

Biome area analyses

Altogether the simulations separate the global vegetation into approximately equal distributed areas of grass and forest groups. However the tundra types, relevant for the snow cover albedo feedback, are inferior on a global scale – merely 7 % of the terrestrial modern vegetation (Table 4-8 top). Under mid-Holocene conditions tundra decreases in addition to that by ca. -1.5 % at the expense of forest and grass types. Here, the ECHAM5-MPIOM simulation (AO-6ka) generates forest the most. Concerning the classification of megabiomes, xerophytic grass and tropical forest dominate the terrestrial landscape. Interactive vegetation (AOV-6ka) within the model led xerophytic grass increase about +5.7 % (Table 4-8 middle) – representing a quarter of the global vegetation ($32*10^6$ km^2). This supposed signal of moisture limitation is contributed by the increase of tropical and temperate shrublands, but the synchronously reduction of desert areas rather implies contradicted augmentation of humidity.

In the region north of 40 °N the tropical grass and shrublands are not existent and most of the desert areas are limited, whereas tundra types are more pronounced instead. Forest types dominate and occupy almost 70 % of the extratropical habitats. The amount of tree sufficient area analogous twice the area of summarised savanna, grass, desert and tundra types (Table 4-8 down). The AO-6ka simulation, rather than the forest decreasing AOV-6ka run, keeps the amount of forests equivalent to the modern situation. Main changes in the Extratropics concern the non-woody vegetation – more precisely a unique and substantial decrease of tundra for all simulations (-4.4 %, Table 4-8) whereas an increase of xerophytic grass appears. The boreal forest represents an evidently enlarged area computed by the AO-6ka and the AOV-6ka model in contrast to ECHAM3 (Figure 4-20a). This primarily takes place

in mid-continental regions in competition to southern vegetation (temperate forest in southern Canada and temperate forest and grassland along the southern margin of Siberia) instead of further pole-wards receding tundra. Even though temperate forest decrease and boreal forest increase compared to the BIOME4 standard, the AO-6ka expands the boreal forests area compared to AOV-6ka favouring the temperate forest (Table 4-8). The distinct magnification of the temperate deciduous broadleaf forest biome in ECHAM3 is not reflected by the AO-6ka or by AOV-6ka simulations (Figure 4-20b). Analogues to previous simulations, the temperate grassland benefits most by mid-Holocene climate change preferring drier interior environments with some summer rain for short time water supply in the topsoil layer. This feature of moisture disturbance in the temperate regions between 40 - 60 °N is more affected by

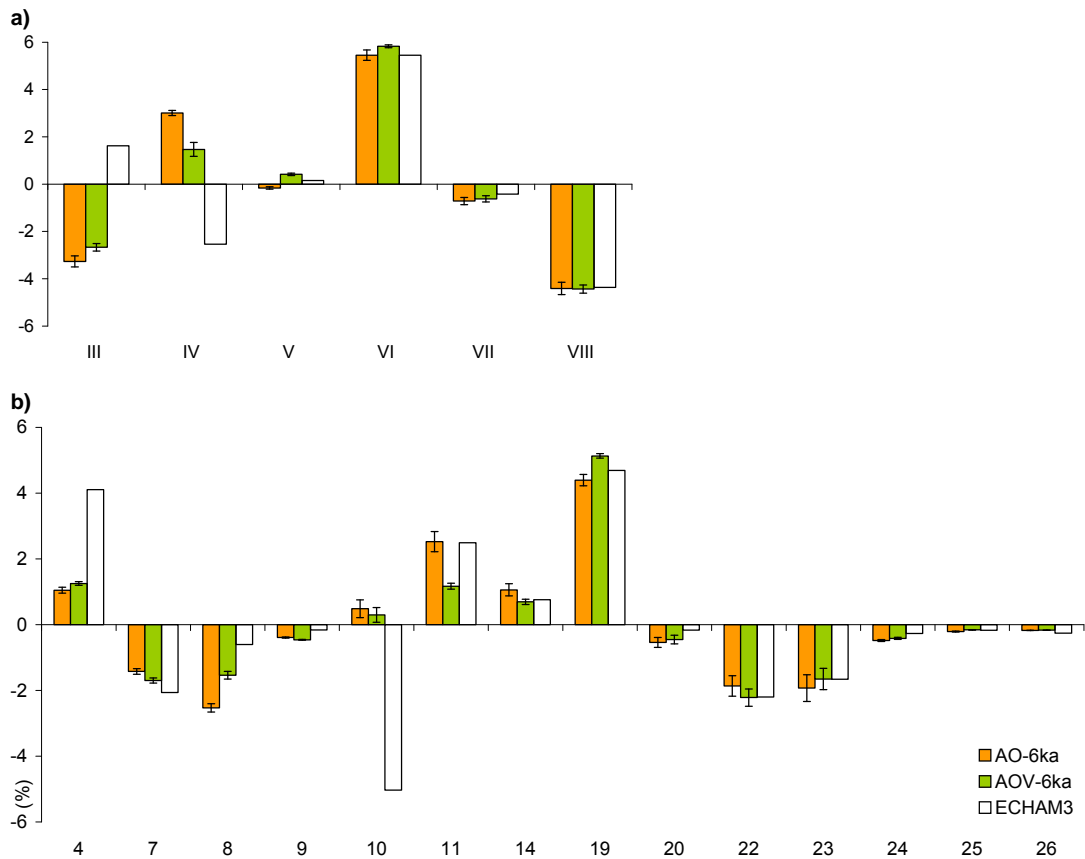**Figure 4-20**: Simulated changes of area compared to BIOME4 modern potential vegetation north of 40 °N in (%). Comparison **a)** illustrates changes in biome and **b)** changes in megabiome classification. The appropriate axis legends are given in Table 4.4-1 and the error bars show the standard deviation for AO-6ka and AOV-6ka derived from AO-0ka and AOV-0ka variability analyses (Table 4-8).

the atmosphere than by the ocean response, causing a reduction of summer precipitation, further enhanced by dynamic vegetation feedbacks and additional synergies. The most common low & high shrub tundra, just like the erect dwarf-shrub tundra are reduced evidently, consigning a tree-suitable prolongation of the growing season (GDD_0) mainly influenced by ocean heat storage in autumn. A majority of the differences between AO-6ka and AOV-6ka changes are significant with respect to the individual standard deviations, except the change of common tundra biomes (Figure 4-20b22-23). The large standard deviations of tundra types are caused by the high variability derived by the analyses for biome variability of the control simulations (Table 4-8) with intra-tundra types exchanges.

Differences in megabiomes

For assessing the biome distribution for 6 ka more precisely the range between lost and new recovered area in relation to net changes and the direction of substitution is analysed. Such a validation of migration patterns serves detailed features of climate induced vegetation changes.

More area of the dominant boreal forest megabiome in the modern BIOME4 simulation is confirmed by the 6ka run of the AO rather than by the AOV simulation.

Table 4-9: Matrix of megabiomes simulated for 6 ka replacing BIOME4 potential modern megabiomes in (10^3 km^2) for north of 40 °N. Read column; 6ka Simulation megabiome is replacing x km^2 of modern BIOME4 megabiome.

(10^3 km^2)	6ka simulation						
AO-6ka replaces	warm-temperate forest	temperate forest	boreal forest	savanna	grassland	desert & barren	tundra
warm-temperate forest	0	27.7	0	25.3	2.3	0	0
temperate forest	98.2	0	658.6	140.3	1419.7	68.8	0
boreal forest	0	671.3	0	0	824.7	29.2	22.3
savanna	0	167.0	0.0	0	103.4	0.0	0
grassland	0	83.2	206.7	31.1	0	116.3	0
desert & barren	0	6.9	4.2	2.4	470.9	0	42.3
tundra	0	0	1994.1	0	1.3	0	0
AOV-6ka replaces	warm-temperate forest	temperate forest	boreal forest	savanna	grassland	desert & barren	tundra
warm-temperate forest	0	3.8	0	34.4	0	0	0
temperate forest	48.3	0	261.7	281.3	1567.8	71.1	0
boreal forest	0	869.1	0	0	903.3	35.4	10.4
savanna	0	46.3	0	0	92.6	0	0
grassland	0	142.6	205.0	2.3	0	129.4	0
desert & barren	0	0	2.1	2.4	463.8	0	42.3
tundra	0	0	1990.3	0	1.3	2.1	0

In addition to this unchanged area the AO-6ka boreal forest reaches a higher gain of new covered area by replacing other megabiomes (Figure 4-21a). As a consequence the increase of AO-6ka predicted boreal forest (+3 %) is double those of the AOV-6ka run (+1.5 %, Figure 4-20bIV). Analysing the individual substitution of modern megabiomes by predicted megabiomes for 6 ka, the AO-6ka simulated boreal forest replaces $1994*10^3$ km^2 of colder-type modern tundra area and $658*10^3$ km^2 of warmer-type modern temperate forest (Table 4-9). In contrast to that, AOV-6ka boreal forest occupies the same amount of tundra area ($1990*10^3$ km^2) but only $261*10^3$ km^2 of temperate forest. This implies that boreal forest equally extends northward in both models but AO-6ka boreal forest also extends southward, while AOV-6ka boreal forest shifts northward at the southern border of distribution, too. The gain of tundra by replacing boreal forest – little enlarged in the AO-6ka run – is neglect able.

However, the AO-6ka boreal forest gains supplementary more area from warmer forest types compared to AOV-6ka. This feature is supported by a strengthened distribution of warmer types like the temperate forest extending into cold modern boreal forest area in the AOV-6ka run. This indicates a shortening of the winter season (GDD_5 >1200, Table 2-1) in the AOV simulation by vegetation feedbacks and additionally an increase of the mean temperature of the coldest month (MTCO) by amplified ocean feedbacks enhanced by synergistic effects through dynamic vegetation.

The mid-Holocene change in radiation provides climate conditions that favour broad extensions of dry and xerophytic vegetation in the mid-latitudes (Figures 4-20aVI, 4-22). In the AOV-6ka simulation the gain for the grass megabiome is higher compared to the gain for boreal forest, whereas the AO-6ka donates both megabiomes equally (Figure 4-21aIV-VI). Nevertheless, the change of boreal forest is evidently minor (Figure 4-20a) because the lost area for grass is 28 % (AO-6ka) respectively 26 % (AOV-6ka) of the strong loss of boreal forest, only (Figure 4-21a).
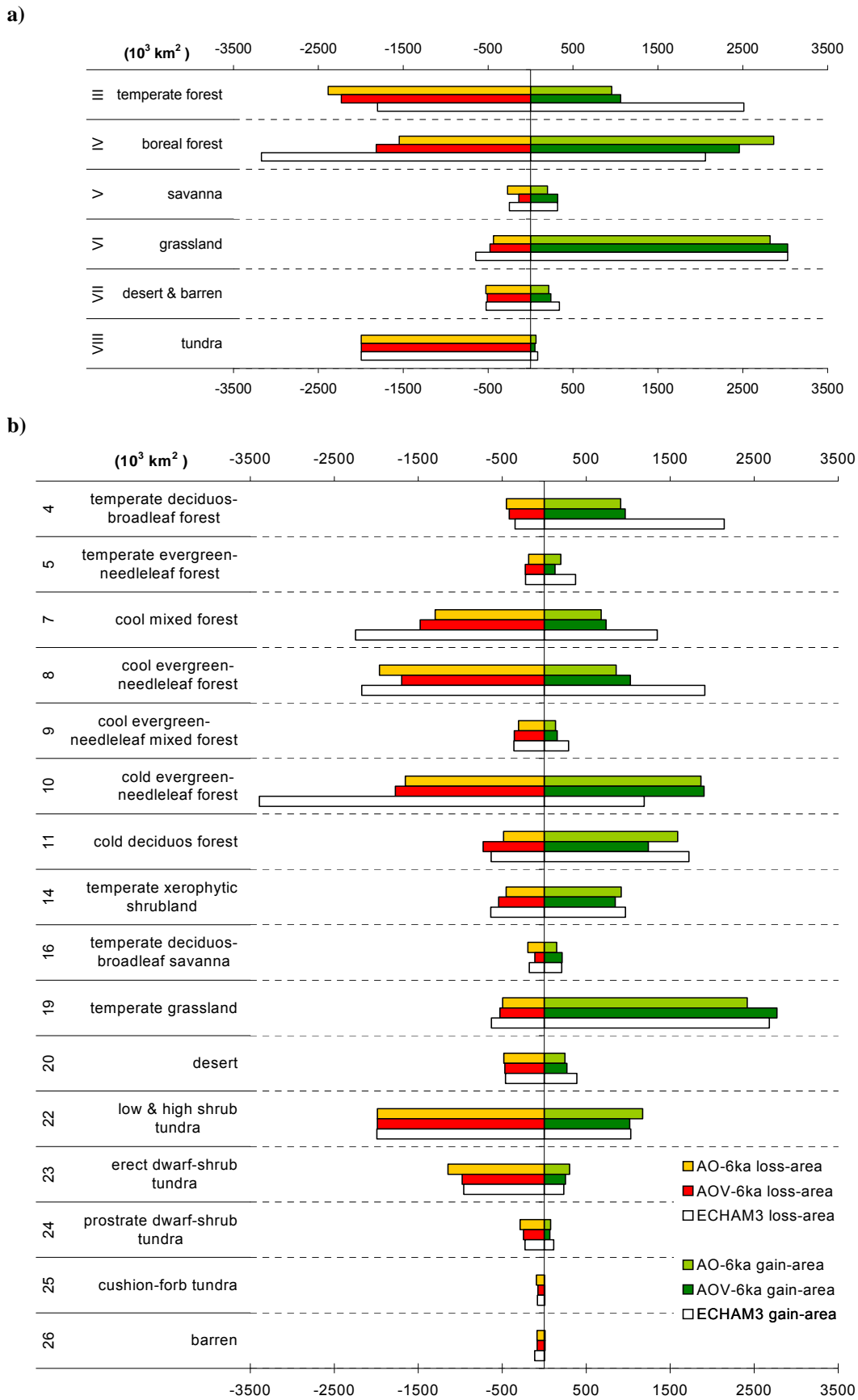
a)

b)

Figure 4-21: Comparison of lost (red) and gained (green) area for 6 ka simulations against BIOME4 modern vegetation in 10^3 km^2 for **a)** megabiome and **b)** biome classification.

So, the overall modification (lost and gained area) of modern boreal forest by 6 ka conditions is even stronger than those of grassland. Although in the AO-6ka simulation a vast area of $2244*10^3$ km^2 of temperate forest or boreal forest is recovered by temperate grassland. Additional vegetation feedbacks in the AOV-6ka run let increase the dry environments by supplementary $+227*10^3$ km^2 (Table 4-9).

On the other hand, the AO-6ka predicted immigration of temperate forest into the modern dryer regions of savanna, grassland and desert is more pronounced with $257*10^3$ km^2 compared to $188*10^3$ km^2 for AOV-6ka (Table 4-9). Moreover savanna-, grassland- and desert-takeovers from modern forest areas in the AOV-6ka simulation is clearly amplified. This AOV-6ka moisture-limiting pattern is assisted by the ratio of gain and loss (Figure 4-21a).

Important in this regard is the individually distribution of the savanna megabiome – representing a sensitive combination of competing tree and grass PFTs. In AO-6ka more temperate forest is replacing modern savanna and in AOV-6ka modern savannas is substituted predominantly by grass. Notable – despite the fact that some more modern grass area is shrivelled and transformed into desert and barren ($+13*10^3$ km^2, Table 4-9) in AOV-6ka – is the contrast that AOV-6ka produces more forest in modern grass areas than AO-6ka ($+58*10^3$ km^2 combined for temperate and boreal forest, Table 4-9). However, this decrease of modern grass is minor compared to the strong extensions by mid-Holocene simulations, but nevertheless they show the high flexible potential of possible migration of grasses in the AOV simulation.

The main discrepancy between the ECHAM3 model and the ECHAM5-MPIOM simulations exist in the extraordinary gain of temperate forest in the ECHAM3 simulation (3 times higher than AO-6ka, respectively 2.4 times higher than AOV-6ka; Figure 4-21a) which is directly correlated to the loss of boreal forest. ECHAM3 computed distinct warmer winter conditions leading to an extension of temperate deciduous broadleaf forest chiefly in Central and East Europe (Figure 4-22). Thus, the complete belt of cool mixed forest, cool evergreen needleleaf forest and the cold evergreen needleleaf forest are shifted further northeast.

Temperate deciduous broadleaf forest
Temperate evergreen needleleaf forest
Warm-temperate evergreen broadleaf & mixed forest
Cool mixed forest
Cool evergreen needleleaf forest
Cool-temperate evergreen needleleaf & mixed forest
Cold evergreen needleleaf forest
Cold deciduous forest
Temperate xerophytic shrubland
Temperate sclerophyll woodland & shrubland

Temperate deciduous broadleaf savanna
Temperate evergreen needleleaf open woodland
Temperate grassland
Desert
Graminoid & forb tundra
Low and high shrub tundra
Erect dwarf shrub tundra
Prostrate dwarf shrub tundra
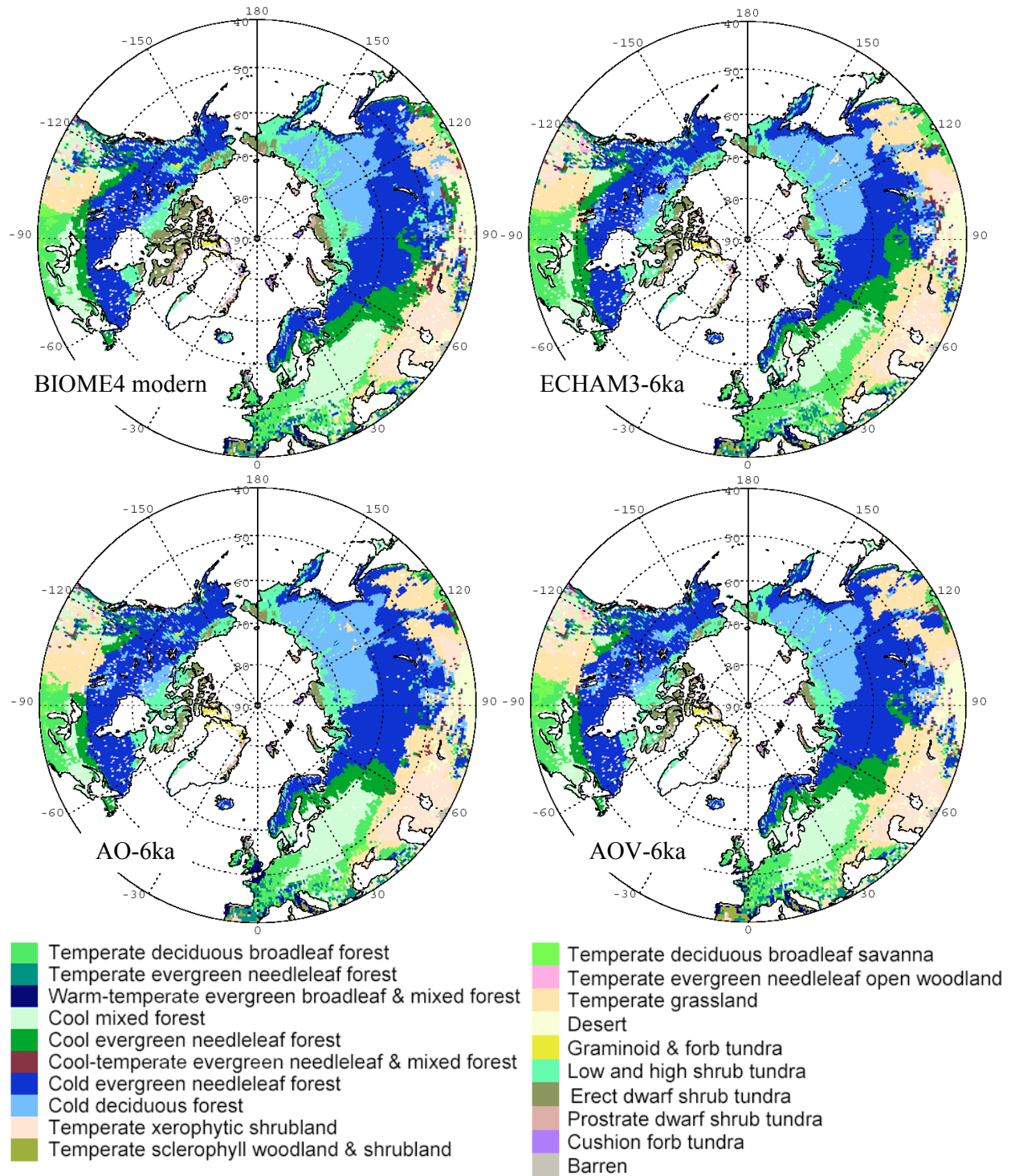Cushion forb tundra
Barren

Figure 4-22: Vegetation patterns for 6 ka simulated by BIOME4 driven by the anomalies from the ECHAM3-LSG (ECHAM3), the ECHAM5-MPIOM (AO-6ka) and the ECHAM-MPIOM-LPJ (AOV-6ka) models. The modern vegetation map (BIOME4 modern, upper left) is driven by a modern climatology (CLIMATE 2.1; Cramer).

Since the plant productivity (NPP) in the high latitudes is more restrictive than the moderate winter warming, the cold evergreen needleleaf forest cannot regain the lost area of southern estates from the northern tundra region and therefore decreases considerably. Conversely, ECHAM3 predicts more deserts, replacing former grassland. In general the ECHAM3 migration rate of forest megabiomes is much higher (Figure 4-21a). Losses and gains are more exposed and a fluctuation between the forest types is strongly pronounced.

Differences in biome changes

The main signals analysed for megabiome migration are broadly recovered within the replacing regimes of individual biome types. Most differences between the two mid-Holocene biome simulations of AO-6ka and AOV-6ka are captured along the boarders of population distribution, although some biome changes are scattered and occur within a common biome stand (Figure 4-23).
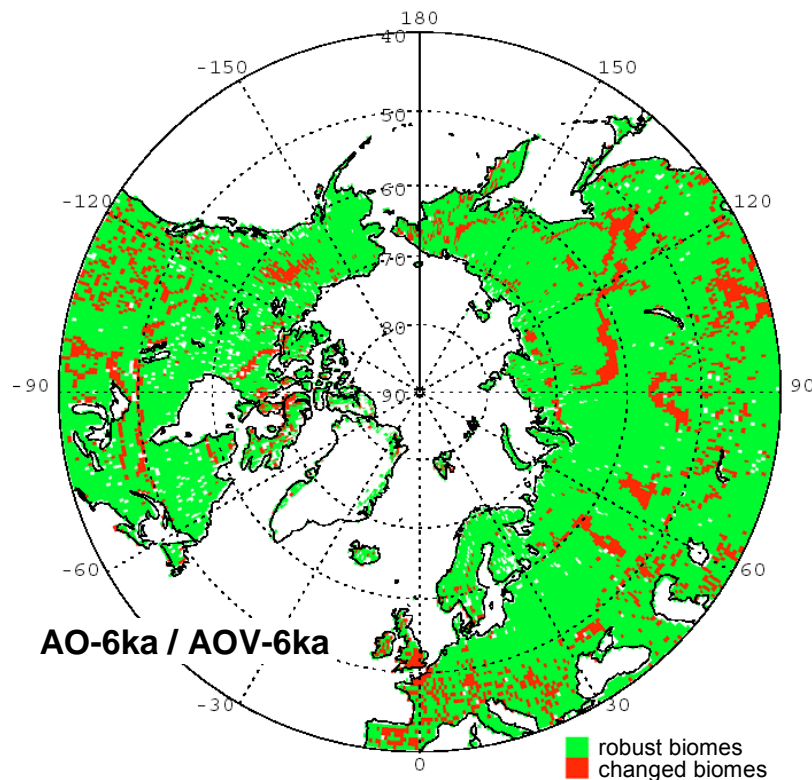

Figure 4-23: Differences between the mid-Holocene biome simulations of AO-6ka and AOV-6ka.

The tendency of warmer conditions simulated by AOV-6ka in contrast to AO-6ka is underlined by several substitutions. A higher amount of $+179*10^3$ km^2 of cool evergreen needleleaf forest substitutes modern cold evergreen needleleaf forest ($613*10^3$ km^2 for AO-6ka compared to $792*10^3$ km^2 for AOV-6ka, Table 4-10[8/10]). Vice versa the replacement of modern cool evergreen needleleaf forest by cold evergreen needleleaf forest ($-368*10^3$ km^2, Table 4-10[10/8]) is strongly reduced; especially in the Eurasian regions of Southern Ural and the Altai mountains. This feature appears by a warming in summer rather than winter-warming, because in these regions the mean temperatures of warmest month (MTWA) are increased but not the yearly minimum temperatures.

The replacing of modern cold deciduous forest by AOV-6ka simulated cold evergreen needleleaf forest is generally enhanced ($+250*10^3$ km^2, Table 4-10[10/11]) along the entire V-shaped northern transition line in Siberia. The associated opposing migration of cold deciduous forest to modern cold evergreen needleleaf forest is strongly reduced in the AOV-6ka simulation and almost restricted to the North-Canadian Mainland ($-159*10^3$ km^2, Table 4-10[11/10]). Thereby the chilling temperatures as decisive factor define the limit of competition between both boreal forest biomes whereat minimum temperatures below -60 °C and/or monthly mean temperatures below -32.5 °C exclude cold evergreen needleleaf forest while cold deciduous forest can still survive (Table 2-1).

A few minor and regional restricted differences maintain the warmer characteristics of the AOV-6ka simulation, such as a supplementary area of $+74*10^3$ km^2 temperate deciduous broadleaf forest recovering modern cool mixed forest (Table 4-10[4/7]). This additional AOV-6ka increase of temperate deciduous broadleaf forest is mainly taking place in Central Europe by eastward extension (Figure 4-22). Likewise, an enhanced increase of cool mixed forest is replacing modern cool evergreen needleleaf forest ($+98*10^3$ km^2, Table 4-10[7/8]) in SW-Canada, the western part of central Europe and southern Scandinavia focus warmer seasonal conditions.

In addition to that the AOV-6ka simulation predicts advanced substitution of the modern cool forest types and modern cold evergreen needleleaf forest by strongly increasing temperate grassland ($+261*10^3$ km^2, Table 4-10[19/7,8,9,10]), based on amplified water-stress compared to the AO-6ka simulation. In the AOV-6ka simulation the temperate grassland is creating a dominant area in the modern highly diverse region of southwest North-America and broadly along the 50th latitude in Central Eurasia – foremost northwards directed – but also effecting modern temperate xerophytic shrubland in more southern parts of this Central Eurasia region ($+71*10^3$ km^2, Table 4-10[19/14]).

Table 4-10: Matrix of 6 ka simulated biomes replacing BIOME4 potential modern biomes in (10^3 km^2) for north of 40 °N. Legend numbers refer to Table 4-8.

AO-6ka replace matrix (10^3 km^2) — 6ka simulation

(10^3 km^2)	4	5	6	7	8	9	10	11	14	15	16	17	19	20	21	22	23	24
4	0	69	75	88	0	5	0	0	0	0	105	0	111	0	0	0	0	0
5	78	0	23	29	0	0	0	0	5	5	2	14	31	0	0	0	0	0
6	19	7	0	0	2	0	0	0	0	25	0	0	2	0	0	0	0	0
7	730	7	0	0	185	25	0	0	98	0	13	0	220	23	0	0	0	0
8	2	0	0	523	0	33	598	22	99	0	0	0	648	37	0	0	0	0
9	10	0	0	14	24	0	2	36	42	0	0	2	167	8	0	0	0	0
10	0	0	0	0	613	6	0	485	6	0	0	0	508	17	9	8	0	0
11	0	0	0	0	13	39	106	0	0	0	0	0	310	2	0	6	0	0
14	0	0	0	2	0	5	7	13	0	0	0	0	313	114	0	0	0	0
15	0	44	0	2	0	0	0	0	0	0	0	0	5	0	0	0	0	0
16	56	61	0	0	0	0	0	0	0	0	0	0	78	0	0	0	0	0
17	0	0	0	5	0	0	0	0	9	0	0	0	11	0	0	0	0	0
19	16	11	0	13	14	22	145	42	198	2	29	0	0	2	0	0	0	0
20	0	0	0	2	5	0	2	0	460	0	0	2	11	0	0	0	0	0
21	0	0	0	0	0	0	12	0	0	0	0	0	0	0	0	11	15	21
22	0	0	0	0	0	0	992	990	1	0	0	0	0	0	4	0	0	0
23	0	0	0	0	0	0	0	0	0	0	0	0	0	0	0	1147	0	0
24	0	0	0	0	0	0	0	0	0	0	0	0	0	0	0	0	287	0

(Row labels down the left = BIOME4 modern)

AOV-6ka replace matrix

	4	5	6	7	8	9	10	11	14	15	16	17	19	20	21	22	23	24
4	0	102	26	51	0	5	0	0	0	0	142	0	91	0	0	0	0	0
5	34	0	22	24	0	0	0	0	5	32	53	23	31	0	0	0	0	0
6	4	0	0	0	0	0	0	0	0	34	0	0	0	0	0	0	0	0
7	803	6	0	0	175	12	0	0	137	0	15	11	296	23	0	0	0	0
8	8	0	0	621	0	37	230	8	59	0	0	0	691	44	0	0	0	0
9	20	0	0	21	27	0	2	22	48	0	4	2	207	4	0	0	0	0
10	0	0	0	0	792	4	0	326	4	0	0	0	611	23	0	10	0	0
11	0	0	0	0	11	62	356	0	2	0	0	0	286	2	0	0	0	0
14	5	0	0	5	0	2	7	13	0	0	0	0	384	127	0	0	0	0
15	0	2	0	2	0	0	0	0	0	0	0	0	2	0	0	0	0	0
16	33	8	0	0	0	0	0	0	0	0	0	0	70	0	0	0	0	0
17	0	0	0	0	0	0	0	0	11	2	0	0	9	0	0	0	0	0
19	57	9	0	11	20	34	147	38	207	2	0	0	0	2	0	0	0	0
20	0	0	0	0	0	0	2	0	371	0	0	2	93	0	0	0	0	0
21	0	0	0	0	0	0	0	4	0	0	0	0	0	2	0	31	6	23
22	0	0	0	0	0	0	1159	827	1	0	0	0	0	0	0	0	0	0
23	0	0	0	0	0	0	0	0	0	0	0	0	0	0	1	976	0	0
24	0	0	0	0	0	0	0	0	0	0	0	0	0	0	1	0	247	0

(Row labels down the left = BIOME4 modern)

Further minor differences in biome changes with spatial significance show a magnified expanding of temperate sclerophyll wood & shrubland and temperate deciduous broadleaf savanna into the area of modern temperate evergreen needleleaf forest (+79*10^3 km^2, Table 4-10[15,16/5]) in southern Mediterranean-Europe for AOV-6ka. This implies that moisture disturbances obstruct an optimised development of LAI and NPP of woody plants and furthermore increase potential fire risk which limits the growth of tree-type biomes. For that reason – but with the opposite effect – the AO-6ka simulation predicts temperate evergreen needleleaf forest replacing the modern temperate sclerophyll wood & shrubland and modern temperate deciduous broadleaf savanna in that region.

Even though the 6-ka simulations tend to calculate dryer conditions especially in mid-continents, the absolute limiting conditions which prevent vegetation to develop are condensed in both simulations. Therefore modern extratropical desert areas are broadly settled by xerophytic biome types. Whereby it occurs that in the AO-6ka run more temperate xerophytic shrubland establishes at the arid surroundings of lake Aral, and in the AOV-6ka run more temperate grassland establishes in the Mongolian deserts (Table 4-10[14,19/20]).

Admittedly there are some crucial results and some exceptions of the general trend of warmer and/or dryer biome predictions by the AOV-6ka simulation compared to the AO-6ka. As prescribed for the megabiome of boreal forest, these cold forest types are shifting northward in the 6 ka simulations by replacing modern tundra areas. This seems to take place by equal extension as the amount of area is almost equivalent. However, the biome-type analysis shows that there are particular differences in how the boreal forest conquers the high northern habitats in the mid-Holocene. In both ECHAM5 simulations the change from modern low & high shrub tundra to cold evergreen needleleaf forest or cold deciduous forest represents the strongest modifications of vegetation cover for 6 ka. But in case of the AO-6ka run additional +163*10^3 km^2 of modern low & high shrub tundra is replaced by cold deciduous forest (Table 4-10[11/22]) and -167*10^3 km^2 less tundra area is replaced by cold

evergreen needleleaf forest (Table 4-10[10/22]) than predicted in the AOV-6ka run. This diverse feature occurs in apparent different regions and refers to varying climate signals.

Supplementary area of AO-6ka cold deciduous forest is replacing modern tundra area solely at far northern locations by shifting the margin of trees (taiga-tundra-boundary) further pole-wards (Figure 4-24). This takes place along the asymmetric SE-NW striking borderline at Keewatin in central Northern-Canada, and at two North-Siberian sites – specified in the Taimyr region and further east along the Verkhojansk-mountain range.

The additional area of cold evergreen needleleaf forest replacing modern tundra in the AOV-6ka run shows another pattern and is mainly situated at less high latitudes in Eurasia (Figure 4-24). Most of this area ($135*10^3$ km^2) is concentrated in the east of the continent – prevailingly in Chukotka, Kamchatka and along the coast of the Ochotski-sea – and supported by Northern Pacific conditions. A second area is
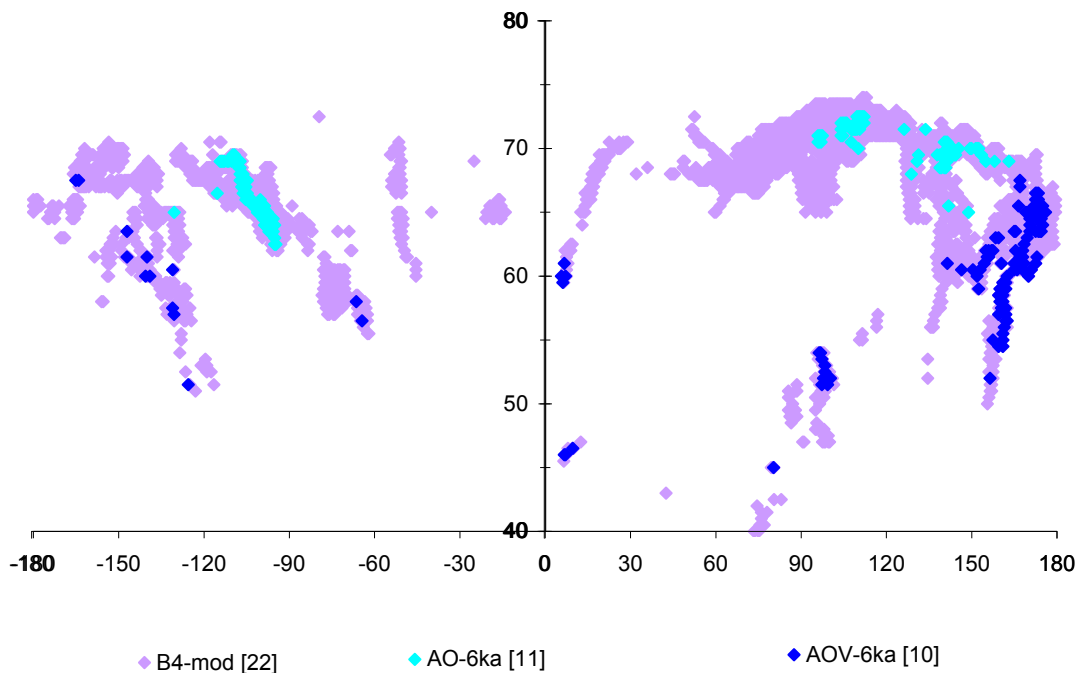

Figure 4-24: Total area of modern low & high shrub tundra as simulated by standard BIOME4 modern (B4 mod[22]), and grids where the AO-6ka run replaces tundra by cold deciduous forest while in the AOV-6ka run tundra is unchanged (AO-6ka[11]) plus grids where the AOV-6ka run replaces tundra by cold evergreen needleleaf forest and the AO-6ka run left tundra unchanged (AOV-6ka[10]).

located at the Sajan-mountains in the southern part of Central-Siberia and some minor spots are sited in the Western-Alps and SW-Scandinavia (Figure 4-24).

Both patterns of distribution are due to a warming signal but they are reflecting different kind of warming aspects. The amplified northwards distribution of AO-6ka cold deciduous forest is caused by the prolongation of the growing-season – warming in the half-year of summer and mainly in autumn – in connection with increased sunshine. The extended distribution of cold evergreen needleleaf forest in the AOV-6ka run is due to warmer winter temperatures (MTCO) and the rise of chilling temperatures (T_{min}), respectively.

One exceptional signal of regionally cooler conditions in the AOV-6ka run compared to the AO-6ka run is located in the N-Canadian Arctic within the tundra area. The increased substitution of modern erect dwarf-shrub tundra by low & high shrub tundra ($171*10^3$ km^2, Table 4-10[22/23]) refers to a more pronounced prolongation of the growing-season ($GDD_0>500$) in the AO-6ka than in the AOV-6ka simulation. This is associated with reduced cloudiness in the AO-6ka run (Figure 4-15c) as an important factor for the calculation of incoming radiation by high latitude sunshine angles. Further north this feature is relived but continued with modern prostrate dwarf-shrub tundra replaced by additional AO-6ka erect dwarf-shrub tundra ($40*10^3$ km^2, Table 4-10[23/24]).

Another regional exception refers to less dryer conditions in the AOV-6ka run compared to the AO-6ka run. At a few spots in warm regions of the extratropics with existing temperate grassland in the modern BIOME4 run temperate deciduous broadleaf forest can develop under AOV-6ka conditions ($+41*10^3$ km^2 compared to AO-6ka, Table 4-10[4/19]). This occurs in a separate enclave in N-Kazakhstan north of the Caspian-sea and moreover at the foremost southern part of the examined region along the Chinese Inner- (Southern-) Mongolia range of the river Huang He.

Even though these features are minor and locally restricted, they still demonstrate a highly differentiated climate structure due to dynamic vegetation, having the potential to affect atmosphere and ocean models at spatial regions in multiple directions.

Arctic tree line

One of the most important tasks in simulating vegetation of the high latitudes is the positioning of the northern border of forests, the so called taiga-tundra-boundary. This arctic tree-/timber-line describes the edge of the habitat at which trees are capable of growing – mainly restricted by low temperatures – and in case of the BIOME4 model it defines a threshold of ≥50 % tree types of the grid cell vegetation.

In comparison to the modern situation the most part of the mid-Holocene taiga-tundra-boundary was situated further north. Nevertheless, the shift of the tree-line between 6 ka and modern is characterised by a strong asymmetrically shape, and varies from the most exposed poleward shifts in central Siberia, small shifts in Europe, little or no changes in Beringia, down to even southward positions in eastern Canada, documented by pollen data analyses (TEMPO Members 1996; CAPE Project

Table 4-11: Approximate changes in the position of arctic tree line at 6 ka compared to modern shown by pollen, interpreted by Bigelow et al. (2003) and Kaplan et al. (2003) from the PAIN data set. The results from Kaplan et al. are deduced from 1° (=110km) deviations.

Sector	Change 6ka - modern	
	Bigelow et al 2003	Kaplan et al. 2003
Mackenzie	100 km N	no change
Keewatin	280 km S	ca. 110 km S
Labrador	170 km S	ca. 660 km S
Greenland	no evidence for treeline	-
Atlantic	no evidence for treeline	-
Europe West	70 km N	ca. 110 km N
Europe East	insufficient data	-
Siberia West	insufficient data	ca. 220 km N
Siberia Central (Taimyr)	180 km N	ca. 330 km N
Siberia Central (Lena)	70 km N	-
Siberia East	no change	ca. 220 km N
Beringia West (Chukotka)	no evidence for treeline	-
Beringia East (Alsaka)	no change	-

Members 2001; Bigelow et al. 2003) (Table 4-11). Especially the advanced northern existence of forests in contrast to the orbital reduction of winter insolation on the northern Hemisphere – sometimes called the biome paradox (e.g. Ganopolski et al. 1998) – is reflecting the taiga-tundra feedback with synergistic effects by sea ice-albedo feedbacks and is referred as one of the main indications beside the 'green Sahara' for the late Holocene climate optimum and their modelling. Most of the 6 ka adapted modifications of the tree line recognised in the pollen-data are reproduced by the 6 ka simulations (Figure 4-25). However, the strength of this arctic tree line shift is more pronounced in the models without dynamic vegetation.

In average for the entire North-American continent the ECHAM3 model shifts the boreal tree line about 129 km northwards. The AO-6ka simulation moves the mean tree line 106 km further north and the AOV-6ka simulation 80 km N, only. The main
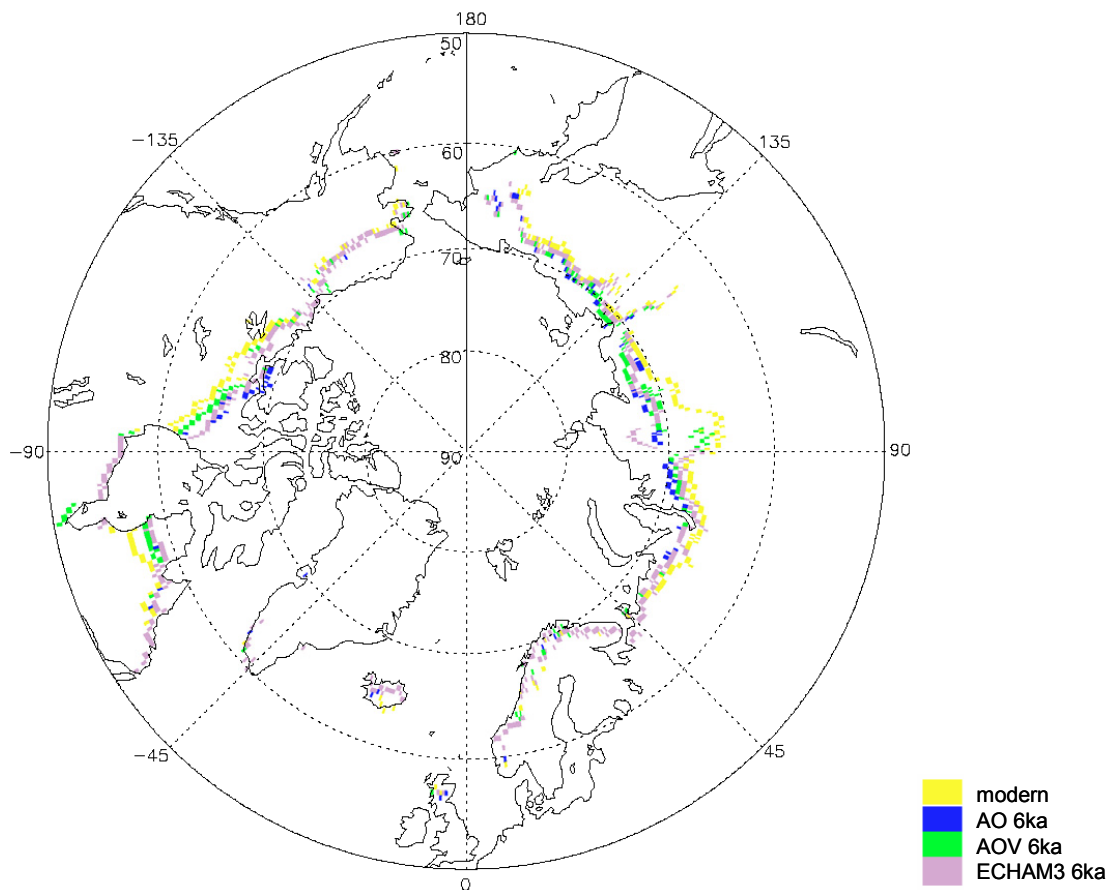

Figure 4-25: The foremost northern location of calculated tree line (taiga-tundra-boundary) for modern and 6 ka simulations. The purple line of ECHAM3 is plotted ahead and overlaps others when covering the same grid cell.

disparity of the simulations is to be found in the Keewatin region west of the Hudson Bay, with greatest northward shifts about 200 km (AOV) – 600 km (ECHAM3) (Figure 4-26a). Conversely, in this part of the continent the remnants of the Laurentide ice sheet – which are not included in the models – prevent a realistic distribution, and the pollen data reconstructions show a clear southern position of the tree line in Keewatin and Labrador, even further south than our days (Table 4-11).

In Eurasia the differences of the averaged shifts for the whole continent are minor. And it is the AO-6ka simulation moving the tree line 134 km furthermost north, while ECHAM3 shifts the trees 116 km north, and the AOV-6ka simulation about 111 km north. In Europe and West Siberia the models show minor and almost identical shifts (Figure 4-26b) – comparable with the pollen data (Table 4-11) – whereas a significant northern deviation of the tree line position occurs in Central Siberia. In this region among 90 and 100 °E longitude the differences between the AO-6ka and AOV-6ka
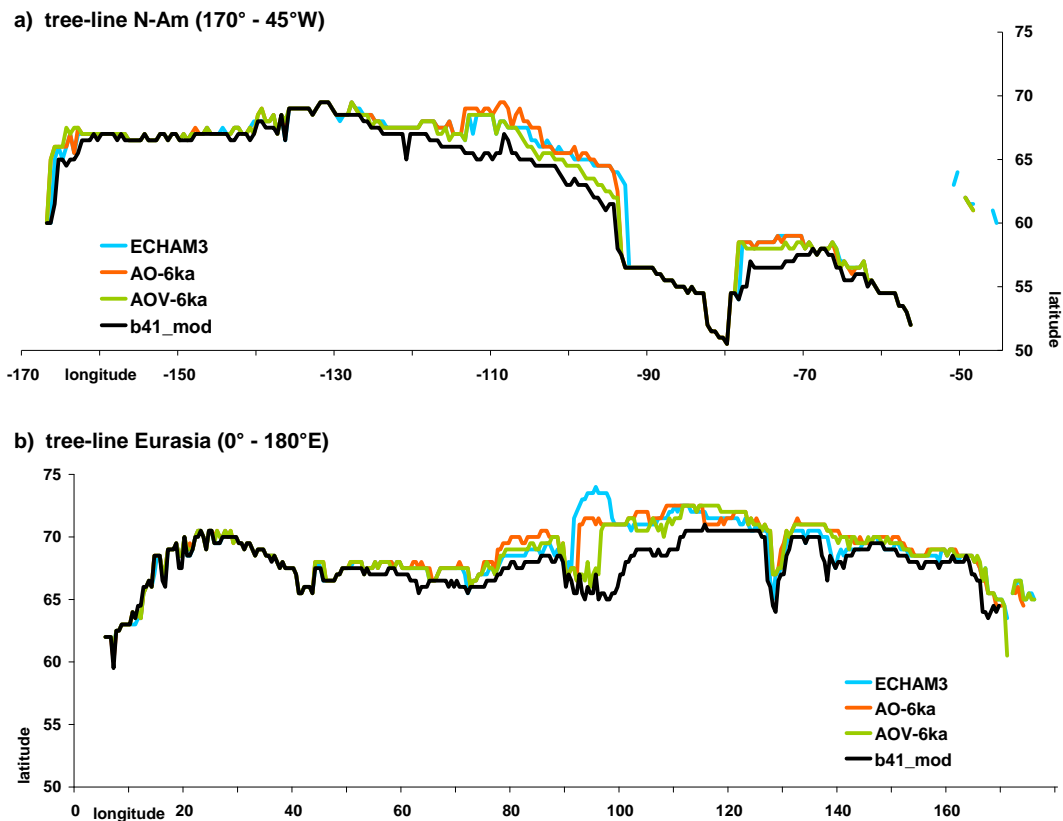

Figure 4-26: Position of the arctic tree line simulated for 6 ka (ECHAM3, AO-6ka, AOV-6ka) and modern (b41_mod) (black line) in **a)** North-America (170-45 °W) and **b)** Eurasia (0-180 °E).

simulation amounts up to a maximum of 555 km, which equivalents 5° in latitude or 10 grid cells in BIOME4 resolution. The leap between the AOV-6ka and ECHAM3 northern tree line is even more obvious and signifies a further shift about 611 km. Such a tremendous differentiation which is auxiliary local restricted has to bare additional possessions than climate conditions. In the AO-6ka and the ECHAM3 simulations a small band of cold deciduous forest is able to settle along the northern rim of the Putarona mountain range spreading from occupied places further east (Figure 4-22). So in fact, the gap between AO-6ka and AOV-6ka represents a geomorphologic structure where still tundra residents on the topographic highlands of the Putarona mountain range, and the visualisation of the northern tree line is someway misleading in this case.

4.4.1.4 Data-model comparison for 6 ka

The comparison of the biome simulations for the mid-Holocene with the Biome6000/PAIN observation data set shows the reliability of the models' reconstruction of vegetation.

The fairly warmer conditions of the AOV-6ka run can match the field data slightly better than the AO-6ka run, with three megabiome data points ahead of 1062. This equivalent 71.2 % for the AO-6ka and 71.5 % for the AOV-6ka of matching (Table 4-12a) and with respect to the variability analyses of the 0 ka control runs the standard deviations confirms no significant signal of improvement. As the polar region north of 70 °N contains 20 data points merely, the validity somehow is limited, albeit the AO-6ka matching is enhanced compared to the AOV-6ka (Table 4-12a) relating to locations of tundra oversimulation in West Siberia. The mean information refer to the

latitudinal bands of the boreal (60-70 °N), the cold-temperate (50-60 °N) and the warm-temperate (40-50 °N) regions.

The good matching of the AOV-6ka run origins by the increased agreement of simulation grid cells with data points in the cold-temperate and boreal regions between 50 ° and 70 ° northern latitude, reaching a 2.1 % higher match for 537 sites in the band between 50 and 70 °N. This obtains the southern front of the northward shifting boreal forests and the distribution and placement of the temperate forest community, where the AOV-6ka simulation is advanced. Remarkable is the high agreement of the AOV-6ka run in the boreal region of 60 – 70 °N, where the match of 66.9 % is significantly higher considering the potential variability described by the calculated standard deviation from the control run analyses (Chapter 4.4.1.2) and given in Table 4-7.

Further south, in the band of 40 – 50 °N, the AOV-6ka climate conditions cause a reduction of the matching compared to the AO-6ka run. Most of these differences between the two models are located in the western part of Central North America and in the south-eastern part of Siberia, where the AOV-6ka simulation predicts some more mismatched xerophytic and forest vegetation. Nevertheless, about qualitatively

Table 4-12: Comparison of observed (Biome6000/PAIN) and simulated vegetation for the mid-Holocene for **a)** megabiome and **b)** biome classification in (%) of matching. The simulated vegetation derives from BIOME4 model simulations driven by the anomalies of the ECHAM5-MPOIM (AO-6ka), the ECHAM5-MPOIM-LPJ (AOV-6ka) and the ECHAM3-LSG2 (ECHAM3) climate models.

simulation-observation-estimation, N of 40 °N (%)

a)	Megabiome	AO-6ka	AOV-6ka	ECHAM3	data points
	N of 40°	71.2	71.5	69.6	1062
	N of 70°	75	65	55	20
	60°-70°	63.7	66.9	64.9	245
	50°-60°	77.4	78.4	72.3	292
	40°-50°	71.1	69.9	70.9	505

b)	Biome	AO-6ka	AOV-6ka	ECHAM3	data points
	N of 40°	44.2	44.7	40.9	1062
	N of 70°	30	25	25	20
	60°-70°	41.2	42.9	42.4	245
	50°-60°	54.5	56.2	47.9	292
	40°-50°	40.2	39.8	36.6	505

high 70 % of the predicted megabiomes match the 505 observed data points between 40 and 50 °N of the warm-temperate region.

For the biome classification the matching of both models shrinks by 27 % (Table 4-12b). Some small advances of the AOV-6ka simulation by the placing of biomes lead to a +0.5 % increased matching of 44.7 % compared to the AO-6ka run. However, the latitudinal structure of reliability is predominantly left unchanged with worse matching in the southern warm-temperate and the northern polar regions. Only small variations between the two models are detectable with the best results for the cold-temperate region (50 – 60 °N), where the AOV-6ka run is matching 95 % of the cool mixed forest and 78 % of the cold evergreen needleleaf forest observation data sites. However, the differences by the simulation-observation estimation between the two ECHAM5-MPIOM models can be seen as minor.

On the other hand, the improvements in simulation-observation estimation by the two ECHAM5-MPIOM models in contrast to the former ECHAM3-LSG model are notable. The 1.9 % higher match of the ECHAM5-MPIOM-LPJ simulation compared to the ECHAM3-LSG simulation for megabiomes is significantly better (Table 4-12a), referring to the standard deviation of the ECHAM5-MPIOM-LPJ control runs (Table 4-7). Even the matching of the ECHAM5-MPIOM simulation is significantly improved. Regarding the specific biome classification this enhancement is additionally amplified. Both ECHAM5-MPIOM models increase their matching considerably by 3.3 % (AO-6ka), respectively 3.9 % (AOV-6ka) compared to ECHAM3-LSG. This progress is reasoned in the specific latitudinal band of temperate to boreal transition between 50 and 60 °N, where the ECHAM5-MPIOM simulations can mainly improve the matching by 6.6 % for AO-6ka and 8.3 % for AOV-6ka (Table 4-12b). Commonly, most of the mismatches in the ECHAM3-LSG simulation that are correctly predicted in the AOV-6ka run - a difference of 24 sites - refer to warmer forest types than seen in the observation reconstruction.
Similarly, those ECHAM3-LSG conditions are locally over-simulating warmer forest types along the costal areas of the temperate North-Atlantic regions reaching less

quantitative agreement in the already described key areas of Chapter 4.3 (Table 4-13c). Although the results for Europe of ECHAM3-LSG were already good in the 7 model estimation, the new ECHAM5-MPIOM simulations are consequently advanced; a fact for all the listed key areas. Besides the placing of the forest types in the oceanic influenced areas, preferably the mid-continental distribution of dry xerophytic vegetation is more realistic (Table 4-13b). Hereby the AO-6ka simulation shows little advances around the Hudson-Bay – despite the missing Laurentide ice sheets - and in Central Eurasia (58.9 %), dealing with only one more correct predicted forest biome versa the lumped dry vegetation of steppe, savanna and grass compared to the AOV-6ka simulation with 57.9 %. In the polar areas of both northern continents the estimation of tundra decrease and forest shifting shows little advances by the less strong winter warming vegetation coupled model.

This advance in the simulation-observation estimation by the ECHAM5-MPIOM and the ECHAM5-MPIOM-LPJ model in contrast to the ECHAM3-LSG model is supported by the Kappa statistics for megabiomes classification. Hereby, the 1062 grid cells corresponding between the simulation and observation reconstructions for 6 ka are estimated by the realised agreement against what might be expected by chance. The ECHAM5-MPIOM simulation (AO-6ka) and the ECHAM5-MPIOM-LPJ simulation (AOV-6ka) reach a Kappa statistics value of k = 0.53, a quote that can be

Table 4-13: Comparison of observed (Biome6000/PAIN) and simulated biome groups for the mid-Holocene in the key regions **a)** of northern taiga-tundra shifting, **b)** of central xerophytic spreading and **c)** the coastal temperate forest mixing in (%) of matching. The appropriate number of data points is given on the right side.

simulation-observation-estimation of megabiomes for specific key regions in %	AO-6ka	AOV-6ka	ECHAM3	data points
a) tundra-taiga estimation				
N-America (170-10°W, N of 60°N)	66.3	67.4	66.3	86
Eurasia (10°W-170°W, N of 60°N)	84.4	84.9	80.4	179
b) xerophytics estimation				
NW-America (120-90°W, 40-55°N)	74.2	75.0	67	120
Central-Eurasia (70-140°E, 40-60°N)	58.9	57.9	52.6	96
c) temperate forests estimation				
NE-America (90-60°W, 40-55°N)	65.2	62.4	57.1	210
Europe (10°W-30°W, 40-60°N)	60.4	61.3	57.9	236

assessed as a quite fair agreement. Both simulations are obviously improved compared to a Kappa statistics result of k = 0.49 by the preceding ECHAM3-LSG simulation.

4.4.2   Discussion

Comparison of AO versus AOV model simulation

The study of AOGCM (ECHAM5-MPIOM) and AOVGCM (ECHAM5-MPIOM-LPJ) simulations for modern and the mid-Holocene show that there are a number of comparable changes in climate and vegetation in response to orbital forcing, but also considerable differences. To separate the robust signals, insignificant changes arising from internal variability have to be separated.

For this purpose the control runs for present time are analysed first to consider the variability of vegetation reconstructions by the examine of the mid-Holocene. The time span of the simulations is divided into five successive periods to include centennial variations of temperatures, precipitation and cloudiness which define the vegetation reconstruction with the BIOME4 biogeography model. Solely for the analysis of the modern situation the relevant climate model output is used to run the BIOME4 model directly to obtain the potential vegetation distribution. However, these reconstructed vegetation patterns compared to the standard BIOME4 modern simulation shows large deviations, like e.g. an unrealistically enlarged area of tundra, so that some of the resulting features must be specific to the ECHAM model. More precisely, the mean temperatures of the control runs of the two types of simulations differ: the AOV model produces warmer conditions for the whole globe as well as for the land mass of the Extratropics north of 40 °N. This is furthermore linked to an intensified water cycle. Altogether, the AOV simulations show weaker differences in biome area distribution than the AO simulations and are, so to say, more comparable

to the BIOME4 modern map which is tuned to interpolated climate observations. On the other hand, the intra-model variability of differences from run to run of each individual biome type is more pronounced. It is obvious that the additional model component of interactive vegetation in AOV as compared to AO creates locally higher centennial fluctuations. And in contrast to the results of the IPSL study of Chapter 3 (Table 3-3), here the additional submodel improves results. This is corroborated by a better agreement with the pollen record of Biome6000/PAIN which contains more than 5000 sites for present time slice (0 ka).

Although the analysis identifies a cold bias in the high northern latitudes for the present day control runs – which is kind of a common problem of GCMs (e.g. Brovkin et al. 2003; Gallimore et al. 2005; Chapman and Walsh 2006) – both models show similar climate patterns in the extratropic region north of 40 °N, leading in both models to an over-estimation of tundra biomes. To prevent this problem, the whole biome analysis for the mid-Holocene is based here on an anomaly approach, by driving the BIOME4 model with the 6ka - 0ka (Holocene - modern) differences. Thereby the interpretation of the vegetation distributions is directly related to the skills of the simple diagnostic vegetation model, instead of the comprehensive general circulation model.

Mid-Holocene biome changes (6 ka)

One of the most important changes of vegetation characteristic for the mid-Holocene climate optimum on the Northern Hemisphere is the northward shift of the tree line (e.g. COHMAP members 1988, TEMPO members 1996, Tarasov et al. 1998, Edwards et al. 2000, Williams et al. 2000, Bigelow et al. 2003). This shift of the taiga-tundra-boundary leads to a remarkable shrinkage of tundra area which both simulations obtain almost equally well. However, this does not imply an equal expansion of cold boreal forest in the two simulations: the area of boreal forest in the AO-6ka compared to the AOV-6ka simulation is substantially larger, because tundra is partly reduced by cold deciduous forest in far arctic regions and in addition – this is

the major contrasting signal between both models – by southward growth, thereby replacing temperate forest types. The northward expansion of cold deciduous forest is reflecting the orbital forced summer warming and the response to ocean feedbacks prolonging the growing season into autumn in connection with a simulated increase of fractional sunshine (cloudiness), playing an important role in the high-latitudes since it allows more photosynthesis (Kaplan et al 2003; Holland and Bitz 2003). In contrast, the AOV-6ka cold evergreen needleleaf forest replaces tundra, caused by a winter warming and less extreme chilling.

The analysis of ocean and vegetation feedbacks from Chapter 3 revealed that coupling of vegetation with an atmosphere-ocean model includes synergies which affect high-latitude temperature. In this case the further northern gradation of the cold evergreen needleleaf forest as well as the northern extension of temperate forest in the AOV run are deduced from a reduction of extreme frost in boreal and arctic regions during the winter season chiefly by synergistic effects (Figure 3-5). This very fact proves the important role of interactions between ocean and vegetation feedbacks to attain locally strong, even reverse signals, leading to more realistically vegetation simulations matched up with proxy-data.

As all of the examined GCMs in this validation – and several other recent ones (PMIP2; Braconnot et al. 2007a) – both ECHAM5 simulations over-estimate the distinct increase of dry xerophytic vegetation types in the continental region of Eurasia between 40 – 60 °N. Particularly the increase of the temperate grassland and temperate xerophytic shrubland in the interior of Siberia and the increase of temperate sclerophyll woodland & shrubland in the northern Mediterranean regions are resulting from water limited water availability, differ from what was found in observations. The small amounts of simulated summer rain as a direct response of the atmosphere to radiative forcing in July and August – the most humid month in Siberia (Tarasov et al. 2002) – cannot sustain extensive forests. In case of the dryer AOV simulation, supplementary xerophytic vegetation expands as a result of vegetation feedbacks and synergies. For the Central-Eurasian signal, it is likely that the dry

westerlies are strengthened and therefore the sub-meridional monsoon can not reach the far interior regions (Tarasov et al. 2002). Likewise, this unrealistic pattern, commonly obtained in 6 ka GCM simulations but not necessarily in simulations with EMICs (Earth system models of intermediate complexity) (see the studies by Brovkin et al. 2002 and Renssen et al. 2005), could possibly be linked to the land-surface water treatment and insufficient soil properties associated with surface energy fluxes, since some of the evaluated AOGCM models of Chapter 4.3 can perform potentially sufficient precipitation but cannot prevent such a strong increase of xerophytic vegetation. The fact, that even the diagnostic vegetation model BIOME4 has problems to cover this Central-Eurasian region in agreement with the sparse field data for the modern state (Chapter 2.3), illustrates the difficulties that emerge if vegetation reconstructions in this region are discussed.

However, the increase of temperate grassland extent is minor, since the majority of modifications in the Extratropics like shifts, gains and losses of vegetation area relates to the boreal biome of cold evergreen needleleaf forest.

Pollen data versus model agreement

Comparison of the simulated biomes with the reconstructed biomes of the Biome6000/PAIN data set shows small improvements of the AOV-6ka simulation as against the AO-6ka. Globally and in most of the key-regions for cold, temperate and arid conditions the additional coupling with the dynamic vegetation model gives superior results. Except for the dry pattern in Central Eurasia, that is confirmed as a very small expansion of arid environments by the palaeo-record but over-estimated by the models, the matching of pollen sites by the AOV-6ka reconstruction is still not as good as by the AO-6ka reconstruction. Likewise the analysis of the IPSL model, asynchronously coupled to a vegetation model in Chapter 3, has already indicated. Nevertheless, the regional increase of mismatches from AOGCM to AOVGCM is clearly minimised. Furthermore, the similarly increased over-estimation of dry vegetation in Central North-America in the IPSL-AOV is not existent in the ECHAM5-MPIOM-LPJ.

Improvements of ECHAM5-MPOIM versus ECHAM3-LSG

Judged by the match of simulated biomes with pollen data reconstructions the later versions of ECHAM5-MPIOM and ECHAM5-MPIOM-LPJ are superior compared to the ECHAM3-LSG, irrespective of type of testing. This is the case in the entire region of the Extratropics in the Northern Hemisphere, in the individual latitudinal bands, as well as in key-areas of vegetation highly sensitive to changes in temperature, moisture or circulations patterns.

The enhanced agreement with observation reconstructions entails a greater credibility of a) the shift of the northern taiga-tundra-boundary; b) the mid-continental moisture limited dispersion of xerophytic vegetation, and c) the near-coastal pattern of temperate forest communities within the zone of transition from ocean to terrestrial regimes, all in all created by radiative forcing changes. Even though simulations with the ECHAM5-MPIOM model partly tend to over-estimate the pole-ward shift of boreal forest, both more recent simulations capture the mean range of the 6 ka tree-lines produced by several AOGCMs evaluated in Chapter 4.3, where the ECHAM3 simulation displays the limits of minimum and maximum shift in Eurasia.

The proportion of tree and grass PFTs especially in Central-Siberia is still improvable. But a closer examination of key areas of the extended xerophytic vegetation shows clear enhancements in the ECHAM5-MPIOM and the ECHAM5-MPIOM-LPJ simulations as compared to ECHAM3 simulations, obvious from a better agreement with the pollen records, and this improvement is more distinct in the central North American region.

The prediction of the correct placing of temperate forest types in Europe is not a trivial task (Masson et al. 1999, Bonfils et al. 2004, Brewer et al. 2007), because the Biome6000/PAIN data set and the bioclimatic reconstruction based on pollen and lake-level data over Europe by Cheddadi et al. (1997) reveal that the climate system response to the 6 ka solar forcing must be complex because of the at that time non-simple pattern of warmer summers in the north and cooler summers in the south, accompanied by winters milder in the northeast but colder in the southwest as

compared to present conditions (Davis et al. 2003). This biparted situation of northern warming and southern cooling is catched better in the AO run, while the AOV run can not reproduce lower temperatures in the summer season in South Europe. This is well seen in a small but better match of the AO simulated forest biomes with the Biome6000/PAIN data in most of the southern region between 40-50 °N, although the agreement for Mid-and North Europe is enhanced in the AOV reconstruction.

In eastern North America a similar northern but over-estimated shift of the warmer forest types (warm-temperate evergreen broadleaf mixed forest and temperate deciduous broadleaf forest) as a result of winter warming is the only result of the AO simulation clearly superior to the AOV simulation as judged by the 6 ka pollen data. Though, one has to be aware that the northern impact of the Laurentide ice-sheet cooling is missing in these simulations, which renders the good model-observation match for eastern North America somewhat arbitrary.

However, when discussing the forest shifts around the North Atlantic coast line, it has to be remembered that this analysis deals with related biomes of one and the same vegetation type and even the same megabiome. This directly indicates a higher variability of changes which increases potential errors. And it postulates a high quality of the vegetation defining parameters in the diagnostic BIOME4 model, which is the case not in general. The parameterisation of temperate forest competition gives an excellent match of >80 % for the related forest groups compared with the 0 ka (present-day) Biome6000/PAIN data for the BIOME4 reconstruction in eastern North-America. But in Europe the placement of the temperate deciduous forests agrees merely with 45 % for the appropriate biomes in the observation data, already mentioned by Kaplan et al. (2003). This is due to the small scaled higher diversity and geomorphic structures and the tendency of the BIOME4 model to under-estimate warm-temperate evergreen broadleaf mixed forest in southern Europe.

Nevertheless, both new ECHAM5 climate simulations can reconstruct more realistic vegetation distributions for the mid-Holocene with a total change of 28 % of the biome area in the ECHAM5-MPIO and the ECHAM5-MPIOM-LPJ simulations against 35 % in the ECHAM3-LSG simulation, whereby the circumstances of climate

change were only driven by monthly different insolation rates with equal amounts of radiation over the year compared to present day.

5. Conclusions and outlook

5.1 Conclusion

Recent climate system models simulate physically consistent climate states on a global scale at several time-scales. The most comprehensive ones are general circulation models (GCMs) with interactive couplings between submodels for atmosphere, ocean, vegetation and cryosphere and, depending on purpose, other sub-model components. These GCMs provide a vast amount of information about the state and statistics of the simulated climate. Vegetation is sensitive to climate. Therefore, climate simulations can be assessed by comparison with observed vegetation or, especially for past climates, their traces in form of pollen distributions. To this end some parameters (temperature, precipitation and cloudiness) have been selected in this study to drive the diagnostic vegetation model (BIOME4). Thereby, a combination of climate conditions can be translated into a distribution of plant ecosystems, here as aggregated to biomes.

The mid-Holocene (6 ka) is frequently used as a reference period to evaluate the sensitivity of GCMs to a change in solar irradiation (e.g. PMIP: Joussaume and Taylor 2000; PMIP2: Harrison et al. 2002, Braconnot et al. 2007a,b, Wanner et al. 2008). By now, there is a history of almost 30 years of experience with simulations of Holocene climate (e.g. Kutzbach 1981). The main reason of interest to examine the mid-Holocene pertains to the well known differences in the parameters of orbitally induced radiative forcing, namely an increased northern summer insolation of ca. +6 W/m^2 (JJAS at 65 °N) and reduced winter insolation of ca. –6 W/m^2 (Berger 1978). Another point raising interest in this period is the lower atmospheric greenhouse gas concentrations (ca. 280 ppm CO_2; e.g. Barnola et al. 1987; Indermühle et al. 1999) compared to present, while differences in coast lines or ice shields are almost

neglectable (e.g. Lauretide ice sheet). Certainly, the impact of these changes on the vegetation with remarkable differences like the green Sahara or the further northern boreal tree-line (the so called "biome paradox" (Ganopolski e al. 1998; Berger 2001)) underline intense interest to invoke this time-slice for the assessment of climate system models – an interest that is not purely academic because in view of the large changes expected for future climate, climate modellers must prove that their models have predictive skill for a large range of different climatic conditions.

The comparison of palaeo-data with simulation results is very much facilitated by the availability of a data synthesis of pollen collections from the mid- and high latitudes generated as part of the PAIN (Pan-Arctic INitiative project: Bigelow et al. 2003) and the Biome6000 (Global Palaeovegetation Mapping Project: Prentice et al. 2000) data sets. Such a comparison is in particular facilitated because the pollen and plant macrofossil data have been translated into biome types which are directly comparable with the biome classification in the BIOME4 vegetation model used for the reconstruction of vegetation distribution from GCM simulations. Furthermore, the selected pollen data focus on the time-span of the mid-Holocene (6 ka) and supply in addition an abundant number of recent samples from present days climate. This observation data provide a target against which in this thesis the realism of the 6 ka simulations has been assessed.

The thesis presented here concentrates on the Extratropics of the Northern Hemisphere north of 40 °N and particular on the vegetation patterns in the temperate, boreal and arctic zones. A large number of simulations from several different models have been examined with respect to the change in vegetation distribution and the

basing climate for the mid-Holocene. The aim was to distinguish robust signals from model specific signals and to relate them to climatic circumstances and the controls of the model components. Thereby several distinct sensitive regions could be located.

Chapter 3 presents an analysis of a series of simulations with the IPSL atmosphere-ocean model in response to orbital-induced changes in mid-Holocene insolation. By means of these simulations the dominant impacts of ocean and vegetation feedbacks and their synergy on mid- and high-latitude climate could be examined. To separate these, a series of AGCM, AOGCM, AVGCM and AOVGCM simulations were examined. It was found that the atmospheric response to orbital forcing produces a more than one degree °C warming over the continents in summer and a cooling during the rest of the year. Ocean feedback reinforces the cooling in spring but counteracts the autumn and winter cooling. The vegetation feedback produces a warming in all seasons, with largest changes in spring. Synergy between ocean and vegetation feedbacks leads to further warming, which can be as large as the independent impact of these feedbacks. The combination of these effects causes the high northern latitudes to be warmer than today throughout the year in the ocean-atmosphere-vegetation simulation. Furthermore the feedbacks also impact on the precipitation. The atmospheric response to orbital forcing reduces precipitation throughout the year. Ocean feedback reduces aridity during autumn, winter and spring, but does not affect summer precipitation. Vegetation feedback increases spring precipitation but amplifies summer drying. The synergy between the feedbacks increases precipitation in autumn, winter and spring, and reduces precipitation in summer. The combined changes amplify the seasonal contrast in precipitation in the ocean-atmosphere-vegetation simulation. The simulated vegetation changes resulting from this year-round warming are broadly consistent with observed mid-Holocene vegetation patterns.

In conclusion of Chapter 3, ocean and vegetation feedbacks are clearly important in modulating the Northern Hemisphere climate response to orbital forcing. Differences between the results of the IPSL simulations and those made with the CLIMBER

model suggest that the role of these feedbacks is not yet completely understood. These discrepancies between the impacts of feedbacks in different models suggest that the treatment of these feedbacks in climate models needs careful attention.

Recent studies by Gallimore et al. (2005), Braconnot et al (2007b) and Otto et al. (2009) suggest a smaller effect of a northward migration of forests on mid-Holocene warming in the northern Extratropics. In the model of Gallimore et al. (2005), an increase of northern grass- and shrub lands produces a cooling which partially compensates the warming snow– albedo feedback induced by boreal forests. The analysis by Otto et al. (2009) was performed with the ECHAM5-MPIOM-JSBACH model and feedbacks were computed by factor separation technique proposed by Stein and Alpert (1993). In contrast to the results obtained in the present study for the IPSL model, Otto et al. (2009) found an almost negligible contribution from vegetation changes and a smaller synergistic contribution from atmosphere-ocean and atmosphere-vegetation feedbacks in the winter season. This situation calls for a model intercomparison exercise on the basis of a unified model set-up and agreed boundary conditions with a special focus on regional impacts of ocean and vegetation feedbacks.

In Chapter 4.3 seven mid-Holocene simulations obtained from six different AOGCMs have been evaluated. A number of diagnostics that measured differences of simulated regional vegetation changes and reconstructions of northern extratropical vegetation patterns from pollen data have been introduced. These diagnostics provide a quantitative assessment of the match between the simulations and observations, and the possibility to identify the implications of the mismatches. The above mentioned vegetation data set (Prentice et al. 2000; Bigelow et al. 2003, Pickett et al. 2004) used for this purpose in the present study, represents the most comprehensive data set for 6 ka currently available. Nevertheless, there are some regions where the data are sparse (e.g. Central and North Eurasia) and other regions where the sites are not well dated (e.g. in Central Canada or Eastern Europe). Both of these issues place limits to the ability to assess climate simulations via this data base. Thus, it would be very

valuable if the work of the Biome6000 project could be continued to expand and improve the existing data sets.

It could be shown that the diagnostics introduced in this study can discriminate between correct (e.g. the simulation of changes in the tundra-taiga boundary) and broadly incorrect (e.g. the simulation of increased aridity in central Eurasia) model responses. It could also be demonstrated that these diagnostics can discriminate between the performances of different models. For example in showing that lowering CO_2 concentration from modern to 6 ka conditions produces a different response in western North America. Accordingly, these diagnostics provide a useful tool for the evaluation of coupled general circulation model simulations on a global and regional scale. Furthermore, it could be shown that differences in the averaging period used in processing the simulation data, can have an impact on the simulated area of specific biomes of up to 20 %, which reflects the large interannual to decadal variability of climate in mid- and high-latitudes.

In the following (Chapter 4.4) simulations from the AOGCM 'ECHAM5-MPIOM' and the AOVGCM 'ECHAM5-MPIOM-LPJ' models were evaluated employing once more the diagnostics which were established in the Chapter before. In addition the effect of climate variability was taken into account by examine an ensemble of model control runs. The variability of the modern simulations was introduced as a reference for assessing the climate signal in the mid-Holocene simulations.

North of 40 °N, forests occupy almost 70 % of the habitats in the vegetation reconstruction for present day. In the mid-Holocene (6ka) runs, the area covered with boreal forest is increased significantly – primarily in the AO 6 ka simulation – in contrast to a reduction in most of the simulations evaluated in the previous Chapters. A northward expansion of forest and therefore a substantial decrease of tundra area is a robust signal in all 6 ka GCM simulations which were evaluated. But the enlarged area of boreal forest is also a result of southward extension, reflecting a competitive advantage over more southern vegetation under 6 ka climate conditions. The patterns of boreal forest extent are related to a northward increase of the cold deciduous forest and additional substitutions of warmer temperate forests at the southern boarder of

distribution in the AO-6ka simulation in contrast to a northern increase of cold evergreen needleleaf forest but a decrease by southern temperate forest types extension in the AOV-6ka simulation. The loss of boreal forest in the former ECHAM3-LSG run − one of the simulations evaluated in Chapter 4.3 − is linked to the substantial increase of the warmer temperate forest whereas all simulations with different versions of the ECHAM model show a similar replacement of tundra.

The initial orbital forced summer warming/winter cooling caused in the higher latitudes of the AO model a warmer autumn season in the arctic zone and a colder winter season in the temperate zone compared to the control run. Whereas the AOV model simulates a warmer winter season in the arctic zone and a warmer winter and spring season in the temperate zone due to the response of vegetation dynamics including synergistic effects between the ocean and vegetation feedbacks.

Another main response to mid-Holocene climate change refers to the simulated increase of temperate grassland caused by drier interior environments in Central-North-America and Central-Eurasia. This change reflects the largest increase of all biome types in the ECHAM5-MPIOM and the ECHAM5-MPIOM-LPJ simulation. Although the mid-continental spread of dry xerophytic vegetation is another robust signal in all GCM simulations analyzed in this thesis, there is no evidence in the pollen data for such an extensive increase in the mid-Holocene, especially not in Central-Eurasia. Unfortunately, the number of data sites in this region is small and the BIOME4 model bares a bias in this area, either. Nevertheless, the BIOME4 model tends to over-estimate tree types in this region today, which would even shrinks the expansion bias of dry xerophytic vegetation in the 6 ka GCM simulations. Examinations of the 6 ka lake-level status (e.g. Harrison et al. 1996, Dorofeyuk and Tarasov 1998, Grunert et al. 2000, Kohlfeld and Harrison 2000, Rudayaa et al 2008, An et al. 2008) support conditions as moist as today. Similar to the first study, where the IPSL model showed a stepwise expansion of xerophytics in Central-Eurasia when coupled to a vegetation model, the ECHAM5-MPIOM-LPJ simulation predicts more unrealistic xerophytics than the ECHAM5-MPIOM. Hereby the mismatches against the observation data were enlarged. Even though the differences between AO and

AOV simulation are narrowed in the ECHAM5 simulations, still the additional dynamic vegetation cannot reverse this problematic signal.

On the other hand, those additional effects by the climate model with dynamic vegetation can even improve the pattern of vegetation distribution. The forest types in the temperate and southern boreal zone of Europe are more congruent with the pollen data in the AOV simulation. In the West-European region a manifold mixture of seasonal climate regimes dominates the competition between the biome types. Although the cooler and wetter than present summer signal in the Mediterranean (Cheddadi et al. 1997, Davis et al. 2003) could be much better reproduced in the AO simulation, over the entire European region the AOV simulation is more consistent with observations. Especially the AOV simulated changes in the northern temperate forest belts – indicating warmer than present winter in North- and East-Europe (Cheddady et al. 1997, Davis et al. 2003) – are more realistic.

Since many previous GCM 6ka simulations failed to reproduce the cooler and wetter summer reconstruction in southern Europe, this has led to a discussion if a sufficient increase in precipitation and the availability of water may be interpreted as a cooling signal from the represented vegetation (Brewer et al. 2007). More likely, a decrease in the winter temperature effects the growing season (reduced GDD_5) even when the summer temperature increase and thus could induce the changes in the Mediterranean mid-Holocene vegetation (Brewer et al. 2007).

Putting all pieces from the three studies together, it appears that two different patterns of vegetation changes occur in the mid-Holocene simulations: 1) a linear shift of vegetation boundaries, representing the direction of transition (e.g. eastern North-America) and 2) a scattered substitution in areas with a high diversity of vegetation (e.g. western North-America). The "shifting pattern" follows the change in a single climatic limit for the particular vegetation distribution (e.g. chilling), while the "scattered pattern" indicates several parallel climatic changes (e.g. seasonal moist availability and seasonal temperatures).

With the diagnostics introduced in this thesis, several sensitive regions in the Extratropics could be identified. The following is an attempt for a synopsis of vegetation changes induced by climate change for mid-Holocene according to the analysis presented in this study (Figure 5-1). To this end, the vegetation changes are assigned to simplified climatic signals.

Clear robust simulated warming signals are:

- an overall northward shift of the tree-line in Siberia triggered by prolonged growing season,
- a northward shift of the temperate forest belts in the eastern part of North-America triggered by winter warming.

Robust simulated cooling signals are:

- a westward extension of cool evergreen needleleaf forest in East-Europe triggered by chilling,
- a dispersal of cold deciduous forest in the central part of Canada triggered by chilling.

A combined cooling and humid signal (except for the IPSL-CM1 simulation) is:

- the increase of cool forests in Central-Asia triggered by a colder spring season and more humid summer and autumn seasons.

Signals of drying (except the CSM1.2Δ simulation in N-America) are:

- an increase of temperate grassland in East-Central-Asia triggered by less precipitation in the spring season and a strongly warmer summer season rising the potential risk of fire disturbance,
- an increase of temperate grassland in Central-North-America triggered by more precipitation in the summer season and less during the rest of the year.

Regions with contrary simulated signals are:

- the different distributions of warm-temperate evergreen mixed forest, temperate deciduous broadleaf forest and temperate evergreen needleleaf forest along the Atlantic coast of Western Europe resulting from different mean winter and summer temperatures,

- the different distributions of warm-temperate evergreen mixed forest, temperate deciduous broadleaf forest and temperate shrubland and savannas in South-Europe caused by different mean winter and summer temperatures and precipitation,
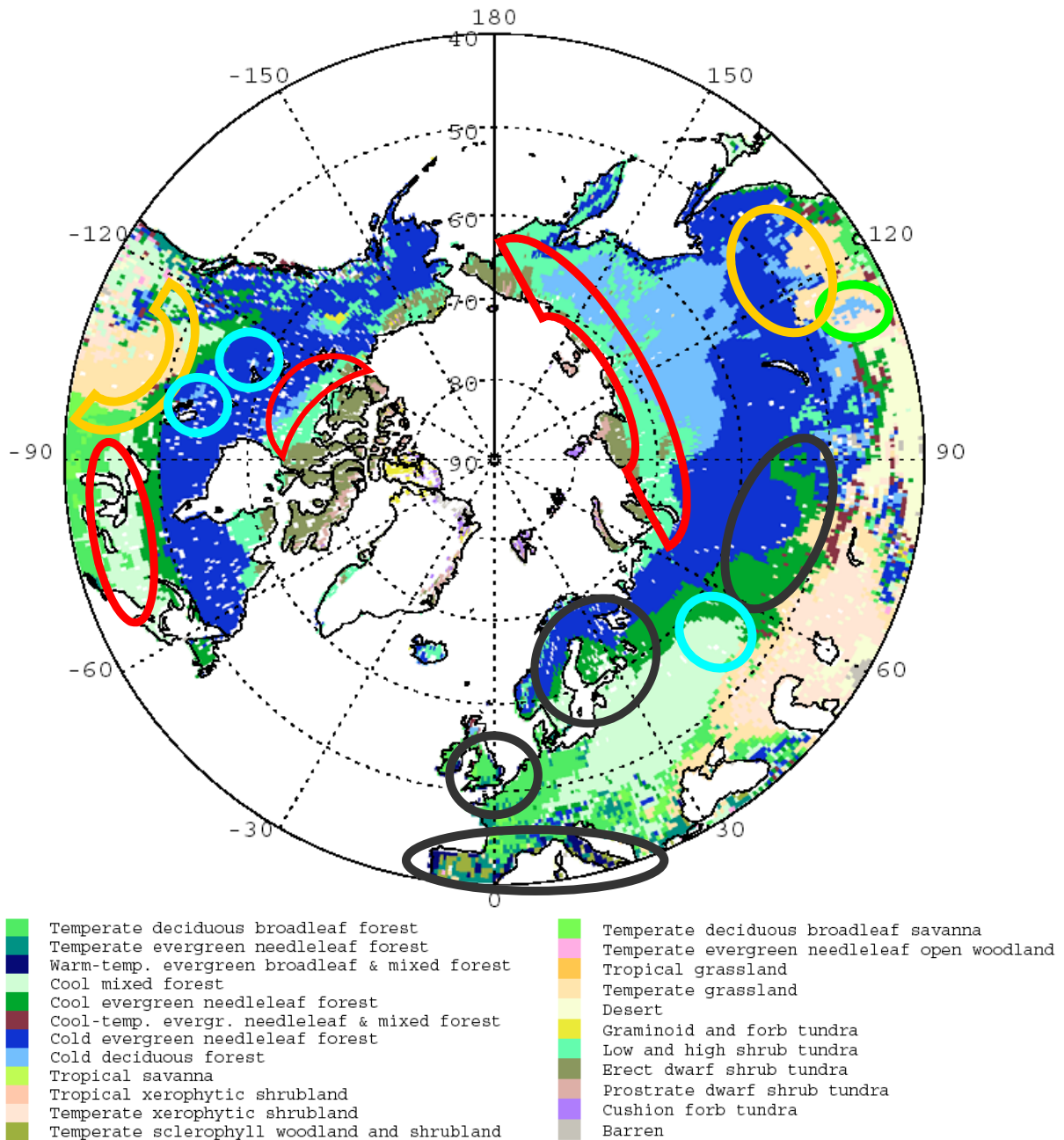

Temperate deciduous broadleaf forest
Temperate evergreen needleleaf forest
Warm-temp. evergreen broadleaf & mixed forest
Cool mixed forest
Cool evergreen needleleaf forest
Cool-temp. evergr. needleleaf & mixed forest
Cold evergreen needleleaf forest
Cold deciduous forest
Tropical savanna
Tropical xerophytic shrubland
Temperate xerophytic shrubland
Temperate sclerophyll woodland and shrubland

Temperate deciduous broadleaf savanna
Temperate evergreen needleleaf open woodland
Tropical grassland
Temperate grassland
Desert
Graminoid and forb tundra
Low and high shrub tundra
Erect dwarf shrub tundra
Prostrate dwarf shrub tundra
Cushion forb tundra
Barren

Figure 5-1: Detected sensitive regions in vegetation reconstruction by the BIOME4 model with GCM climate simulations for mid-Holocene. Warming signals are marked in red, cooling signals in blue, cool and humid signal in green, drying signal in yellow and contrasting signals of the simulations in black.

135

- the different direction of shift of cool mixed and cool evergreen needleleaf forest in North-Europe as a consequence of different mean winter temperatures and chilling.
- The different distribution of cool evergreen needleleaf forest in central West-Asia induced by different winter temperatures.

Not all of the robust simulated signals are realistic and supported by mid-Holocene pollen records. But the expansion of boreal forests is supported by pollen evidence and thus gives hints for vegetation changes under future climate scenarios. It is expected on the basis of several simulations e.g. in the 4th IPCC report (Meehl et al. 2007) and proxy data estimations (e.g. Chapin et al. 2005) that by the end of this century, the northern latitudes will be significantly warmer than present. This expected warming seems to be comparable to the warming from mid-Holocene insolation forcing in the boreal and polar zones, so that the 6 ka vegetation change gives an indication of vegetation changes to be expected in the next century in this northern regions.

This analogy does not hold for other sensitive Extratropical regions. In the Mediterranean region of Southern Europe the mid-Holocene situation differs from what the simulations of the future scenarios in the 4th IPCC report project. The locally cooler and wetter 6 ka climate conditions are strengthened by biogeophysical processes forced by insolation in contrast to the predicted warmer and dryer conditions appearing by upcoming greenhouse gas increases.

So, the partly strong signals of the climate conditions at 6 ka would for the future imply a migration of biomes into nowadays agriculturally productive areas, a possibility to be excluded because of the expected growth of human population far into the 21st century with its increasing food demands.

Although the simulations of an asymmetric northward shift of boreal forest in 6 ka are robust and agrees with observations (Frenzel et al. 1992; TEMPO et al. 1996; Cheddadi et al. 1997; Tarasov et al. 1998; Prentice and Webb III 1998; MacDonald et al. 2000), the prediction of the tree-line varies partly by about several hundreds of kilometres between the evaluated GCM simulations (Figure 5-2). However, a view at the furthest northern position of forest reveals some complications: a thin westward extension of boreal forest in Northwest-Siberia along the Verkhojansk-mountain range produces the obviously strongest poleward shift in some simulations (Figure 5-2,right). In fact, there are trees north of the 70th latitude. However due to orography, a vast area of tundra is found south of the region and a second tree-line exist further south along the 67th latitude. An additional complication arises with respect to the position of the actual taiga-tundra-boundary. A comparison with the reconstructed tree-line derived by a synthesis of land cover satellite data (SYNMAP; from Jung et al. 2006) shows for North-America a deviation from the BIOME4 reconstruction for present day climate that is partly larger than the differences between the 6 ka simulations (Figure 5-2,left). Those differences for the present position of the tree-line infers from the detection method and from the definition for trees and shrubs, namely the fractional threshold for vegetation cover at which a grid cell switches from forest to tundra.

The question where and at what extent boreal forest exists is important, because the vegetation–snow albedo feedback is expected to have a strong impact on the temperatures at high latitudes (deNoblet et al. 1996; Texier et al. 1997; Crucifix et al. 2002; Foley 2005; Claussen et al. 2006; Notaro and Liu 2008).

5.2 Outlook

The mid-Holocene optimum at 6 ka represents only a snap shot at the end of the Holocene thermal maximum with several successive and shifting phases that started in North-western North-America between 11 ka and 9 ka (Kaufman et al. 2004), followed by a continuous weakening of the strong summer insolation. Ice-cover, sea-level, vegetation-cover, bare ground and the circulations of the atmosphere and the ocean were in a highly transient phase. Hence to capture the situation at 6 ka, transient simulations like those that have been done with EMIC models by Claussen and Gayler (1997), Claussen et al. (1999), Brovkin et al. (2002) and Renssen et al. (2003), or those GCM runs with limitations e.g. in the ocean dynamics (Schmidt et al. 2004, Lorenz et al. 2004, Otto-Bliesner et al. 2006, Schurgers et al. 2006, Liu et al. 2007) could possibly improve the unrealistic signals in the equilibrium model simulations and help to re-define the overall role of biogeophysical and biogeochemical feedbacks in the climate system (Claussen 2009). The exploration of transient Holocene vegetation and climate change using pollen reconstructions and simulations provides an interesting challenge to plant geography and involved research.

Another effort to enhance the quality of global climate simulations could be a better treatment of the soils. This implies soil parameters, soil evolution, moisture memory, flux exchanges to the atmosphere, respiration and additional landcover types like peat or wetlands. For instance the diagnostic vegetation model BIOME4 uses in addition to the standard temperature and precipitation parameters also water holding capacity and water percolation as input fields. So far these soil parameters are not routinely provided by the GCM simulation output.
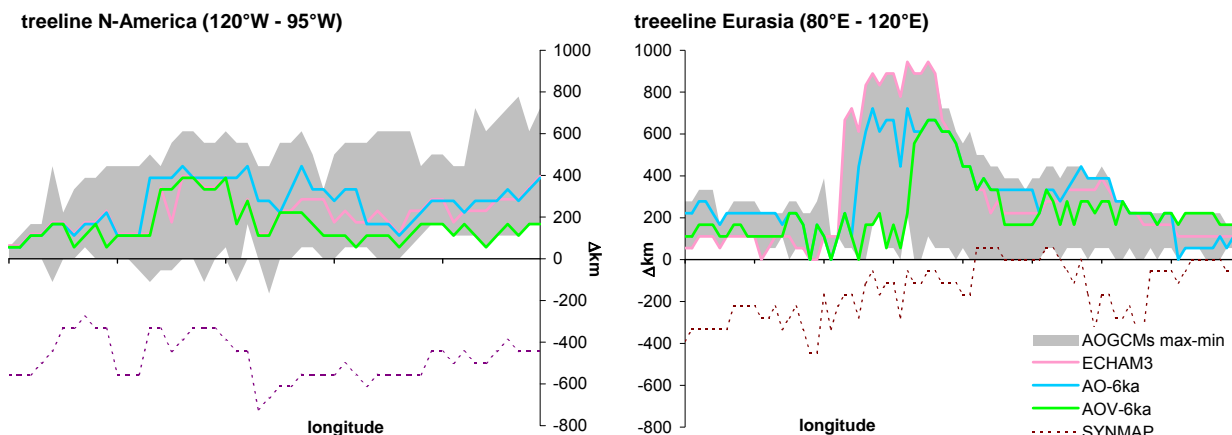
Figure 5-2: Shift of the arctic tree line simulated for 6 ka by ECHAM3-LSG (ECHAM), ECHAM5-MPIOM (AO-6ka), ECHAM5-MPIOM-LPJ (AOV-6ka) and the range of the minimum and maximum shift referred to the AOGCM simulations of CSM1.2, CSM1.2D, ECBilt, HADCM2, ECHAM3, IPSL-CM1 and MRI compared to the BIOME4 modern reconstruction (x-axis) in North-America (120-95 °W) and Eurasia (80-120 °E). The spotted line shows the relative position of the actual tree-line derived from land cover satellite data (SYNMAP) from Jung et al. (2006).

Comprehensive climate system models are still growing in complexity. Potential problems, e.g. introduced by the continuous further development of the models, could be detected early by routinely applying the vegetation diagnostics introduced and analyzed in this study to the simulation output of GCMs – e.g. as standard part of the post processing. In view of the importance of climate projections for anticipating future climate changes, such a procedure could strengthen the confidence in the reliability of their results. From this point of view, palaeovegetation studies, like the one presented here, can provide a substantial support to climate change science.

Bibliography

Literature

Ana, C-B., Chena, F-H, Barton, L., (2008) Holocene environmental changes in Mongolia: A review. Global and Planetary Change 63: 4, doi: 10.1016/j.gloplacha.2008.03.007.

Arctic Climate Impact Assessment scientific report (ACIA): Impacts of a warming Arctic Cambridge University Press, (2005) Hassol, S.J. 1042p., http://www.acia.uaf.edu.

Barnola, J.-M., Raynaud, D., Korotkevich, Y.S., Lorius. C. (1987) Vostok ice core provides 160,000-year record of atmospheric CO2. Nature 329: 408-14.

Bartalev, S.A., Belward, A.S., Erchov, D.V., Isaev, A.S., Bartholomé, E. (2003) Land Cover Map of the Northern Eurasia based on the SPOT-Vegetation data. Global Land Cover 2000 project. TerraNorte Information System. RAS Space Research Institute. (http://terranorte.iki.rssi.ru).

Berger, A. (1978) Long-term variations of daily insolation and Quaternary climatic changes. Journal of the Atmospheric Sciences 35:2362-2367.

Berger, A. (2001) The role of CO2, sea level and vegetation during the Milankovitch-forced glacial-interglacial cycles. In: Hammer, C.U., (ed) Geosphere-biosphere interactions and climate. Pontifical Academy of Sciences. Cambridge University Press, Cambridge, 119-146.

Beringer, J., Tapper, N. J., McHugh, I., Lynch, A. H., Serreze, M. C., & Slater, A. (2001) Impact of Arctic treeline on synoptic climate. Geophysical Research Letters 28 (22): 4247-4250.

Bigelow, N.H., Brubaker, L.B., Edwards, M.E., Harrison, S.P., Prentice, I.C., Anderson, P.M., Andreev, A.A., Bartlein, P.J., Christensen, T.R., Cramer, W., Kaplan, J.O., Lozhkin, A.V., Matveyeva, N.V., Murray, D.F., McGuire, A.D., Razzhivin, A.Y, Ritchie, J.C., Smith, B., Walker, D.A., Galjewski, K., Wolf, V., Holmquist, B., Igarashi, Y., Kremenetskii, K., Paus, A., Pisaric, M.F.J., Volkova, V.S. (2003) Climate change and Arctic ecosystems I. - Vegetation changes north of 50°N between the last glacial maximum, mid-Holocene and present. Journal of Geophysical Research 108: doi: 10.1029/2002JD002558.

Bonan, G.B., Pollard, D., Thompson, S.L. (1992) Effects of boreal forest vegetation on global climate. Nature 359: 716-718.

Bonan, G.B. (1998) The land surface climatology of the NCAR Land Surface Model coupled to the NCAR Community Climate Model. Journal of Climate 11: 1307-1326.

Bonfils, C., N. de Noblet-Ducoudré, J. Guiot, and P. Bartlein, (2004) Some mechanisms of mid-Holocene climate change in Europe, inferred from comparing PMIP models to data. Climate Dynamics 23: 79-98.

Braconnot, P., Marti, O., Joussaume, S. (1997) Adjustment and feedbacks in a global coupled ocean-atmosphere model. Climate Dynamics 13: 507-519.

Braconnot, P., Joussaume, S., Marti, O., de Noblet, N. (1999) Synergistic feedbacks from ocean and vegetation on the African monsoon response to mid-Holocene insolation. Geophysical Research Letters 26: 2481-2484.

Braconnot, P., Joussaume, S., de Noblet, N., Ramstein, G. (2000a) Mid-Holocene and Last Glacial Maximum African monsoon changes as simulated within the Paleoclimate Modelling Intercomparison Project. Global and Planetary Change 26: 51-66.

Braconnot, P., Marti, O., Joussaume, S., Leclainche, Y. (2000b) Ocean feedback in response to 6 kyr BP insolation. Journal of Climate 13: 1537-1553.

Braconnot, P., Loutre, M.F., Dong, B., Joussaume, S., Valdes, P. (2002) How the simulated change in monsoon at 6 ka BP is related to the simulation of the modern climate: results from the Paleoclimate Modeling Intercomparison Project. Climate Dynamics 19: 107-121.

Braconnot, P., Otto-Bliesner, B., Harrison, S., Joussaume, S., Peterchmitt, J.-Y., Abe-Ouchi, A., 15 Crucifix, M., Driesschaert, E., Fichefet, Th., Hewitt, C. D., Kageyama, M., Kitoh, A., Laˆıne´ , A., Loutre, M.-F., Marti, O., Merkel, U., Ramstein, G., Valdes, P., Weber, S. L., Yu, Y., and Zhao, Y, (2007a) Results of PMIP2 coupled simulations of the Mid-Holocene and Last Glacial Maximum – Part 1: experiments and large-scale features. Climate of the Past, 3: 261–277, http://www.clim-past.net/3/261/2007/.

Braconnot, P., Otto-Bliesner, B.L., Harrison, S., Joussaume, S., Peterchmitt, J.-Y., Abe-Ouchi, A., Crucifix, M., Driesschaert, E., Fichefet, T., Hewitt, C.D., Kageyama, M., Kitoh, A., Laıˆne´ , A., Loutre, M.-F., Marti, O., Merkel, U., Ramstein, G., Valdes, P., Weber, S.L., Yu, Y., Zhao, Y., (2007b). Results of PMIP2 coupled simulations of the Mid-Holocene and Last Glacial Maximum – Part 2: feedbacks with emphasis on the location of the ITCZ and mid- and high latitudes heat budget. Climate of the Past 3: 279–296.

Bradley, R.S., Briffa, K.R., Cole, J., Hughes, M.K., Osborn, T.J., (2002) In: Alverson, K.D., Bradley, R.S., Pedersen, T.F., (Eds), 2003: Paleoclimate, Global Change and the Future 105-141.

Brewer, S., Guiot, J., Torre, F. (2007) Mid-Holocene climate change in Europe: a data model comparison. Climate of the Past 3: 499–512.

Brewer, S., Francois, L., Cheddadi, R., Laurent, J.-M., Favre, E. (2009) Comparison of simulated and observed vegetation for the mid-Holocene in Europe. Climate of the Past Discussion, 5: 965–1011.

Broström, A., Coe, M., Harrison, S.P., Gallimore, R., Kutzbach, J.E., Foley, J., Prentice, I.C., Behling, P. (1998) Land surface feedbacks and paleomonsoons in northern Africa. Geophysical Research Letters 25: 3615-3618.

Brovkin, V., Bendtsen, J., Claussen, M., Ganopolski, A., Kubatzki, C., Petoukhov, V., Andreev, A. (2002) Carbon cycle, vegetation and climate dynamics in the Holocene: experiments with the CLIMBER-2 model. Global Biogeochemical Cycles 16(4): 1139 DOI: 10.1029/2001GB001662.

Brovkin, V., Levis, S., Loutre, M.F., Crucifix, M., Claussen, M., Ganopolski, A., Kubatzki, C., Petoukhov, V. (2003) Stability analysis of the climate-vegetation system in the northern high latitudes. Climate Change 57(1): 119-138.

Canadell, J., Jackson, R.B., Ehleringer, J.R., Mooney, H.A., Sala, O.E., Schulze, E.D., (1996) Maximum rooting depth of vegetation types at the global scale. Oecologia 108:583-595.

CAPE Project Members (2001) Holocene paleoclimate data from the Arctic: testing models of global climate change. Quaternary Science Review 20: 1275-1287.

Chapin, F.S.; Sturm, M.; Serreze, M.C.; McFadden, J.P.; Key, J.R.; Lloyd, A.H.; McGuire, A.D.; Rupp, T.S.; Lynch, A.H.; Schimel, J.P.; Beringer, J.; Chapman, W.L.; Epstein, H.E.; Euskirchen, E.S.; Hinzman, L.D.; Jia, G.; Ping, C.L.; Tape, K.D.; Thompson, C.D.C.; Walker, D.A.; Welker, J.M. (2005) Role of land-surface changes in Arctic summer warming. Science 310: 657-660.

Chapman, W. L., Walsh, J. E. (1993): Recent variations of sea ice and air temperature in high latitudes. Bulletin of the American Meteorological Society 74, 33-47.

Chapman, W.L.,. Walsh, J.E. (2006) Simulations of Arctic temperature and pressure by global climate models. Journal of Climate 20(4) 609–632, doi: 10.1175/JCLI4026.1.

Cheddadi, R., Yu, G., Guiot, J., Harrison, S.P., Prentice, I.C., (1997) The climate of Europe 6000 years ago. Climate Dynamics 13: 1–9.

Clark, C.D., Knight, J.K., Gray, J.T. (2000) Geomorphological reconstruction of the Labrador Sector of the Laurentide Ice Sheet. Quaternary Science Reviews 19: 1343-1366.

Claussen, M. (1994) On coupling global biome models with climate models. Climate Research 4: 203-221.

Claussen, M. (1997). Modeling bio-geophysical feedback in the African and Indian monsoon region. Climate Dynamics 13(4): 247-257.

Claussen, M., Gayler, V. (1997) The greening of the Sahara during the mid-Holocene: results of an interactive atmosphere-biome model. Global Ecology and Biogeography Letters 6: 369-377.

Claussen, M. (1998) On multiple solutions of the atmosphere – vegetation system in present-day climate, Global Change Biology 4: 549-559.

Claussen, M., Brovkin, V., Ganopolski, A., Hoelzmann, P., Pachur, H.-J., (1999). Simulation of an abrupt change in Saharan vegetation in the mid-Holocene. Geophysical Research Letters 26, 2037–2040.

Claussen, M. (2001) Biogeophysical feedbacks and the dynamics of climate. In: Max-Planck-Institute for Biogeochemistry J, Germany, ed. Global Biogeochemical Cycles in the Climate System. Academic Press, San Diego 61-69.

Claussen M. (2003). Does land surface matter in weather and climate? In: Kabat P, Claussen M, Dirmeyer P, Gash JHC, Guenni L, Meybeck M, Pielke RA, Vörösmarty CJ, Lütkemeier S (eds) Vegetation, Water, Humans and the Climate: A New Perspective on an Interactive System. Springer-Verlag Heidelberg

Claussen, M., Fohlmeister, J., Ganopolski, A., Brovkin, V. (2006) Vegetation dynamics amplifies precessional forcing. Geophysical Research Letters 33: L09709, doi:10.1029/2006GL026111.

Claussen, M. (2009) Late Quaternary vegetation – climate feedbacks. Climate of the Past Discussions 5: 635–670, [www.clim-past-discuss.net/5/635/2009/].

CLIMAP (1981). Seasonal reconstructions of the Earth's surface at the last glacial maximum in Map Series, Technical Report MC-36. Boulder, Colorado: Geological Society of America.

COHMAP members (1988) Climatic change of the last 18,000 years: observations and model simulations. Science 241: 1043-1052.

Cubash, U., Meehl, G.A., et al. (2001) Projections of future climate change, in Climate Change 2001: The Scientific Basis, edited by J.T. Houghton et al., Cambridge Univ. Press, New York. 525-582

Curry, J.A., Rossow, W.B., Randall, D., Schramm, J.L., (1996) Overview of Arctic cloud and radiation characteristics. Journal of Climate 9: 1731-1764, doi:10.1175/1520-0442(1996)009<1731:OOACAR>2.0.CO;2.

Crucifix, M., Loutre, M.F., Tulkens, P., Fichefet, T., Berger, A., (2002) Climate evolution during the Holocene: a study with an Earth system model of intermediate complexity. Climate Dynamics 19 (1): 43–60.

Davis, B.A.S., Brewer, S., Stevenson, A.C., Guiot, J., and Data contributors, (2003) The temperature of Europe during the Holocene reconstructed from pollen data. Quaternary Science Review 22: 1701–1716,. 967, 968, 977.

de Noblet, N.I., Prentice, I.C., Joussaume, S., Texier, D., Botta, A., Haxeltine, A. (1996) Possible role of atmosphere-biosphere interactions in triggering the last glaciation. Geophysical Research Letters 23: 3191-3194.

Dorofeyuk, N.I., Tarasov, P.E. (1998) Vegetation and lake levels of northern Mongolia since 12,500 yr B.P. based on the pollen and diatom records. Stratigraphy. Geological Correlation 6(1), 70-83.

Douville, H., Royer, J.F. (1996) Sensitivity of the Asian summer monsoon to an anomalous Eurasian snow cover within the Meteo-France GCM. Climate Dynamics 12: 449-466.

Ducoudré, N.I., Laval, K., Perrier, A. (1993) SECHIBA, a new set of parameterizations of the hydrologic exchanges at the land atmosphere interface within the LMD atmospheric general circulation model. Journal of Climate 6: 248-273.

Edwards, M.E., Anderson, P.M., Brubaker, L.B., Ager, T.A., Andreev, A.A., Bigelow, N.H., Cwynar, L.C., Eisner, W.R., Harrison, S.P., Hu, F.-S., Jolly, D., Lozhkin, A.V., MacDonald, G.M., Mock, C.J., Ritchie, J.C., Sher, A.V., Spear, R.W., Williams, J.W., Yu, G. (2000) Pollen-based biomes for Beringia 18,000, 6000 and 0 14C yr BP. Journal of Biogeography 27: 521-554.

Elenga, H., Peyron, O., Bonnefille, R., Jolly, D., Cheddadi, R., Guiot, J., Andrieu, V., Bottema, S., Buchet, G., de Beaulieu, J. L., Hamilton, A. C., Maley, J., Marchant, R., Perez-Obiol, R., Reille, M., Riollet, G., Scott, L., Straka, H., Taylor, D., Van Campo, E., Vincens, A., Laarif, F., Jonson, H. (2000) Pollen-based biome reconstruction for southern Europe and Africa 18,000 yr BP. Journal of Biogeography 27(3): 621-634.

FAO (1995) Digital soil map of the world and derived soil properties. Food and Agriculture Organization, Rome.

Foley, J.A., Kutzbach, J.E., Coe, M.T., Levis, S. (1994) Feedbacks between climate and boreal forests during the Holocene epoch. Nature 371: 52-54.

Foley, J.A., Prentice, I.C., Ramankutty, N., Levis, S., Pollard, D., Sitch, S., Haxaltine A., (1996) An integrated biosphere model of land surface processes, terrestrial carbon balance, and vegetation dynamics. Global Biogeochemical Cycles 10(4): 603-628.

Foley, J.A. (2005) Tipping points in the Tundra. Science 310: 627–628.

Frenzel, B., Pecsi, B., Velichko. A.A. (1992). (Ed.s). Atlas of Palaeoclimates & Palaeoenvironments of the Northern Hemisphere. INQUA/Hungarian Academy of Sciences. Budapest.

Gallimore, R.G., Kutzbach, J.E. (1996) Role of orbitally induced changes in tundra area in the onset of glaciation. Nature 381: 503-505.

Gallimore, R.G., Jacob, J., Kutzbach, J.E (2005) Coupled atmosphere-ocean-vegetation simulations for modern and mid-Holocene climates: role of extratropical vegetation cover feedbacks. Climate Dynamics 25: 755–776.

Ganopolski, A., Kubatzki, C., Claussen, M., Brovkin, V., Petoukhov, V. (1998) The influence of vegetation-atmosphere-ocean interaction on climate during the mid-Holocene. Science 280: 1916-1919.

GLC2000 database, European Commision Joint Research Centre, 2003. http://www-gem.jrc.it/glc2000.

Gloersen, P., Campbell, W.J. (1991) Recent variations in arctic and antarctic sea-ice covers. Nature 352: 33-36.

Gond, V., Vogt, P., Achard, F., Zubkov, A.M., Mollicone , D., Yu Savin, I., Fritz, S., Repina, G., Hartley, A.. Vavrus, S.J. (1999) The response of the coupled Arctic sea ice atmosphere system to orbital forcing and ice motion at 6 kyr and 115 kyr BP. Journal of Climate 12: 873 – 896.

Guilyardi, E., Madec, G., Terray, L. (1999) The role of lateral ocean physics in the upper ocean thermal balance of a coupled ocean-atmosphere model. Institut Pierre Simon Laplace Note 13:19.

Guiot, J., Boreux, J.J., Braconnot, P., Torre, F., Participants, (1999) Data-model comparison using fuzzy logic in paleoclimatology. Cimate Dynamics 15: 569-581.

Grunert, J., Lehmkuhl, F., Walther, M. (2000) Paleoclimatic evolution of the Uvs Nuur basin and adjacent areas (Western Mongolia). Quaternary International 65-66: 171-192.

Harrison, S.P., Yu, G., Tarasov, P.E. (1996) Late Quaternary lake-level record from northern Eurasia. Quaternary Research 45: 138-159.

Harrison, S.P., Jolly, D., Laarif, F., Abe-Ouchi, A., Dong, B., Herterich, K., Hewitt, C., Joussaume, S., Kutzbach, J.E., Mitchell, J., de Noblet, N., Valdes, P. (1998) Intercomparison of simulated global vegetation distributions in response to 6 kyr BP orbital forcing. Journal of Climate 11: 2721-2742.

Harrison, S.P., Yu, G., Takahara, H., Prentice, I.C. (2001). Palaeovegetation - Diversity of temperate plants in east Asia. Nature 413: 129-130.

Harrison, S.P., Braconnot, P., Joussaume, S., Hewitt, C., Stouffer, R.J. (2002) Comparison of palaeoclimate simulations enhances confidence in models. Eos, Transactions, American Geophysical Union 83: 447-447.

Harrison, S.P., Kutzbach, J.E., Liu, Z., Bartlein, P.J., Otto-Bliesner, B.L., Muhs, D., Prentice, I.C., Thompson, R.S (2003) Mid-Holocene climates of the Americas: a dynamical response to changed seasonality. Climate Dynamics 20: 663-688, doi:10.1007/s00382-002-0300-6.

Harrison, S.P., Prentice, I.C. (2003) Climate and CO2 controls on global vegetation distribution at the last glacial maximum: analysis based on palaeovegetation data, biome modelling and palaeoclimate simulations. Global Change Biology 9: 983-1004.

Hantel, M., Kraus, H., Schönwiese, C.-D. (1987). Climate definition. Landolt-Börnstein N. Serie, V/4c/1. Berlin: Springer Verlag: 1-28.

Haxeltine, A., Prentice, I.C. (1996) BIOME3: An equilibrium terrestrial biosphere model based on ecophysical constraints, resource availability, and competition among plant functional types. Global Biogeochemical Cycles 10(4): 693-709.

Heiskanen, J. (2008) Evaluation of global land cover data sets over the tundra-taiga transition zone in northernmost Finland. International Journal of Remote Sensing 29 (13) 3727-3751, doi: 10.1080/01431160701871104.

Hewit, C.D., Mitchell, J.F.B. (1998) A fully coupled GCM simulation of the climate of the mid- Holocene. Geophysical Research Letters 25: 361-364.

Hewitt, C.D., Broccoli, A.J., Mitchell, J.F.B., Stouffer, R.J. (2001) A coupled model study of the last glacial maximum: Was part of the North Atlantic relatively warm? Geophysical Research Letters 28: 1571-1574.

Holland, M.M., Bitz, C.M., (2003) Polar amplification of climate change in the coupled model intercomparison project. Climate Dynamics 21, 221-232.

Indermühle, A., Stocker, T.F., Joos, F., Fischer, H., Smith, H.J., Wahlen, M., Deck, B., Mastroianni, D., Tschumi, J., Blunier, T., Meyer, R., Stauffer, B. (1999) Holocene carbon-cycle dynamics based on CO_2 trapped in ice at Taylor Dome, Antarctica. Nature 398: 121–126, doi:10.1038/18158,. 972.

Jackson, R.B., Canadell, J., Ehleringer, J.R., Mooney, H.A., Sala, O.E., Schulze, E.D. (1996) A global analysis of root distributions for terrestrial biomes. Oecologia 108: 389-411.

Johns, T.C., Carnell, R.E., Crossley, J.F., Gregory, J.M., Mitchell, J.F.B., Senior, C.A., Tett, S.F.B., Wood, R.A. (1997) The second Hadley Centre coupled ocean-atmosphere GCM: model description, spinup and validation. Climate Dynamics 13: 103-134.

Jolly, D., Prentice, I.C., Bonnefille, R., Ballouche, A., Bengo, M., Brenac, P., Buchet, G., Burney, D., Cazet, J.P., Cheddadi, R., Edorh, T., Elenga, H., Elmoutaki, S., Guiot, J., Laarif, F., Lamb, H., Lezine, A.M., Maley, J., Mbenza, M., Peyron, O., Reille, M., Reynaud-Farrera, I., Riollet, G., Ritchie, J.C., Roche, E., Scott, L., Ssemmanda, I., Straka, H., Umer, M., Van Campo, E., Vilimumbalo, S., Vincens, A., Waller, M. (1998) Biome reconstruction from pollen and plant macrofossil data for Africa and the Arabian peninsula at 0 and 6000 years. Journal of Biogeography 25(6) 1007-1027.

Joussaume, S., Taylor, K.E. (1995) Status of the Paleoclimate Modeling Intercomparison Project (PMIP). In: Gates WL (ed) Proceedings of the First International AMIP Scientific Conference, 15-19 May 1995. Vol WMO/TD-No. 732. WCRP (World Climate Research Programm) - 92, Monterey, California, USA, 425-430.

Joussaume, S., Braconnot, P. (1997) Sensitivity of paleoclimate simulation results to season definitions. Journal of Geophysical Research-Atmospheres 102: 1943-1956.

Joussaume, S., Taylor, K.E., Braconnot, P., Mitchell, J.F.B., Kutzbach, J.E., Harrison, S.P., Prentice, I.C., Broccoli, A.J., Abe-Ouchi, A., Bartlein, P.J., Bonfils, C., Dong, B., Guiot, J., Herterich, K., Hewitt, C.D., Jolly, D., Kim, J.W., Kislov, A., Kitoh, A., Loutre, M.F., Masson, V., McAvaney, B., McFarlane, N., de Noblet, N., Peltier, W.R., Peterschmitt, J.Y., Pollard, D., Rind, D., Royer, J.F., Schlesinger, M.E., Syktus, J., Thompson, S., Valdes, P., Vettoretti, G., Webb, R.S., Wyputta, U. (1999) Monsoon changes for 6000 years ago: Results of 18 simulations from the

Paleoclimate Modeling Intercomparison Project (PMIP). Geophysical Research Letters 26: 859-862.

Joussaume, S., Taylor, K.E. (2000) The Paleoclimate Modeling Intercomparison Project. In: Braconnot, P. (ed) Paleoclimate Modelling Intercomparison Project (PMIP). Proceedings of the third PMIP workshop. Vol WCRP-111; WMO/TD-No. 1007. WCRP, La Huardière, Canada, 4-8 October 1999, pp 9-25.

Jung, M., Henkel, K., Herold, M., Churkina, G., (2006) Exploiting synergies of global land cover products for carbon cycle modelling. Remote Sens. Environment., 101(4): 534–553.

Jungungclaus, J. H., Haak, H., Esch, M., Roeckner, E., Marotzke, J. (2005): Will Greenland melting halt the thermohaline circulation? Geophysical Research Letters 33: L17708, doi: 10.1029/2006GL026815.

Kageyama, M., Valdes, P.J., Ramstein, G., Hewitt, C., Wyputta, U. (1999) Northern hemisphere storm tracks in present day and Last Glacial Maximum climate simulations: A comparison of the European PMIP models. Journal of Climate 12: 742-760.

Kaufman, D.S., Ager, A., Anderson, N.J., Anderson, P.M., Andrews, J. T., Bartlein, P.J., Brubaker, L.B., Coats, L.L., Cwynar, L.C., Duvall, M.L. , Dyke, A.S., Edwards, M. E., Eisner, W.R., Gajewski, K., Geirsdóttir, A., Hu, F.S., Jennings, A.E., Kaplan, M.R., Kerwin, M.W., Lozhkin, A.V., MacDonald, G M., Miller, G.H., Mock, C J., Oswald, W.W., Otto-Bliesner, B.L., Porinchu, D.F., Rühland, K., Smol, J.P., Steig, E.J., Wolfe B.B. 2004. Holocene thermal maximum in the Western Arctic (0 to 180W). Quaternary Science Reviews, 23, 529-560.

Kaplan, J.O., Bigelow, N.H., Prentice, I.C., Harrison, S,P., Bartlein, P.J., Christensen, T.R., Cramer, W., Matveyeva, N.V., McGuire, A.D., Murray, D.F., Razzhivin, V.Y., Smith, B., Walker, D.A., Anderson, P.M., Andreev, A.A., Brubaker, L.B., Edwards, M.E., Lozhkin, A.V. (2003) Climate change and arctic ecosystems II. Modeling, paleodata-model comparisons, and future projections. Journal of Geophysical Research 108: doi:10.1029/2002JD002559.

Kitoh, A., Murakami, S. (2002) Tropical Pacific climate at the mid-Holocene and the Last Glacial Maximum simulated by a coupled ocean-atmosphere general circulation model. Paleoceanography 17: doi:10.1029/2001PA000724.

Kohfeld, K. E., and Harrison, S. P. (2000). How well can we simulate past climates? Evaluating the models using global palaeoenvironmental datasets. Quaternary Science Reviews 19(1-5), 321-346.

Kohfeld, K.E., Harrison, S.P. (2000) How well can we simulate past climates? Evaluating the models using global palaeoenvironmental datasets. Quaternary Science Reviews 19: 321-346.

Kraus, H. (2000): Die Atmosphäre der Erde. Eine Einführung in die Meteorologie. - Vieweg, Braunschweig.

Kubatzki, C., Claussen, M. (1998) Simulation of the global bio-geophysical interactions during the Last Glacial Maximum. Climate Dynamics 14:461-471.

Kubatzki, C., Montoya, M., Rahmstorf, S., Ganopolski, A., Claussen, M. (2000) Comparison of the last interglacial climate simulated by a coupled global model of intermediate complexity and an AOGCM. Climate Dynamics 16 :799-814

Kutzbach, J.E. (1981) Monsoon climate of the early Holocene: climate experiment with the earth's orbital parameters for 9000 years ago. Science 214: 59-61

Kutzbach, J.E., Otto-Bliesner, B.L. (1982) The sensitivity of the African-Asian monsoonal climate to orbital parameter changes for 9000 years B.P. in a low-resolution general circulation model. Journal of the Atmospheric Sciences 39: 1177-1188.

Kutzbach, J.E., Street-Perrott, F.A. (1985) Milankovitch forcing of fluctuations in the level of tropical lakes from 18 to 0 kyr BP. Nature 317: 130-134.

Kutzbach, J.E., Guetter, P.J. (1986) The influence of changing orbital parameters and surface boundary conditions on climate simulations for the past 18000 years. Journal of the Atmospheric Sciences 43: 1726-1759.

Kutzbach, J.E., Gallimore, R.G. (1988) Sensitivity of a coupled atmosphere mixed layer ocean model to changes in orbital forcing at 9000 years BP. Journal of Geophysical Research-Atmospheres 93: 803-821.

Kutzbach, J.E., Guetter, P.J., Behling, P.J., Selin, R. (1993) Simulated climatic changes: Results of the COHMAP climate-model experiments. In: Wright, Jr. H.E., Kutzbach, J.E., Webb III, T., Ruddiman, W.F., Street-Perrott, F.A., Bartlein, P.J. (Editors), Global Climates since the Last Glacial Maximum. University of Minnesota Press, Minneapolis, pp. 24-93.

Kutzbach, J.E., Liu, Z. (1997) Response of the African monsoon to orbital forcing and ocean feedbacks in the middle Holocene. Science 278: 440-443.

Kutzbach, J.E., Harrison, S.P., Coe, M.T. (2001) Land-ocean-atmosphere interactions and monsoon climate change: A palaeo-perspective. In: Schulze, E.-D., Heimann, M., Harrison, S.P., Holland, E., Lloyd, J., Prentice, I.C., Schimel, D.S., (Max-Planck-Institute for Biogeochemistry, Jena, Germany) (Editors), Global Biogeochemical Cycles in the Climate System. Academic Press, San Diego, pp. 73-83.

Latifovic, R., Zhu, Z.L., Cihlar, J., Giri, C. (2002) Land cover of North America 2000. Natural Resources Canada, Canada Center for Remote Sensing, US Geological Service EROS Data Center.

Le Clainche, Y. (2000) Etude du Couplage Ocean-Glace-Atmosphère et de l'Impact de la Glace de Mer sur le Climate des Haute Latitudes. Thèse de doctorat Université Paris VI.

Leemans, R., Cramer, W. (1991) The IIASA database for mean monthly values of temperature, precipitation and cloudiness of a global terrestrial grid. International Institute for Applied Systems Analysis (IIASA). RR-91-18.

Levis, S., Foley, J.A., Pollard, D. (1999) Potential high-latitude vegetation feedbacks on CO2-induced climate change. Geophysical Research Letters 26:747-750.

Levis, S., Foley, J.A., Pollard, D. (2000) Large-scale vegetation feedbacks on a doubled CO2 climate. Journal of Climate 13: 1313-1325.

Levitus, S. (1982) Climatological atlas of the world's oceans. NOAA/ERL/GFDL 13: 173 pp.

Liu, Z., Gallimore, R.G., Kutzbach, J.E., Xu, W., Golubev, Y., Behling, P., Selin, R. (1999) Modeling long-term climate changes with equilibrium asynchronous coupling. Climate Dynamics 15: 325-340, DOI: 10.1007/s003820050285.

Liu, Z., Harrison, S.P., Kutzbach, J.E., Otto-Bliesner, B. (2004) Global monsoons in the mid-Holocene and oceanic feedback. Climate Dynamics 22: 157-182, DOI:110.1007/s00382-00003-00372-y.

Liu, Z., Wang, Y., Gallimore, R., Gasse, F., Johnson, T., deMenocal, P., Adkins, J., Notaro, M., Prentice, I.C., Kutzbach, J., Jacob, R., Behling, P., Wang, L., Ong, E., (2007) Simulating the transient evolution and abrupt change of Northern Africa atmosphere–ocean–terrestrial ecosystem in the Holocene. Quaternary Science Reviews 26: 1818–1837.

Lorenz, S.J., Lohmann, G., (2004) Acceleration technique for Milankovitch type forcing in a coupled atmosphere-ocean climate circulation model: method and application for the Holocene. Climate Dynamics 23: 727–747.

Lucht, W., Prentice, I.C., Myneni, R.B., Sitch, S., Friedlingstein, P., Cramer, W., Bousquet, P., Buermann, W. and Smith, B. (2000). Climatic control of the high-latitude vegetation greening trend and Pinatubo effect, Science 296, 1687-1689.

MacDonald, G.M., Felzer, B., Finney, B.P., Forman, S.T. (2000) Holocene lake sediment records of Arctic hydrology. Journal of Paleolimnology 24: 1-14.

Madec, G., Imbard, M. (1996) A global ocean mesh to overcome the North Pole singularity. Climate Dynamics 12: 381 – 388.

Madec, G., Delecluse, P., Imbard, M., Lévy, C. (1998) OPA8.1 ocean general circulation model reference manual. Institut Pierre Simon Laplace Note 11: (http://www.ipsl.jussieu.fr/modelisation/note11.html)

Marshall, S.J., Tarasov, L., Clarke, G.K.C., Peltier, W.R. (2000) Glaciological reconstruction of the Laurentide Ice Sheet: physical processes and modelling challenges. Canadian Journal of Earth Sciences. 37: 769-793.

Marsland, S., Haak, H., Jungclaus, J., Latif, M., Röske, F. (2003) The Max-Planck-Institute global ocean/sea ice model with orthogonal curvilinear coordinates. Ocean Modeling, 5, S. 91-127.

Masson, V., Joussaume, S. (1997) Energetics of the 6000-yr BP atmospheric circulation in boreal summer, from large-scale to monsoon areas: A study with two versions of the LMD AGCM. Journal of Climate 10:2888-2903.

Masson, V., Cheddadi, R., Braconnot, P., Joussaume, S., Texier, D. (1999) Mid-Holocene climate in Europe: What can we infer from PMIP model data comparisons? Climate Dynamics 15: 163-182.

Maycut, G.A., Untersteiner, N. (1971) Some results from a time-dependent, thermodynamic model of sea-ice. Journal of Geophysical Research 76:1550-1575.

Meehl, G.A., Stocker, T.F., Collins, W.D., Friedlingstein, P., GayeGregory, A.T., J.M., Kitoh, A., Knutti, R., Murphy, J.M., Noda, A., Raper, S.C.B., Watterson, I.G., Weaver, A.J., Zhao, Z.-C., (2007): Global Climate Projections. In: Climate Change 2007: The Physical Science Basis. Contribution of Working Group I to the Fourth Assessment Report of the Intergovernmental Panel on Climate Change [Solomon, S., D. Qin, M. Manning, Z. Chen, M. Marquis, K.B. Averyt, M. Tignor and H.L. Miller (eds.)]. Cambridge University Press, Cambridge, United Kingdom and New York, NY, USA.

Melillo, J.M., McGuire, A.D., Kicklighter, D.W., Moore III, B., Vorosmarty, C.J., Schloss, A.L. (1993). Global climate change and terrestrial net primary production. Nature. 363:234-240.

Mikolajewicz, U., Scholze, M., Voss, R. (2003) Simulating near-equilibrium climate and vegetation for 6000 cal. years BP. Holocene 13: 319-326.

Mitchell, J.F.B., Grahame, N.S, Needham, K.J. (1988) Climate simulations for 9000 years before present: seasonal variations and effect of the Laurentide ice sheet. Journal of Geophysical Research-Atmosphere 93: 8283-8303.

Monserud, R.A., (1990) Methods for comparing global vegetation maps, IIASA WP-90-40, International Institute For Applied System Analyses, Laxenburg, Austria.

Monserud, R.A., Leemans, R. (1992) Comparing global vegetation maps with Kappa statistic, Ecological Modelling, 62: 275-293.

Myneni, R.A., Keeling, C.D., Tucker, C.J., Asrar, G., Neman, R.R. (1997): Increased plant growth in the northern high latitudes from 1981 to 1991. Nature, 386: 698-702.

Ni, J., Harrison, S.P., Prentice, I.C., Kutzbach, J.E., Sitch, S. (2005). Impact of climate variability on present and Holocene vegetation: A model-based study. Ecological Modelling, doi:10.1016/j.ecolmodel.2005.05.019.

Ni, J., Harrison, P.S., Prentice, I.C., Kutzbach, J.E., Sitch, S. (2006) Impact of climate variability on present and Holocene vegetation: A model-based study. Ecological Modelling; 191, 469-486.

Notaro, M., Liu, Z. (2008) Statistical and dynamical assessment of vegetation feedbacks on climate over the boreal forest. Climate Dynamics 31: 691-712, doi: 10.1007/s00382-008-0368-8.

Otto, J., Raddatz, T. Claussen, M. Brovkin, V. Gayler V. (2009) Separation of atmosphere-ocean-vegetation feedbacks and synergies for mid-Holocene climate. Geophysical Research. Letters 36: L09701, doi:10.1029/2009GL037482.

Otto-Bliesner, B.L. (1999) El Niño/La Niña and Sahel precipitation during the middle Holocene. Geophysical Research Letters 26 : 87-90.

Otto-Bliesner, B.L., Brady, E.C., Tomas, R., Levis, S., Kothavala, Z., (2006) Last Glacial Maximum and Holocene climate in CCSM3. Journal of Climate 19, 2526–2544.

Overpeck, J., Hughen, K., Hardy, D., Bradley, R., Case, R., Douglas, M., Finney, B., Gajewski, K., Jacoby, G., Jennings, A. , Lamoureux, S. , Lasca, A. , MacDonald, G., Moore, J. , Retelle, M., Smith, S., Wolfe, A. , Zielinski G. (1997). Arctic Environmental Change of the Last Four Centuries. Science. 278. no. 5341: 1251 – 1256. DOI: 10.1126/science.278.5341.1251.

Parkinson, C.L., Cavalieri, D.J., Gloersen, P., Zwally, H.J., Comiso, J.C. (1999).Arctic sea ice extents, areas, and trends. Journal of Geophysical Research 104: 20837–20856.

Parmesan, C., Yohe, G. (2003) A globally coherent fingerprint of climate change impacts across natural systems; nature: 421: 37-42.

Peixoto, J.P., Oort, A.H. (1992). Physics of climate. New York: American Institute of Physics.

Petit, J.R., Jouzel, J., Raynaud, D., Barkov, N.I., Barnola, J.-M., Basile, I., Bender, M., Chappellaz, J., Davis, M., Delaygue, G., Delmotte, M., Kotlyakov, V.M., Legrand, M., Lipenkov, V.Y., Lorius, C., Pepin, L., Ritz, C., Saltzman, E., Stievenard, M. (1999) Climate and atmospheric history of the past 420,000 years from the Vostok ice core, Antarctica. Nature 399 : 429 – 436.

Peltier, W.R. (1994). Time Dependent Topography Through the Glacial Cycle. IGBP PAGES/World Data Center-A for Paleoclimatology Data Contribution Series. 93-015.

Pickett, E., Harrison, S. P., Hope, G., Harle, K., Dodson, J. R., Kershaw, A. P., Prentice, I. C., Backhouse, J., Colhoun, E. A., D'Costa, D., Flenley, J., Grindrod, J., Haberle, S., Hassell, C., Kenyon, C., Macphail, M., Martin, H., Martin, A. H., McKenzie, M., Newsome, J. C., Penny, D., Powell, J., Raine, I., Southern, W., Stevenson, J., Sutra, J.-P., Thomas, I., van der Kaars, S., Ward, J. (2004). Pollen-based reconstructions of biome distributions for Australia, South East Asia and the Pacific (SEAPAC region) at 0, 6000 and 18,000 14C yr B.P. Journal of Biogeography 31(9), 1381-1444.

Prentice, I.C., Cramer, W., Harrison, S.P., Leemans, R., Monserud, R.A., Solomon, A.M. (1992) A global biome model based on plant physiology and dominance, soil properties and climate. Journal of Biogeography 19: 117-134.

Prentice, I.C., Guiot, J., Huntley, B., Jolly, D., Cheddadi, R. (1996) Reconstructing biomes from palaeoecological data: a general method and its application to European pollen data at 0 and 6 ka. Climate Dynamics 12: 185-194.

Prentice, I.C., Webb III, T. (1998) BIOME 6000: reconstructing global mid-Holocene vegetation patterns from palaeoecological records. Journal of Biogeography 25: 997-1005.

Prentice, I.C., Jolly, D., BIOME 6000 Participants (2000): Mid-Holocene and glacial-maximum vegetation geography of the northern continents and Africa. Journal of Biogeography 27: 507-519.

Qin, B.Q., Harrison, S.P., Kutzbach, J.E. (1998) Evaluation of modelled regional water balance using lake status data: A comparison of 6 ka simulations with the NCAR CCM. Quaternary Science Reviews 17: 535-548.

Randall, D. (2000) General Circulation Model Development - Past, Present, and Future. International Geophysics, Volume 70. ISBN: 978-0-12-578010-0.

Raynaud, D., Jouzel, J., Barnola, J.M., Chappellaz, J., Delmas, R.J., Lorius, C. (1993) The ice record of greenhouse gases. Science 259: 926-934.

Renssen, H., Brovkin, V., Fichefet, T., Goosse, H. (2003) Holocene climatic instability during the termination of the African Humid Period. Geophysical Research Letters 30(4): 1184. doi:1029/2002GL016636.

Renssen, H., Braconnot, P., Tett, S.F.B., von Storch, H., Weber, S.L. (2004) Recent developments in Holocene climate modelling. In: Battarbee, R.W., Gasse, F., Stickley, C.E. (eds); Past climate variability through Europe and Africa; Kluwer; Dordrecht; 495-513.

Renssen, H., Goosse, H., Fichefet, T., Brovkin, V., Driesschaert, E., Wolk, F., (2005) Simulating the Holocene climate evolution at northern high latitudes using a coupled atmosphere-sea ice-ocean-vegetation model. Climate. Dynamics 24(1) 23–43.

Reynolds, R.W. (1988) A Real-Time Global Sea Surface Temperature Analysis. Journal of Climate 1: 75-87.

Roeckner, E., Bäuml, G., Bonaventura, L., Brokopf, R., Esch, M., Giorgetta, M., Hagemann, S., Kirchner, I., Kornblueh, L., Manzini, E., Rhodin, A., Schlese, U. , Schultzweida U., Tompkins, A. (2003) The atmospheric general circulation model ECHAM5. Part I: Modeldescription. MaxPlanckInst. F. Meteor., Report No. 349. Hamburg.

Rudayaa, N., Tarasov, P., Dorofeyuk, N., Solovieva, N., Kalugine, I., Andreev, A., Daryin, A., Diekmann, B., Riedel, F., Tserendash N., Wagner, M., (2008) Holocene environments and climate in the Mongolian Altai reconstructed from the Hoton-Nur pollen and diatom records: a step towards better understanding climate dynamics in Central Asia. Quaternary Science Reviews 28: 5-6, doi:10.1016/j.quascirev.2008.10.013.

Sadourny, R., Laval, K. (1984) January and July performance of the LMD general circulation model. In: Nicolls ,C. (ed) New Perspectives in climate modelling. Vol. 16: Developments in atmospheric science. Elsevier, Paris, pp 173-197.

Schaaf, C., Strahler, A., Feng, Gao, Lucht, W., Yufang, Jin, Xiaowen Li, Xiaoyang, Zhang, Tsvetsinskaya, E., Muller, J.-P., Lewis, P., Barnsley, M., Roberts, G., Doll, C., Shunlin Liang, Roy, D., Privette, J. (2002) First Operational BRDF, Albedo and Nadir Reflectance Products from MODIS, Remote Sensing of Environment., 83: 135-148.

Schellnhuber, H.-J. (1999): 'Earth system' analysis and the second Copernican revolution. Nature 402, C19–C26.

Schellnhuber, H.-J., Wenzel, V. (eds) (1998): Earth System Analysis – Integrating science for sustainability. Heidelberg: Springer, 530 pp.

Schmidt, G.A., Shindell, D.T., Miller, R.L., Mann, M.E., Rind, D., (2004). General circulation modelling of Holocene climate variability. Quaternary Science Reviews 23, 2167–2181.

Schurgers, G., Mikolajewicz, U., Gröger, M., Maier-Reimer, E., Vizcaıno, M., Winguth, A., (2006). Changes in terrestrial carbon storage during interglacials: a comparison between Eemian and Holocene. Climate of the Past 2: 449–483.

Schurgers, G., Mikolajewicz, U., Gröger, M.; Maier-Reimer, E., Vizcaino, M., Winguth, A. (2007): The effect of land surface changes on Eemian climate. Climate Dynamics 29, 357-393. DOI:10.1007/s00382-007-0237-x.

Serreze, M.C., Walsh, J.E., Chapin III, F.S., Osterkamp, T., Dyurgerov, M., Romanovsky, V., Oechel, W.C., Morison, J., Zhang, T., Barry, R.G. 2008. Observational evidence of recent change in the northern high-latitude environment. Climatic Change 46(1-2): 159-207, doi:10.1023/A:1005504031923.

Semtner, A.J. (1976) Model for thermodynamic growth of sea ice in numerical investigations of climate. Journal of Physical Oceanography 6: 379-389.

Sitch, S., Smith, B., Prentice, I., Arneth, A., Bondeau, A., Cramer, W., Kaplan, J., Levis, S., Lucht,W., Sykes, M., Thonicke, K., Venevsky, S. (2003) Evaluation of ecosystem dynamics, plant geography and terrestrial carbon cycling in the LPJ Dynamic Global Vegetation Model. Global Change Biology 9: 161–185.

Stein, U., Alpert, P. (1993) Factor separation in numerical simulations. Journal of the Atmospheric Sciences 50: 2107-2115.

Steffen, W., Walker, B.(1992) The terrestrial biosphere and global change: Implication for natural and managed ecosystems. A synthesis of GCTE and related research. IGBP Science No.1.

Street-Perrott, F.A., Perrott, R.A. (1993) Holocene vegetation, lake levels, and climate of Africa. In: Wright, H.E., Kutzbach, J.E., Webb III, T., Ruddiman, W.F., Street-Perrott, F.A., Bartlein, P.J. (Ed), Global climates since the last glacial maximum. University of Minnesota Press, Minneapolis, pp. 318-356 (569 p.).

Takahara, H., Sugita, S., Harrison, S.P., Miyoshi, N., Morita, Y., Uchiyama, T. (2000). Pollen-based reconstructions of Japanese biomes at 0, 6000 and 18,000 14C yr BP. Journal of Biogeography 27(3): 665-683.

Tarasov, P.E., Webb III, T., Andreev, A.A., Afanas'eva, N.B., Berezina, N.A., Bezusko, L.G., Blyakharchuk, T.A., Bolikhovskaya, N.S., Cheddadi, R., Chernavskaya, M.M., Chernova, G.M., Dorofeyuk, N.I., Dirksen, V.G., Elina, G.A., Filimonova, L.V., Glebov, F.Z., Guiot, J., Gunova, V.S., Harrison, S.P., Jolly, D., Khomutova, V.I., Kvavadze, E.V., Osipova, I.M., Panova, N.K., Prentice, I.C., Saarse, L.,

Sevastyanov, D.V., Volkova, V.S., Zernitskaya, V.P. (1998) Present-day and mid-Holocene biomes reconstructed from pollen and plant macrofossil data from the former Soviet Union and Mongolia. Journal of Biogeography 25: 1029-1053.

Tarasov, P. E., Volkova, V. S., Webb III, T., Guiot, J., Andreev, A.A., Bezusko, L.G., Bezusko, T.V., Bykova, G.V., Dorofeyuk, N.I., Kvavadze, E.V., Osipova, I.M., Panova, N.K., Sevastyanov, D.V. (2000). Last glacial maximum biomes reconstructed from pollen and plant macrofossil data from northern Eurasia. Journal of Biogeography 27(3), 609-620.

Tarasov, P.E., Dorofeyuk, N.I., Vipper, P.B. (2002) The Holocene Dynamics of Vegetation in Buryatia. Stratigraphy and Geological Correlation 10(1): 88-96.

TEMPO-Members, Kutzbach, J.E., Bartlein, P.J., Foley, J.A., Harrison, S.P., Hostetler, S.W., Liu, Z., Prentice, I.C., Webb III, T. (1996) Potential role of vegetation feedback in the climate sensitivity of high-latitude regions: a case study at 6000 years before present. Global Biogeochemical Cycles 10: 727-736.

Texier, D., de Noblet, N., Harrison, S.P., Haxeltine, A., Jolly, D., Joussaume, S., Laarif, F., Prentice, I.C., Tarasov, P. (1997) Quantifying the role of biosphere-atmosphere feedbacks in climate change: coupled model simulation for 6000 years BP and comparison with palaeodata for northern Eurasia and northern Africa. Climate Dynamics 13: 865-882.

Texier, D., de Noblet, N., Braconnot, P. (2000) Sensitivity of the African and Asian monsoons to mid-Holocene insolation and data-inferred surface changes. Journal of Climate 13: 164-181.

The Global Land Cover Map for the Year 2000 (2003), GLC2000 database, European Commission Joint Research Centre. http://www-gem.jrc.it/glc2000.

Thompson, R.S., Anderson, K.H. (2000). Biomes of western North America at 18,000, 6000 and 0 14C yr BP reconstructed from pollen and packrat midden data. Journal of Biogeography 27(3): 555-584.

Vavrus, S.J. (1999). The response of the coupled arctic sea ice-atmosphere system to orbital forcing and ice motion at 6 kyr and 115 kyr BP. Journal of Climate 12, 873-896.

Vavrus, S.J., Harrison, S.P. (2003) The impact of sea-ice dynamics on the Arctic climate system. Climate Dynamics 20: 741-757, doi: 710.1007/s00382-00003-00309-00385.

Voss, R., Mikolajewicz, U. (2001) The climate of 6000 years BP in near-equilibrium simulations with a coupled AOGCM. Geophysical Research Letters 28: 2213-2216.

Wanner, H., Beer, J., Bütikofer, J., Crowley, T.J., Cubasch, U., Flückiger, J., Goosse, H., Grosjean, M., Joos, F., Kaplan, J.O., Küttel, M., Müller, S.A., Prentice, I.C., Solomina, O., Stocker, T. F., Tarasov, P., Wagner, M., Widmann, M. (2008) Mid- to Late Holocene climate change: an overview. Quaternary Science Reviews 27: 1791–1828, doi: 10.1016/j.quascirev.2008.06.013.

Warrilow, D.A., Sangster, A.B., Slingo, A. (1986) Modelling of land surface processes and their influence on European climate. Technical report DCTN 38, United Kingdom Meteorological Office, Bracknell, Berkshire RG12 2SZ, UK, Bracknell, UK.

Weatherley, J.W., Briegleb, B.P., Large, W.G., Maslanik, J.A. (1998) Sea ice and polar climate in the NCAR Csm. Journal of Climate 11: 1472-1486.

Weber, S.L. (2001) The impact of orbital forcing on the climate of an intermediate-complexity coupled model. Glob Planet Change 30: 7-12.

Weber, S.L., Oerlemans, J. (2003) Holocene glacier variability: three case studies using an intermediate-complexity climate model. Holocene 13: 353-363.

Weber, S.L., Crowley, T.J., van der Schrier, G. (2004) Solar irradiance forcing of centennial climate variability during the Holocene. Climate Dynamics 24: 539-553.

Williams, J.W., Webb III, T., Richard, P.H., Newby, P. (2000) Late Quaternary biomes of Canada and the eastern United States. Journal of Biogeography 27: 585-607.

Wohlfahrt, J., Harrison, S.P., Braconnot, P. (2004) Synergistic feedbacks between ocean and vegetation on mid- and high-latitude climates during the mid-Holocene. Climate Dynamics 22: 223-238.

Wohlfahrt J., Harrison, S.P., Braconnot, P., Hewitt, C.D., Kitoh, A., Mikolajewicz, U., Otto-Bliesner, B.L., Weber, L. (2008) Evaluation of coupled ocean-atmosphere simulations of the mid-Holocene using palaeovegetation data from the northern hemisphere extratropics. Climate Dynamics 31(7-8): 871-890, doi: 10.1007/s00382-008-0415-5.

Woodruff, S., Slutz, R.J., Jenne, R.L., Steurer, P. (1987) A comprehensive ocean-atmosphere data set. Bulletin of the American Meteorological Society 68: 1239-1250.

Woodward, F.I. (1987) Stomatal numbers are sensitive to increases in CO2 from preindustrial levels. Nature 327: 617-618.

Yu, G., Harrison, S.P. (1995) Holocene changes in atmospheric circulation patterns as shown by lake status changes in northern Europe. Boreas 24: 260-268.

Yu, G., Harrison, S.P. (1995). Lake status records from Europe: data base documentation. NOAA Paleoclimatology Publications Series 3: 451pp, Boulder, Colorado.

Yu, G., Harrison, S.P. (1996) An evaluation of the simulated water balance of Eurasia and northern Africa at 6000 y BP using lake status data. Climate Dynamics 12: 723-735.

Yu, G., Prentice, I.C., Harrison, S.P., Sun, X.J. (1998) Pollen-based biome reconstructions for China at 0 and 6000 years. Journal of Biogeography 25(6): 1055-1069.

Yu, G., Chen, X., Ni, J., Cheddadi, R., Guiot, J., Han, H., Harrison, S.P., Huang, C., Ke, M., Kong, Z., Li, S., Li, W., Liew, P., Liu, G., Liu, J., Liu, Q., Liu, K.-B., Prentice, I.C., Qui, W., Ren, G., Song, C., Sugita, S., Sun, X., Tang, L., van Campo, E., Xia, Y., Xu, Q., Yan, S., Yang, X., Zhao, J., Zheng, Z. (2000). Palaeovegetation of China: a

pollen data-based synthesis for the mid-Holocene and Last Glacial Maximum. Journal of Biogeography 27(3): 635-664.

Zhou, L., Tucker, C.J., Kaufmann, R.K., Slayback, D., Shabanov, N.V., Myneni, R.B. (2001). Variations in northern vegetation activity inferred from satellite data of vegetation index during 1981-1999. Journal of Geophysical Research 106: 20,069-20,083.

CLIMATE 2.1: Cramer: http://www.pik-potsdam.de/~cramer/climate.html).

MPI-Meteorology models: http://www.mpimet.mpg.de/en/ wissenschaft/modelle.

PMIPI & PMIP2 (http://www-lsce.cea.fr/pmip/)

Biome6000: http://www.bridge.bris.ac.uk/resources/Databases/BIOMES_data

List of acronyms

[CO$_2$]	Carbon Dioxide concentration
0 ka	present day
6 ka	6000 years before present
ACIA	Arctic Climate Impact Assessment
AO	atmosphere-ocean
AOGCM	atmosphere-ocean coupled general circulation model
AOV	atmosphere-ocean-vegetation
AOVGCM	atmosphere-ocean-vegetation coupled general circulation model
biome	ecosystems of a specific vegetation compositions
BIOME1	first equilibrium biogeography vegetation model (Prentice et al. 1992)
BIOME4	diagnostic equilibrium biogeography vegetation model (Kaplan et al. 2003)
Biome6000	pollen and macrofossil data set developed by the Global Palaeovegetation Mapping Project (Prentice and Webb 1998)
CAPE	Project for Holocene paleoclimate data from the Arctic (2001)
CLIMAP	Long range Investigation, Mapping, and Prediction: produced a map of climate conditions during the last glacial maximum
CLIMBER	climate system model of intermediate complexity developed at the Potsdam- Institut für Klimafolgenforschung
COHMAP	Cooperative Holocene Mapping Project: observations and simulations of climate change for the last 18,000 years (1988)
CSM1.2	atmosphere-ocean general circulation model (Otto-Bliesner 1999)
DJF	winter season of December, January, February
ECBILT	atmosphere-ocean general circulation model (Weber 2001)
ECHAM3	atmosphere-ocean general circulation model (Voss and Mikolajewicz 2001)
ECHAM3-LSG	AOGCM model (Voss and Mikolajewicz 2001)
ECHAM5	atmosphere general circulation model (Roeckner et al. 2003)
ECHAM5-MPIOM	atmosphere-ocean general circulation model (Jungclaus et al. 2005)
ECHAM5-MPIOM-LPJ	atmosphere-ocean general circulation model (Schurgers et al. 2007)
EMIC	climate system model of intermediate complexity
FAO	Food and Agriculture Organization, Rome
GCM	general circulation model simulating climate parameters on a global scale
GDD	growing-degree-days

GDD_0	growing-degree-days above 0 °C; relevant for the decision between boreal forests and tundra
GDD_5	growing-degree-days above 5 °C; relevant for the decision between boreal and temperate forests
HADCM2	atmosphere-ocean general circulation model (Hewitt and Mitchell 1998)
IGBP	International Geosphere- and Biosphere Programme
IPCC	Intergovernmental Panel on Climate Change: launched by the United Nations departments of UNEP and WMO
IPSL	GCM of the Institute Pierre Simone Laplace, France
IPSL-CM1	atmosphere-ocean general circulation model (Braconnot et al. 1999, 2000a)
JJA	summer season of June, July, August
K	Temperature in Kelvin
LAI	leaf area index
LMD	Laboratoire de Météorologie Dynamique
LPJ	Lund-Potsdam-Jena dynamic global vegetation model (Sitch et al. 2003)
MAM	spring season of March, April, May
megabiome	combination of related biomes
MODIS	Moderate Resolution Imaging Spectroradiometer satellite data
MPIOM	ocean general circulation model (Marsland et al., 2003)
MRI	atmosphere-ocean general circulation model (Kitoh and Murakami 2002)
MTCO	maximum mean temperature of the coldest month
MTWA	mean temperature of the warmest month
NH	Northern Hemisphere
NPP	net primary productivity
OPA	oceanic general circulation model (Madec et al. 1998)
PAGES	Past Global Changes project: to coordinate and promote past global change research
PAIN	Pan-Arctic INitiative project (Bigelow et al. 2003)
PFT	plant functional types (Steffen et al. 1992)
PMIP	Palaeoclimate Modelling Intercomparison Project (Joussaume & Taylor 2000)
ppm	parts per million
SECHIBA	land-surface scheme model (Ducoudré et al. 1993)
SIC	sea ice cover
SON	autumn season of September, October, November
SST	sea surface temperature
TEMPO	Project for modeling the potential response of vegetation to global climate change (1996)
T_{min}	minimum temperature
WCRP	World Climate Research Programme
Wm^2	Watt per square meter

Danksagung

Ich möchte mich an dieser Stelle ganz besonders bei Professor Martin Claussen, meinem Gruppenleiter Christian Reick und meiner Lebenspartnerin Anne bedanken. Ohne Ihre Unterstützung hätte es diese letzte Seite nie gegeben.

Ich danke Martin für die Möglichkeit, als Steineklopfer im Reich der Formelwesen die Tür zwischen planetaren und lokalen Strategien etwas weiter öffnen zu können. Seine Geduld und sein Ideenreichtum haben mich unterstützt. Es war immer wieder motivierend, aus dem eigenen kleinen holozänen Wald heraus das weite unerforschte Land mit Martins Augen zu sehen.

Ich hätte mir keinen besseren, kritischeren und engagierteren Capo und Lektor als Christian wünschen können. Er war da, als ich Ihn brauchte. Vielen dank für die erste und die zweite Hilfe, das wesentlich bessere 'English' und die kniffligen Fragen, die mich immer weiter führten.

Besonders hilfreich für mich waren die vielen Diskussionen, Anregungen, Denkanstöße und Nachhilfestunden von Thomas Wiki-Raddatz, ebenso wie die vielen hilfreichen Tipps von Julia Pongratz. Nur durch die geduldige Hilfestellung von Veronika Gayler haben es meine Biome-Modellläufe aus dem Algorithmen-Maschinenraum bis zur Postergalerie geschafft. Herzlichen Dank dafür.

Der alten Glasturm-Crew aus Jena und der 17er-Crew über Hamburg danke ich für die herzliche und unkomplizierte Zusammenarbeit. Die hervorragenden Arbeits-bedingungen die ich in diesen beiden MPI´s angetroffen habe, ich meine die technischen aber insbesondere die sozialen Strukturen, ließen zahlreiche Umzüge und Umbaumaßnahmen fast unbemerkt an mir vorüber gehen.

Meinen ganz besonderen Dank an die stärkenden Freunde in der Ferne: besonders Andreas und Mandi, sowie Ingo, Alex, Martin, Katrin, Enrico und Jörg.

Und ich danke meiner Mutsch, die, ganz egal wie und was ..., doch immer zu mir stand.

Anne sei Dank: für die Hilfe bei der Formatierung, die unglaubliche Ausdauer, die Liebe und mutige Freundschaft, und vor allem das Vertrauen.